A MATRIX ISOLATION SPECTROSCOPIC INVESTIGATION OF THE REACTION PRODUCTS OF TRANSITION METAL CENTRES WITH ETHENE AND WATER

by

MATTHEW G. K. THOMPSON

A thesis submitted to the Department of Chemistry

in conformity with the requirements for

the degree of Doctor of Philosophy

Queen's University

Kingston, Ontario, Canada

November 2007

Abstract

The reaction products of thermally generated atomic V with ethene and ethene isotopomers have been investigated by matrix isolation ultraviolet visible and Fourier transform infrared (FTIR) spectroscopy. When V is deposited into matrices of pure Ar, evidence for V and V_2 are present in the UV-visible absorption spectra. Addition of trace amounts of ethene results in the elimination of absorptions due to V_2 on deposition, likely due to the formation of $V^{\cdots}(C_2H_4)$ van der Waals complexes on matrix condensation. Irradiation of matrices containing V and trace C_2H_4 in Ar, with light corresponding to atomic V electronic excitations, eliminates all UV-visible absorptions due to atomic V in the matrix.

Infrared analysis of matrices containing V and C_2H_4 give evidence for a new product on deposition, consistent with a kinetically formed H-V-C_2H_3 isomer. Following further irradiation of the matrix, several new products of C-H bond insertion by the metal atom, including additional H-V-C_2H_3 conformational isomers, and $H_2V(\eta^2\text{-}C_2H_2)$ products are observed in the infrared spectrum. Additionally, the formation of ethane is evident as a major product immediately following deposition of V + C_2H_4 + H_2O in Ar. The formation of this product is consistent with alkene insertion into the V-H bond of an H-V-OH intermediate, followed by a photo-induced elimination to give C_2H_6.

Under higher C_2H_4 concentrations, competitive ethane formation in which a sacrificial hydrogenation mechanism involving two ethene molecules is observed, analogous to the mechanism proposed to account for V + H_2O + C_2H_4. Isotopic

investigations aimed at confirming key aspects of the proposed mechanisms are also presented. Similar reactivity is observed for several metals, suggesting that this reaction is a generalized reaction, whenever transition metal hydrides are formed. The additional observation of ethene hydrogenation where the initiating hydride source is either water, or ethene, suggests that this reaction could also easily generalize to other initiating hydride sources. The mechanism could also extend to the insertion of other π-bond containing species, as well.

Acknowledgements

It would be impossible for me to have completed this work entirely on my own. The enormous support of a number of people has contributed to the overall production of this thesis, through numerous valuable discussions, administrative support, and dedicated instruction. While it would take many additional pages to properly thank every person who has been a part of this work, I hope that this small section serves as representative of my sincerest thanks to all those involved.

Without doubt, the departmental administrative assistants at both Queen's University and Trent University have been invaluable in helping me achieve my goals. In particular, Ms. Annette Keyes, and Mrs. Laurie LaPlante are two people who have helped me enormously. Their tireless efforts will never be forgotten, and certainly, their efforts will remain at the forefront of my memories of graduate school. Additionally, members of the staff at each of the universities have been invaluable, as well. In particular, the help of Mr. John LaPlante, and Mr. Barry Best, along with Mr. Ralph Frederick, Mr. Ed Wilson, Mr. Paul Karrel, and Mr. Ken Fowler have been instrumental in ensuring that day to day research could continue, smoothly.

I have also had the privilege of great instruction, in graduate courses at both Queen's University and Trent University, and I would like to thankfully acknowledge the tireless efforts of all of my instructors, who have certainly helped me to learn chemistry in their own ways.

Additionally, I would like to thank Professors Alan Slavin, and William Graham, who served as examiners on my committee. Their kind words, and thought provoking questions helped me to make my written thesis more complete. I am very pleased that both of them agreed to help me with this work, and provide their time, their advice, and their support.

Without doubt, two of my instructors, Professor Donal Macartney, and Professor David Wardlaw, were the most inspirational, and my favourite instructors, at Queen's. It was for this reason that I asked each of them to serve as members of my supervisory committee, and ultimately as examiners during my Ph.D. defence. I am very happy to have had these people along with me, during this journey. If I had to repeat the process, I would certainly hope that both of them would agree to repeat it with me, since they have certainly helped to make my overall Ph.D. experience exceptional.

Finally, I could not conceive of writing this section without thanking Professor J. Mark Parnis, my supervisor, my chemical mentor, and one of my best friends. Were it not for Mark, I would never have considered graduate school, and I would thus have missed out on countless opportunities which have proven, time and time again, to be the perfect choices for me. Through my conversations with Mark, I have learned as much about life as I have about chemistry – and these lessons that I have learned in each case, will undoubtedly serve me well as I continue forward from this point. It is a consequence of these experiences that I have become the person that I am today. I am very proud to be completing this work, in this context, and if I am able to help even one person

have but a fraction of the experience I had during my Ph.D., I would consider that to be a great success.

In memory of my grandfather, Jack Rascon

While he would have realized in advance that he would not have understood a single concept, he would have sat and read this entire document, simply because I had written it. Then, during my convocation, he would have clapped louder, stood taller, and been filled with more pride than anyone has ever been.

Statement of originality

I hereby certify that all of the work described within this thesis is the original work of the author. Any published (or unpublished) ideas and/or techniques from the work of others are fully acknowledged in accordance with the standard referencing practices.

Matthew Gary Karl Thompson

November, 2007

Table of Contents

List of Tables

List of Figures, Illustrations and Schemes

Chapter 1

Introduction

1.0 Origins of the current work

Hydrocarbons represent one of the largest classes of chemical compounds, and many examples exist of their use in synthesis, petrochemistry, and in industry.[1] In particular, saturated hydrocarbons and small unsaturated hydrocarbons are some of the most interesting molecules, since these species are widely available, and relatively inexpensive. However, the strength and relatively inert nature of the non-polar C-H bonds in hydrocarbons makes such species challenging to use as starting points in targeted synthesis. Thus, the chemical properties of the molecules seem to inhibit the advantages of their low cost and wide availability. Consequently, reactions where hydrocarbon C-H bonds can be made reactive are of considerable interest. One method by which such activation of C-H bonds can be made to occur is by the reaction of hydrocarbons with metal containing species.

The present work originated as an exploration of the stepwise mechanism of early transition metal atoms reacting with multiple units of the simplest alkene, ethene ($H_2C=CH_2$). Complementary gas-phase kinetics results had previously demonstrated that early transition metal atoms could coordinate multiple units of ethene, with the observation of extensive dehydrogenation of the ethene subunits.[2] These experimental observations suggested significant liberation of

molecular hydrogen from the metal/ethene reaction system. Furthermore, the surprisingly high level of coordination observed on the metal atom, given the limited availability of space on the atom surface, suggested a metal-mediated process such as oligomerization of the ethene units must occur. Additionally, the observed loss of hydrogen from the hydrocarbon suggested reaction pathways in which multiple insertions of the metal into the C-H bonds of the hydrocarbons must occur. However, the method of detection used in the gas-phase study provided information only of total mass of the various intermediate and product species. Thus no direct evidence for the structures of the reacting species, or the nature of the reaction taking place on the metal atom surface, was available. The current study was performed in order to elucidate these complementary aspects of the gas-phase reaction chemistry of the metal atom with ethene. The intended objective in these complementary studies was: a) to identify reaction intermediates in the overall process, and b) to identify reaction products. The complementary technique of matrix isolation, combined with UV-visible and infrared spectroscopy provide a means to explore these details thoroughly.

A variety of transition metal atoms were studied in the gas-phase with ethene, with the elements in Group VB (V, Nb, Ta) showing significant reactivity. Naturally, the focus on this group of metals became an obvious choice as a starting point. The heaviest of these particular metals have been some of the most difficult metals to generate in the gas-phase, prior to the widespread availability of lasers, and thus it is unsurprising that correspondingly little is known about the reactivity of these atoms. The choice to focus on the simplest

of these atoms, vanadium, V, was made with the expectation that understanding the chemistry of V would provide a basis for understanding the corresponding reaction chemistry with the other species in Group VB. Consequently, the major results presented in this work focus on understanding the reactivity of V with ethene. By varying the concentration of ethene, the goal is to determine structural aspects of V/ethene reaction intermediates and products resulting from the expected C-H bond activation of ethene.

The major technique used to perform these complementary experiments is matrix isolation, with either UV-visible or infrared spectroscopic analysis. Thus, the beginning sections of this introduction focus on the basic nature of matrix-isolation as a technique, and the impact on spectroscopic measurements of using matrix-isolation methods. As these experiments do represent a complementary study of the reaction chemistry observed in gas-phase experiments, and not a direct measurement in the same experimental system, it is necessary to consider the impact, if any, of using the matrix isolation technique for this investigation. As such, factors describing the associated strengths, weaknesses, limitations, and deviations from "true" gas-phase work shall be included.

1.1 Matrix isolation: Technique and spectroscopic analysis

The "modern" matrix-isolation technique was developed by Pimentel in 1954,[3] as a means of stabilizing and trapping reactive intermediates implicated, but not directly observed, for a particular reaction process. In the simplest terms, the technique involves the inclusion of an excess of "inert" gas introduced

simultaneously with reagents that may begin to interact under gas-phase conditions. While these initial interactions between the reagents occur, the excess of the inert material entrains the gas-phase reagents, along with any initially forming reaction intermediates or products. Conveniently, this mixture can be easily directed within the experimental system, by appropriately designing the experimental apparatus. By diverting the gas-mixture toward a cold surface maintained below the freezing point of the excess inert gas, all of the species co-condense on the cold surface, thereby isolating reaction intermediates and products as guest species in a host of the inert support material. This solidified inert support is referred to as the 'matrix', in which the reagents, reaction products, and remaining reaction intermediates are isolated.

Although originally designed for stabilizing products due to gas-phase reactions, later experiments demonstrating that the technique could be extended to simple *in situ* syntheses of molecules within the matrix,[4,5,6] and to the isolation and characterization of products generated following photoexcitation and subsequent decomposition were also performed.[7,8] Thus, the versatility of this approach for generating, characterizing, and studying the reactivity of transient chemical reaction species is well-accepted. To this date, the matrix isolation technique has been cited in more than 16,000 research publications.

The stabilization and isolation of transient species is believed to occur during the "high pressure" condensation of excess inert gas, while a reaction occurs. The high relative pressure results in a significant reduction of the mean free path of any molecule entrained in the inert gas. As a result, repeated

collisions with the excess inert gas occur, and when two species having different internal energies collide, energy transfer can occur between the collision partners. Rare-gas atoms have no additional degrees of freedom for retaining internal energy beyond translational motion and electronic configuration, thus when rare-gases are used, these atoms leave the collision event with some additional translational energy. This process results in cooling of "energized" species, referred to as collisional deactivation. More effective collisional deactivation can be achieved by including "relatively inert" matrix hosts, such as N_2, CH_4, or SF_6, into the gas-mixture.[9] All of these molecules can more efficiently store additional energy following collision with an energized species, since these species have additional degrees of freedom in rotational and vibrational modes. However, these molecules can also be reactive under some experimental conditions, and hence, can result in significant diversion from chemistry under investigation. Consequently, the rare-gases represent the best choices for matrix support materials, and are most commonly used. In particular, the use of argon arises as a practical matrix choice, given its physical characteristics, and relative availability. As a result, argon is used commonly in routine matrix-isolation work.

As mentioned previously, highly energized transient species formed during a reaction are subjected to repeated collision with the rare-gas atoms, resulting in the rapid deactivation of energized molecules. When a transient species can be deactivated below some energy threshold required to overcome a reaction barrier, the species can be isolated in the matrix and subsequently observed. Since the temperature of the rare-gas condensation environment is extremely

low, (< 20 K in Ar), even very small reaction barriers become significant impediments. As such, species considered significantly reactive under ambient thermal conditions can be isolated and observed spectroscopically. One particular application of this technique is the mechanistic investigation of chemical reaction processes.

To perform mechanistic investigations, the modern use of the rare-gases as matrix support materials brings a number of advantages. As the rare-gas matrix host species are closed-shell atoms, they are mostly considered chemically inert, and are not directly detectable in particular forms of spectroscopy such as UV-visible, or infrared. Thus, when these species are used as the matrix support material, only those absorptions arising from the isolated species within the matrix are directly observed. Typically, reagent to host concentrations < 1:1000 are used to ensure that the isolated species are well separated from each other. These low concentration conditions ensure that when spectroscopic characterization is used the acquired spectra emulate the true gas-phase spectra reasonably well. Increasing the concentration beyond 1:1000 host:guest can lead to studies of reactivity of transient species within the matrix. Nevertheless, matrix-isolation of species represents one method of obtaining pseudo gas-phase spectroscopic absorptions, within a solid environment, for species which might otherwise be difficult or impossible to observe in the true gas-phase.

The cold temperature conditions of the matrix support material following condensation of the gas-mixture provide some additional advantages. Species

isolated within the matrix are maintained at very low thermal energies, and thus unimolecular reactions are generally inhibited. As the solid matrix support surrounds species, bimolecular reactions are also generally inhibited once the matrix is formed, as there is extremely limited diffusion within the solid matrix support material. The combination of these factors provides the basis for studying mechanistic reaction chemistry in matrices.

Although it is possible that transient species can be effectively isolated under matrix isolation conditions, generally some fraction of these transient species survives collisional deactivation during condensation, and these species can propagate along the reaction coordinate. The multitude of simultaneous products in the matrix can result in a vast array of spectroscopic absorptions, arising from the numerous species isolated in the matrix. By systematically increasing the concentration of a particular reagent, the spectroscopic features arising from a single transient species will correspondingly change in concert, providing the information necessary to characterize absorptions into groups. By performing careful experiments in this manner, these groups of features can be characterized based on their corresponding behaviour following changes to the chemical system. As a result, spectral features associated with specific species can be identified, and these spectra provide a means for identification of the species. Varying the concentration of reagents in the reaction environment is one of the simplest methods for performing the above characterization. However, increasing the concentration of a reagent eventually leads to the increased likelihood of a transient species to react further with additional reagent

molecules. Nevertheless, by using controlled changes in reagent concentration, this reactivity of the transient species can be effectively characterized, and both reactivity of a precursor molecule and parallel reactivity of a transient species can be simultaneously investigated. Other techniques such as photoexcitation, annealing of the matrix, and isotopic substitutions represent additional tools that can help to perform characterizations of novel species, by using methods similar to concentration variation.

Photoexcitation of species isolated in the matrix is another very beneficial technique which will be used throughout this work. Since the species initially formed during a reaction process can be isolated in the matrix for prolonged periods, it is possible to introduce energy into these matrix-isolated species using light. Provided that an isolated species has an absorption in resonance with a wavelength of light used to irradiate the matrix, absorption of that photon may lead to an increase in internal energy of the isolated species. This rapid transfer of energy to the isolated species can result in the species overcoming a thermal energy barrier, thereby leading to additional product formation. Thus, reactivity can be introduced even following matrix condensation, and changes that arise in measured spectra following this form of induced reactivity allow for additional identification of spectral absorptions associated with an individual species. Furthermore, the use of light to induce chemistry in this fashion leads to the possibility of studying the corresponding photochemistry of isolated transient-species, another aspect which may never be available in the gas-phase.

Arguably, the only disadvantages of the matrix-isolation technique involve: a) the extensive equipment necessary for generating and maintaining matrix-isolation conditions, b) the potential for matrix-guest interactions that deviate from the true gas-phase, and additionally, c) the impact of the matrix environment on isolated molecules, which becomes evident through spectroscopic measurements. Each of these topics is described in great detail in books dedicated to the subject of matrix isolation,[10] and also the chemistry and physics of species isolated within a matrix environment.[11] Thus, the consequences of these factors are well understood, and the benefits gained by the use of the matrix isolation technique far outweigh the simple disadvantages. For clarity, in the following sections the impact of the matrix isolation technique that arises in the forms of spectroscopy used in this work will be introduced, to aid interpretations of the mechanistic investigations that follow in later chapters.

1.2 UV-visible spectroscopy and matrix isolation

Spectroscopic transitions arising from UV-visible light correspond to the promotion of electrons from a lower energy orbital, to a higher energy orbital. The energy difference between the two states is $\Delta E = E_{photon} = hc/\lambda_{absorption}$, where $\lambda_{absorption}$ corresponds to the wavelength of the absorbed photon inducing the electronic transition. In many organic molecules, molecular absorptions typically occur only in the energy range associated with UV photons. If, however, significant π-conjugation exists in a molecule, this can lead to absorptions tailing into the blue light range of the visible region.[12] Transition metal compounds, by comparison, frequently have absorptions in the visible light range, corresponding

to weakly allowed transitions of partially filled d-orbitals. As a result, these systems can absorb visible light, appearing highly coloured, and the absorption of light in this manner can cause these species to exhibit considerable photo-induced reactivity.[13]

In order for an electronic transition to be observed for an atom in the UV-visible spectrum, selection rules require that: 1) there be no change in the spin-quantum number, **S**, upon combination of the upper and lower states (*i.e.* $\Delta\mathbf{S} = 0$), and also 2) that there be a unit change in the orbital angular momentum quantum number, **L** (*i.e.* $|\Delta\mathbf{L}| = 1$) during the transition. For heavy nuclei, spin-orbit coupling becomes more and more significant, and the **S** and **L** quantum numbers are no longer considered rigorously separate. Instead, the total angular momentum quantum number, **J**, must then be considered. In such cases, $|\Delta\mathbf{J}| = 0$, or 1 but, transitions for which $\mathbf{J}_{\mathbf{lower}} = 0$ to $\mathbf{J}_{\mathbf{upper}} = 0$ are expressly forbidden. An additional rule, known as the Laporte rule, requires that only those states in which parity is inverted following the transition may be combined.[14] The Laporte rule is quite rigorously observed under all conditions, and in tables such as Moore's tables,[15] special designation of parity-allowed transitions are given, for convenience.

As a result of the condition that, upon absorption of a photon, $|\Delta\mathbf{L}| = 1$, it is thus forbidden for electrons to transition between d orbitals. This is understandable, since such d to d transitions would offer no change in the orbital quantum number, **L**, and hence $\Delta\mathbf{L} = 0$. However, this selection rule rigorously applies only to atoms *in vacuo*, and thus, for atoms in environments where the

symmetry of the system is distorted, such “forbidden” transitions can weakly occur. Thus, weak interactions of an atom with a secondary species (such as is the case for an atom isolated in a matrix), can result in weakly allowed electronic transitions. These weak transitions can sometimes result in the excitation of species within the matrix environment, which may lead to investigation of excited state reactivity, rather than studies of ground-state reactivity.

Since the species that are trapped in a matrix are not completely isolated from their environment, but instead, can interact weakly with the matrix surroundings, the measured spectra are frequently distorted from the corresponding gas-phase spectra. Two factors which are frequently observed include: spectral shifting of absorptions (either to higher or to lower energy relative to the gas-phase) and also spectral broadening of absorption bands (both homogeneous and inhomogeneous cases). Fortunately, each of these cases can be readily understood simply by considering the physical environment of the isolated species.

The shifting of absorptions in the matrix environment relative to true gas-phase absorptions requires consideration of both the structure of the ground and the excited state which are involved in the specific transition, while additionally considering the environment in which the species is isolated. In cases where an interaction of the excited state is repulsive with the environment, the upper-state energy will increase relative to the gas phase energy, and hence, the ΔE associated with the transition will be larger.[11] The required photon inducing the transition will be of lower wavelength, and thus, the matrix isolated absorption in

the spectrum would appear to “shift toward blue” compared from the gas phase. If, instead, the interaction of the excited state species with the matrix environment is attractive relative to the gas-phase, then the upper state energy will be lower relative to the gas-phase. Correspondingly, the ΔE for the transition decreases, and the wavelength of the photon associated with the corresponding absorption will increase in the matrix isolated spectrum, or “shift toward red”. In many cases, knowledge of the excited state cannot be known prior to observation of the absorption spectra and instead these red- and blue-shifts are interpreted in the opposite way, providing evidence of the upper state attraction or repulsion with the matrix environment.

Similarly, broadening effects can be understood in terms of the interaction of the isolated absorber with the surrounding environment. Inhomogeneous broadening arises from the isolation of a species in specific, and unique, trapping environments.[11] For the case of an isolated atom, having a spherical geometry, inhomogeneous broadening is generally insignificant. By comparison, for molecules, inhomogeneous broadening can occur more extensively. Homogeneous spectral broadening arises as a result of the isolated species weakly coupling with motion of the surrounding environment, and the net result is a uniform broadening of absorption features.[11] All absorptions in the spectra of matrix isolated species suffer from some extent of homogeneous broadening.

According to Beer’s law, for a given absorber, the absorption intensity at a given wavelength will be proportional to the number of those absorbers giving rise to the absorption, and the path length over which the absorptions are

possible.[16] As a result, measurement of the absorption intensity is an indirect measure of the concentration of the species giving rise to the absorption. However, when broadening is an issue, the height of a particular absorption is not necessarily a good measurement for species concentration. In such cases, integration of the area under the absorption represents a better indicator of the concentration of the absorbing species. These types of area measurements are thus frequently encountered when performing quantitative measurements in matrix isolation experiments.

In this work, one of the principle applications of UV-visible spectroscopy is to become aware of the absorptions of species isolated in the matrix. Knowing these specific absorptions that are present allows for the controlled introduction of light of specific energy, by irradiating the matrix with a source that emits light corresponding to absorptions of isolated species. In this way, energy can be quickly introduced into a chemical system, possibly advancing a chemical reaction, and helping to identify groups of absorptions in a spectrum that correspond to a single molecule, as mentioned above.

1.3 Infrared spectroscopy and matrix isolation

The absorptions in infrared spectra correspond to the excitation of vibrational normal modes in molecules. These normal modes can be reduced into two general classes of motion: stretching motion of the molecule, and bending or deformational motion of the molecule. A non-linear, polyatomic molecule of N constituent atoms will have 3N-6 vibrational normal modes (3N-5, if linear). However, only those normal modes which result in a change in the

dipole moment upon vibration of the molecule will be observed in an infrared absorption spectrum. For convenience, normal modes are labeled with a symbol ν_k, where k corresponds to the k^{th} vibrational normal mode. The order in which the numbers 1 through k = 3N-6 are assigned to each vibrational normal mode of a molecule are based on rules of specific types of nuclear motion, and of symmetry. Such rules ensure that a consistent nomenclature of the vibrational modes is always used. A very comprehensive account of molecular vibrational motion can be found in the work of Wilson, Decius and Cross.[17]

Generally, stretching mode absorptions involve the predominant motion of only two nuclei in the molecule. In many cases, the solution for the energy in the harmonic oscillator problem can be used as a model for predicting the absorption wavenumber position in the infrared spectrum that corresponds to a stretching normal mode. From the solution to the harmonic oscillator problem,[18] a general expression for the absorption position in the infrared spectrum is given as:

$$\bar{\nu}_{stretching\_absorption} = \frac{1}{2\pi c}\sqrt{\frac{k}{\mu}} \qquad \text{Eq. 1.1}$$

with k representing the associated force constant of the stretching bond being modeled, and μ representing the reduced mass ($\mu = m_a * m_b/(m_a+m_b)$) for two nuclei, a and b, undergoing the stretching motion.[a] By comparison, bending motion is much more complicated, and no simple formula predicting bending type vibrational motion exists. However, by using stretching mode motion as a first

[a] The c and π symbols are physical constants available in an appendix at the end of this work. The value of c is typically quoted in this case in the units of cm/s, rather than m/s, to reflect the standard use of cm^{-1} as the standard wavenumber unit in infrared absorption spectroscopy.

approximation for understanding bending motion, the consequence of multiple nuclei moving during a bending vibration would be expected to result in significant increases in the reduced mass. Since wavenumber position is inversely related to reduced mass for absorptions due to stretching motion, bending absorptions are thus expected to appear in regions of the infrared spectrum that are lower in energy. This region is less specific for determining exactly which nuclei are present, and instead, absorptions in this region represent a fingerprint for specifically identifying molecules. The widespread use of computational methods for predicting infrared spectra of molecules have made computational predictions important tools aiding experimental infrared spectroscopy. By comparison of predicted spectra with the corresponding experimental spectra, identification of molecules can be made fairly accurately.

That the above equation (Eq. 1.1) predicting infrared absorptions is sensitive to the mass of the nuclei involved in the motion allows infrared absorption spectra to be used for the empirical identification of the nuclei in an unknown molecule. With proper implementation, this can often lead to functional group determination in the molecule, as well. As various functional groups will always absorb infrared radiation in very discrete sections of the infrared region, groups of frequency ranges corresponding to different nuclear motion can be tabulated, and used as a reference.[19,20] Using these tables, careful experimentation, and predictive software tools, it is possible to characterize the structure of unknown molecules based solely on their infrared absorption spectrum. Subtle geometric aspects such as conformational isomerism, degree

of unsaturation in a molecule, or even the distinction between planar or pyramidal geometry, can be made by using infrared spectroscopy.[19] As a result, this form of spectroscopy has been widely used for structural determination. Although other tools exist which can aid in structural determination, infrared spectroscopy represents a common, widely available, and simple tool for routine analyses. As an example demonstrating the distinction of degree of unsaturation, for a family of hydrocarbons, a comparison of the C-H stretching mode region of the infrared spectra of matrix-isolated ethane, C_2H_6, ethene, C_2H_4, and ethyne, C_2H_2 is given as Figure 1. As can be seen in this figure, as the degree of unsaturation increases from C_2H_6 to C_2H_4 to C_2H_2, the corresponding C-H stretching absorption band in the infrared spectrum moves to higher wavenumber value. Thus, it is possible to perform analyses of series of infrared spectra to compare relative degrees of dehydrogenation within molecules giving rise to the compared absorptions.

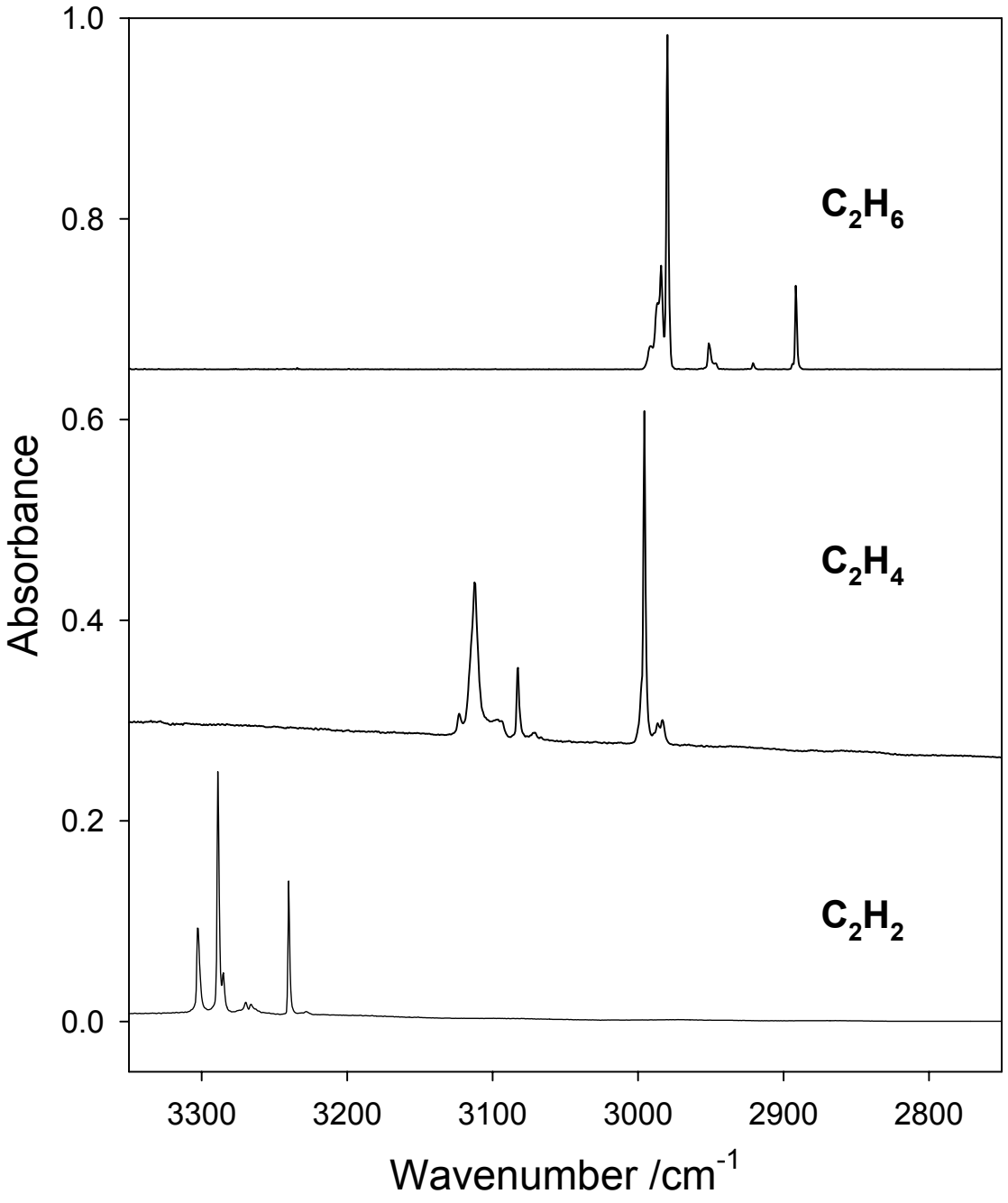

Figure 1: Portions of the infrared spectra in the C-H stretching mode region of matrix-isolated ethane (C_2H_6), ethene (C_2H_4) and ethyne (C_2H_2). Each spectrum has been offset along the absorbance axis by a constant for clarity of comparison.

For proper characterization of unidentified species, it is imperative to use isotopic substitution to unambiguously assign new features. For the smallest of molecules used in this work, which are primarily hydrogen (H) containing, the use of fully deuterated (D) analogues is quite straightforward. Selective substitution of hydrogen for deuterium in various molecules can also help to identify subtle mechanistic steps involved in an overall process. Hydrogen containing motion in the infrared is easiest to identify when switching hydrogen for deuterium in chemical systems. This fact is best highlighted in the absorption positions associated with pure stretching mode vibrations in infrared spectra. Since the force constant of the stretching bond is roughly preserved when exchanging the H nucleus for that of D (i.e. $k_H \sim k_D \sim k$),[21] it follows that the only change in the above equation (Eq. 1.1) stems from the change in the reduced mass. Thus, a ratio of the ν_H/ν_D vibrations simplifies to:

$$\frac{\bar{\nu}_H}{\bar{\nu}_D} = \frac{1/2\pi c}{1/2\pi c}\frac{\sqrt{k/\mu_H}}{\sqrt{k/\mu_D}} = \sqrt{\frac{\mu_D}{\mu_H}} \qquad \text{Eq. 1.2}$$

Since it can be shown that the ratio of μ_D to μ_H is 2, this ratio of pure stretching vibrational wavenumber position involving H to the same vibrational wavenumber position involving D is typically 1.414 (the square root of 2), when the H/D experiments are compared. Vibrational modes which are described in terms of bending components have a ratio less than 1.414, and the ratios of H/D vibrational positions can be between 1.38 and 1.30 in many cases. A more complete description of this type of analysis is given by Nakamoto,[21] and by Wilson, Decius and Cross.[17] Similar ratios exist for isotopic interchanges of other

elements, however, the extreme relative change of μ_D/μ_H provides the most pronounced ratio. In this work, the only other major isotope used is the exchange of ^{12}C for ^{13}C, and when these isotopes are interchanged, the shift in wavenumber position for ^{13}C involving modes compared from the same ^{12}C mode is typically less than 30 cm^{-1}. The expected ratio for a pure stretching vibration would be approximately $\nu(^{12}C)/\nu(^{13}C) = 1.04$, and as is the case with H/D substitution, even less than that value when significant contributions from bending motion are heavily involved the normal mode motion.

The majority of molecules, under ambient conditions, are in the ground vibrational state.[18] Additionally, transitions corresponding to infrared absorptions may occur only between adjacent vibrational states, *i.e.* $|\Delta\upsilon| = 1$. Thus, the most commonly observed transition for an absorption in the infrared spectrum of a molecule corresponds to the $\upsilon_1 \leftarrow \upsilon_0$ transition. A complete description of molecular infrared spectroscopy is described by Herzberg.[22] Since molecules are not perfectly harmonic, additional spectroscopic transitions can be observed, corresponding to $\upsilon_k \leftarrow \upsilon_0$, where $k > 1$. These transitions, known as overtone bands, appear at slightly lower than k times the wavenumber value corresponding to the $\upsilon_1 \leftarrow \upsilon_0$ absorption, as equal spacing of vibrational levels arises from the assumption that the vibrations are purely harmonic. Since some degree of anharmonicity in the vibrational levels of the molecule exists, the energy of the vibrational states slowly converges with increasing vibrational quantum number, υ. The anharmonic nature of the vibrations gives rise to the observation of overtone bands, and also to transitions exciting multiple normal

modes of vibration, simultaneously. Bands in an infrared spectrum corresponding to simultaneous excitation of more than one normal mode are called combination bands, and are generally symbolized $(m*\nu_a \pm n*\nu_b)$,[b] where m and n are natural numbers and ν_a and ν_b are the a^{th} and b^{th} vibrational normal mode of a molecule. Although one might expect that the presence of combination and overtone bands in the spectrum can cause significant cluttering of absorptions in the spectrum, combination and overtone bands are often very weak in the measured absorption spectrum. Thus, these transitions generally appear in the absorption spectrum only when higher concentrations of the absorbing molecule are present.

In some spectra, absorptions are not observed at the expected position, or more than the expected number of absorptions in a given region of the infrared spectrum may be observed. This behaviour can occur for a number of reasons, but one such reason which is often encountered is Fermi resonance. In simplistic terms, Fermi resonance arises when the energy of one fundamental normal mode is accidentally on, or close to, resonance with a combination or overtone mode.[22] As a result of the accidental degeneracy these two "degenerate" states mix and "repel" one another. Consequently, the energy of one state moves to slightly higher energy while the energy of the other moves to slightly lower energy, when each is compared from the originally degenerate states. Additionally, an increase in intensity is observed for the combination/overtone band, giving rise to the additional bands in the spectrum at

[b] Note: additional terms can also be added beyond binary combinations.

lower concentration. Thus, Fermi resonance results in two features where only one would be expected in the absorption spectrum, and can sometimes be used to account for additional absorptions. When isotopes are used, these accidental degeneracies often disappear, and so, spectra of isotopic systems may be free of Fermi resonance. This provides one method of identifying, experimentally, a case involving Fermi resonance.

Coupling of nuclei of similar mass, in a polyatomic molecule, is another form of splitting which transforms a pure vibrational mode into a set of vibrational modes.[17,21,22] In the simplest alkane, CH_4, the C-H bonds are all equivalent. This would suggest that a single C-H stretching mode absorption should be visible in the infrared absorption spectrum, with a degeneracy of four, corresponding to each individual C-H bond. However, that presumption assumes that the C-H bonds are each independent and that during vibrational motion, none of the C-H bonds responds to the motion of the others. This is not accurate and, instead, vibrational motion in which the similarly massed nuclei move in tandem can result, resulting in a lifting of the degeneracy. The lifting of degeneracy results in splitting of the absorption associated with the given vibrational modes, yielding absorptions in the spectrum at increased energy relative to the degenerate set, and similarly in modes having decreased energy relative to the degenerate set. The magnitude of the energy shift for each of the symmetric and asymmetric modes is approximately equal, but displaced in opposite directions. Similarly, since the selection rule for absorption of infrared radiation requires a change in the dipole moment upon vibration, the different

nuclear motion in both the symmetric and asymmetric cases can result in vastly different intensities in the infrared spectrum.

When one of the nuclei involved in a coupled vibration is isotopically substituted, the coupled vibrations disappear, with a new feature appearing in the spectrum at the average position of the absorption position for each of the two coupled features.[22] As a simple example, consider the absorption in the infrared of HCCH, DCCD, and HCCD. In the case of HCCH, two C-H stretching absorptions are observed at 3373.7 cm^{-1} (sym) and 3287 cm^{-1} (asym), and for DCCD, two absorptions are observed at 2700 cm^{-1} and 2427 cm^{-1}, in each case due to symmetric and asymmetric C-H/C-D stretching motion. When the spectrum of HCCD is acquired, absorptions in the spectrum occur for the C-H stretch at 3334.8 cm^{-1} compared from the average symmetric and asymmetric C-H stretching vibration in HCCH at: (3373.7 cm^{-1} + 3287 cm^{-1})/ 2 = 3330 cm^{-1}. Similarly, the C-D stretch of HCCD at: 2584 cm^{-1} compared with the average symmetric and asymmetric C-D stretching vibrations in DCCD = (2427 + 2700) / 2 = 2564 cm^{-1}. At first, this last calculation seems to disagree with the proposal presented above, since the 2564 cm^{-1} value is quite shifted from the expected 2584 cm^{-1} value. However, if one recognizes that the C≡C stretching frequency is similar in energy to the C-D stretching frequency, some degree of coupling with the C≡C stretching motion would be expected as well. Thus, if the C≡C stretching contributions could be decoupled, the 2564 cm^{-1} would be closer to the expected 2584 cm^{-1} value. Nevertheless, this example demonstrates that in cases where coupling of nuclear motion is expected, isotopic substitution can be

used as a means of determining additional geometrical aspects inherent to the molecule.

While infrared spectroscopy is a useful structural tool, some complications arising through the use of infrared spectroscopy for vibrational analysis must also be considered. In the gas phase, molecules are free to rotate, and under ambient thermal conditions, molecules are statistically distributed among a number of rotational levels. Coupling of rotational molecular motion with vibrational motion can occur, and thus, for molecules rotating with differing extents, the spacing between adjacent vibrational levels can change very slightly.[16] As a result, a given absorption in the gas-phase infrared spectrum will exhibit a number of lines around a fundamental vibrational absorption position, corresponding to vibrational transitions for molecules in different rotational states. These absorptions, called rovibrational bands in the spectrum, can span a large wavenumber range, and although information regarding the structure of the molecule can be obtained, such spectra can be extremely complicated for larger molecules.

One of the benefits of isolation of a molecule in a rare-gas matrix is the immediate consequence that most molecules are held rigidly within the matrix environment, and thus, inhibited from rotational motion. Correspondingly, the coupling of rotational motion to vibrational motion is eliminated, and hence, the rovibrational lines in the spectrum disappear. An example of the simplification of the gas-phase and matrix-isolated spectra of H_2O and CO_2 is given as

Figure 2. Although some shifting and broadening occurs in the spectra, similar to that described in the UV-visible spectroscopy sections above, the resultant matrix-isolated infrared absorption spectra are very close to the fundamental absorptions that would be observed in the gas-phase infrared spectra. In some drastic cases, matrix isolation subtly distorts the geometry of the isolated molecule,[11,23] and thus significant deviations from the gas-phase are observed. However, the majority of molecules are not significantly distorted by matrix isolation.

While most rotational motion is inhibited in the matrix, small molecules, in particular small hydrides such as H_2O, can exhibit rovibrational spectra in rare-gas matrices.[24] However, the low temperatures of the matrix-isolation environment significantly reduce the available thermal energy, lowering most molecules into only those rotational levels very close to the rotational ground state. Generally, no more than the first five rotational levels can be populated significantly, and thus, rovibrational spectra are quite compact compared from the gas-phase spectra. Additionally, changes in the host gas used for matrix isolation can completely inhibit the observed rovibrational lines, leading to absorptions representative of the gas-phase fundamentals.[25]

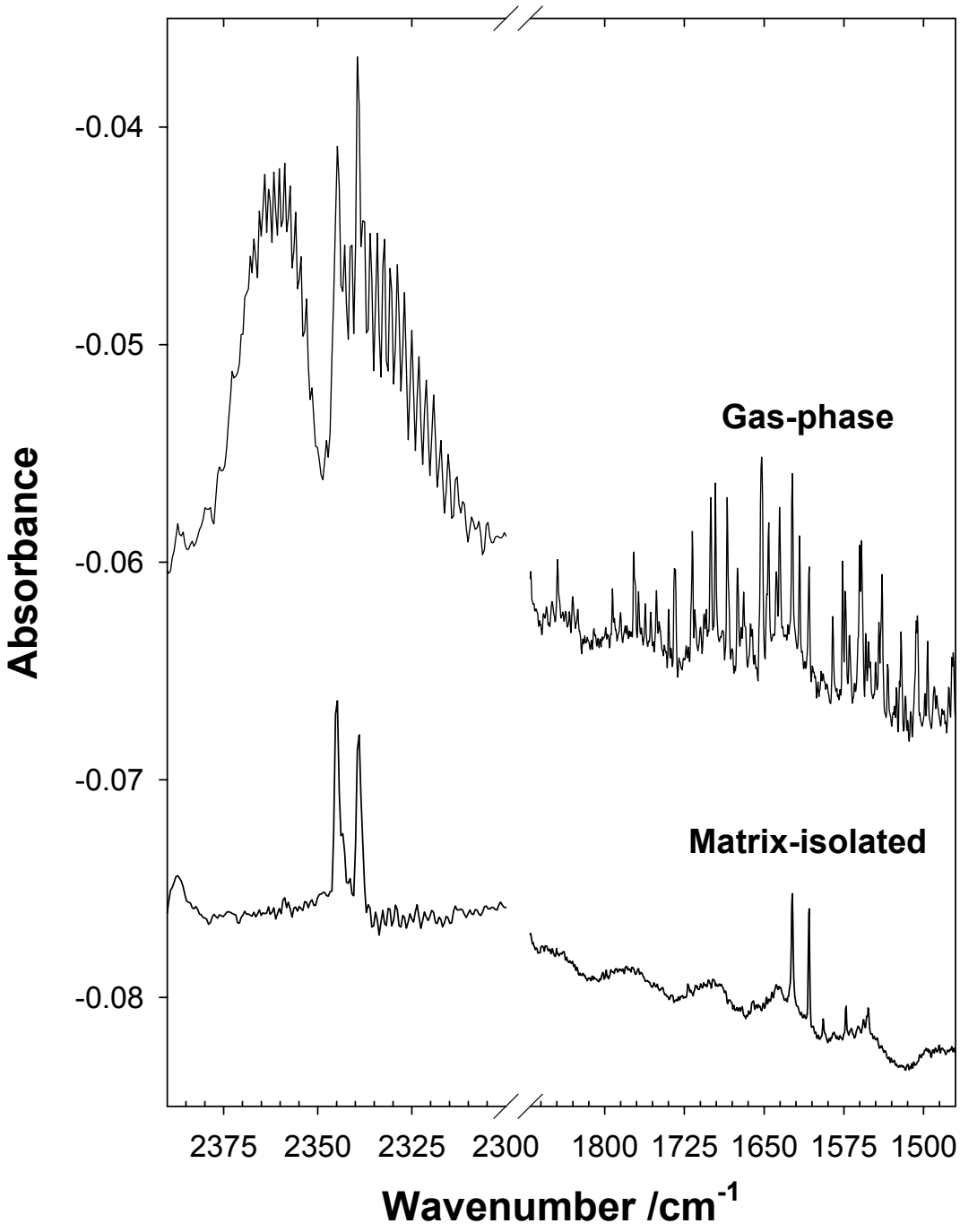

Figure 2: Comparison of portions of the gas-phase and matrix-isolated infrared absorption spectra of CO_2 (left) and H_2O (right).

1.4 General introduction to basic organometallic chemistry

As the major chemistry observed in these studies arises from the reactions of metal atoms with simple alkenes and small inorganic molecules, it is useful to consider some general concepts which will occur as themes within the context of this work. Thus, a few simple considerations of basic organometallic reactions are given here, for introduction. More extensive and complete introductions to this material can be obtained from the works of Crabtree,[1a] and of Cotton and Wilkinson.[1b]

The first row transition series can be broken into two groups: the left side of the d-block (Sc-Mn) is known as the early transition metals, and the right side of this group (Co-Cu) are considered the late transition metals. However, even this classification is somewhat broad, as the region from Cr-Co can behave as either early or late metals, in some cases. In general, the two groups of species differ in their reactivity because of the gradual increase in nuclear charge (Z) that occurs from the left to ride side. This increase in Z is balanced, but incompletely shielded, by electrons in d-orbitals. These d-orbital electrons do not significantly penetrate into the nucleus, and thus, the changes in nuclear charge (or effective nuclear charge, Z_{eff}) among the d-elements result in significantly different reactivity for species involving transition metal atoms. Since these species can be considered as nuclei that have an "excess" nuclear charge, the donation of electrons from other chemical species, leading to coordination of a group at the metal nucleus, is one of the most common types of chemistry. Thus, chemical species having non-bonding electrons, or those species possessing π-electrons,

can donate the excess electron density into the metal atom, forming coordination bonds. Even loosely associated electrons shared between multiple nuclei in a molecule can be shared with the metal nucleus, introducing multi-centre, multi-electron coordination. In such a way, π-containing groups such as ethene or benzene can donate an entire π-bond network to associate with a metal atom. This concept, where multiple nuclei are bonding with a single coordination site on a metal atom is known as hapticity, and is symbolized with η^k, where k is the number of nuclei coordinated to a single site on the metal nucleus. As an example, the donation of the π-bond from ethene into a metal, forming a metal-ethene coordination complex, would be symbolized M(η^2-C_2H_4) and for benzene, M(η^6-C_6H_6). The bonding arising from hapticity can be substantially weaker than a classically covalent bond, and as a result this type of coordination chemistry can be very interesting.

In their ground states, the gas-phase first-row transition series atoms (with the exception of Cr and Cu) have a full 4s valency, and since the LUMO orbitals are protected by the 4s shell, these species behave much like noble gas atoms. As a result, many interactions of these atoms with collision partners are repulsive in the gas-phase, and as such, the atomic species can be relatively inert.[26] Generally, to the neutral atom, only those coordinating species which have “hard” lone pairs,[1] such as H_2O, can penetrate the outer shell, interacting with available d-orbitals, and leading to ground-state chemistry. By comparison, the soft electron cloud of a π-bond may not penetrate the hard 4s-shell, and thus only

weak hydrogen-bonded or van der Waals complexes with the ground-state metal atom are possible.

The repulsion associated with the outer 4s shell of the transition metal atoms can be overcome by oxidation of the 4s electrons. The partially occupied interior d-orbitals then become exposed. Correspondingly, the transition metal atom can become significantly more reactive, and the availability of empty low-lying orbitals can have significant chemical consequence. Some metal atoms will react with another molecule, cleaving a bond, and formally inserting the metal atom into one of the sigma bonds of the coordinating species. The addition of a molecule to the metal atom in this way, which results in the formal removal of the s-electrons, is known as an 'oxidative addition'.[1] Additional reactivity of the transition metal complex can occur, and in some cases, species bonded to the metal centre can be expelled from the complex, returning the oxidized electrons to the metal in a process known as a reductive elimination.[1]

For transition metals reacting with alkenes, a primary reaction involves the metal inserting into one of the C-H bonds of the alkene. This activation of the relatively strong C-H bond by a transition metal is a special case of oxidative addition which is observed in a number of cases throughout this work.[1] Special cases of reductive eliminations are also suspected in later chapters of this work, specifically for cases when metal centres involve a number of coordinated groups where one or more M-H and M-R (R= alkyl) bonds are present. In these species it is often thermodynamically and kinetically viable for elimination of H_2 or R-H from the metal centre. Generally, as the metal becomes more saturated by

coordinating partners, these eliminations become more and more viable.[1] However, when saturation of coordination spots is minimized, the elimination is less feasible, and the addition product is a little lower in energy than the elimination product. The reactivity can be understood by considering factors involving orbital overlap, or relative M-H/M-R and R-H bond strengths. Since the addition and elimination products can be similar in relative energy, the barriers for the associated inter-conversions are sometimes small. However, these barriers are frequently only the endothermicity of the reaction, and thus these types of reactions can often occur quite readily.

Although a great deal of additional information could be provided as background for organometallic chemistry, these ideas will represent the basis for understanding the mechanistic proposals in the reaction of V with ethene, and with water that will be presented in the following chapters.

1.5 References for Chapter 1

[1] See for examples: a) *The Organometallic Chemistry of the Transition Metals*, 4th Ed, Crabtree, R.*;* John Wiley & Sons, Inc.: Hoboken, NJ, **2005**. b) Cotton, F.A.*;* Wilkinson, G.*; Advanced Inorganic Chemistry,* 5th Ed.; Wiley, New York, **1988.**

[2] Parnis, J.M.; Escobar-Cabrera, E.; Thompson, M.G.K.; Jacula, J.P.; Lafleur, R.D.; Guevara-Garcia, A.; Martinez, A.; Rayner, D.M. *J. Phys. Chem. A.*, **2005**, 109, 32, 7046.

[3] Whittle, E.; Dows, D.A.; Pimentel, G.C.; *J. Chem. Phys.*, **1954**, 22, 1943.

[4] Andrews, L.; *J. Chem. Phys.*, **1968**, 50, 4288.

[5] Andrews, L.; Pimentel, G.C.; *J. Chem. Phys.*, **1961**, 44, 2361.

[6] Andrews, L.; Pimentel, G.C.; *J. Chem. Phys.*, **1967**, 47, 3637.

[7] Perutz, R.; *Chem. Rev.*, **1985**, 85, 97.

[8] Frei, H.; Pimentel, G.C.; *Ann. Rev. Phys. Chem.*, **1985**, 36, 491.

[9] Fridgen, T.D.; Parnis, J.M; *J. Phys. Chem. A.*, **1997**, 101, 5117.

[10] See for example: Dunkin, I.R.; *Matrix Isolation Techniques*, Oxford University Press, New York, **1998**.

[11] See, for example: Moskovits, M.; Andrews, L.; *Chemistry and Physics of Matrix Isolated Species,* Elsevier, New York, **1989**.

[12] See, for example: Turro, N.J.; *Modern Molecular Photochemistry*, University Science Books, California, **1991**.

[13] See, for example: Balzani, V.; Carassiti, V.; *Photochemistry of Coordination Compounds*, Academic Press, New York, **1970**.

[14] See, for example: Herzberg, G.; *Atomic Spectra and Atomic Structure,* 2nd Ed., Dover, New York, **1944**.

[15] Moore, C.E.; Circ. U.S. Natl. Bur. Stand., 467, 1, **1947**.

[16] See, for example: Hollas, J.M.; *Modern Spectroscopy*, 3rd Ed., Wiley, New York, **1998**.

[17] See, for example: Wilson, E.B. Jr.; Decius, J.C. and Cross, P.C.; *Molecular Vibrations: The Theory of Infrared and Raman Vibrational Spectra*, Dover, New York, **1980**.

[18] See, for example: McQuarrie, D.A.; *Quantum Chemistry*, University Science Books, California, **1983**.

[19] See, for example: Silverstein, R.M.; Webster, F.X.; Kiemle, D.J.; *Spectrometric Identification of Organic Compounds*, 7th Ed., Wiley, New York, **2005**.

[20] See, for example: Lin-Vien, D.; Colthup, N.B.; Fately, W.G.; Grasselli, J.G.; *The Handbook of Infrared and Raman Characteristic Frequencies of Organic Molecules*, Academic Press, New York, **1991**.

[21] See, for example: Nakamoto, K.; Infrared and Raman Spectra of Inorganic and Coordination Compounds, Part A, B., 5th Ed., Wiley, New York, **1997**.

[22] Herzberg, G. *Infrared and Raman Spectra of Polyatomic Molecules*, Van Nostrand Reinhold Company: New York, **1988**.

[23] Moskovits, M.; Ozin, G.A. (eds), *Cryochemistry*, Wiley: New York, **1976**.

[24] Ayers, G.P.; Pullin, A.D.E.; *Chem. Phys. Lett.*, **1974**, 29, 604.

[25] Tursi, A.J.; Nixon, E.R.; *J. Chem. Phys.*, **1970**, 52, 1521.

[26] Weisshaar, J. C.*; Acc. Chem. Res.*, **1993**, 26, 213.

Chapter 2

Review of transition metal reactivity with hydrocarbons: theory, gas-phase and matrix-isolation studies

2.0 Overview of transition metal chemistry

A great deal of research concerning the chemistry of the elements in the transition series has already been explored, and as such, the resulting literature is expansive. As one moves from group to group within these elements, the chemistry can change dramatically, as a result of the increase in nuclear charge and the increase by a single valence electron. Even localizing within a specific group, moving down that series of elements can result in wild variations in reactivity with respect to a certain molecule. Additionally, the high degeneracy of the orbitals on the metal atoms leads to many low-lying electronic states, with each configuration representing a unique chemical species. Thus, it is quickly evident as to why the chemistry of the transition series has been so widely studied, and fortunately, various themes which help to understand the overall chemistry do occur within these chemicals. Generally, the predominant factors explaining the chemistry are attributed to either orbital occupancy, or electronic configuration.[1,2] By considering the chemistry within each of these contexts, it is

possible to understand, and predict a great deal of the reactivity of the transition series. Collected works such as Cotton and Wilkinson's *Advanced Inorganic Chemistry* represent excellent references toward understanding this diverse area of chemistry, and localizing from the vast array into a specific topic area.[3]

2.1 Transition metal chemistry with hydrocarbons

Of the large body of work considering transition metals, the reactions of these species with hydrocarbons is an interesting subsection, spanning areas of catalysis, petrochemistry, and even photochemistry. Although much of the work occurs in solution, some of the studies do involve transition metal reactions in the gas-phase. A multitude of examples of metal + hydrocarbon reactions exist, for which those focusing on alkenes represent reactions bearing the most relevance to this work. Thus, in further consideration, work involving alkenes, and in particular ethene (C_2H_4), will represent the primary focus. These gas-phase studies represent the best starting points when trying to understand mechanistic aspects of chemical processes, which is the target of the current work. A general introduction to this area is summarized by Weisshaar in an account of the reaction of transition metal atoms, and atomic ions, with hydrocarbons.[4] Considerably more work has been performed on transition metal ions, rather than the corresponding neutrals, since the ions are easier to manipulate, and it is easier to detect their associated products. Furthermore, the metal ions are significantly more reactive in most cases. A comparison summary of neutral metal, and metal singly and doubly charged species is given by Weisshaar. The conclusions of the work state that: M^{n+} + hydrocarbons systems exhibit

significant ion-molecule polarization effects, leading to enhanced reactivity of metal ions when compared to neutral metal atoms. However, the ion-hydrocarbon chemistry in the gas phase is somewhat unrepresentative of corresponding solution-phase chemistry, and also ion-hydrocarbon chemistry is significantly different than corresponding neutral metal-hydrocarbon chemistry. Weisshaar further points out that, since ions in solution are effectively charge-neutralized due to their solvation, in order to further understand solution-phase transition metal chemistry, gas-phase reactions focusing on neutral metal atoms are best representative. As an additional benefit to working with gas-phase systems, the simplicity of solvent-free environments allows for complementary computational investigations, to help identify unknown products.

2.2 Computational investigations of metal atoms with ethene

The application of computations to understanding the chemistry of metal atoms with various species is extensive. One review for computational studies of the first row of transition metals, focusing primarily on hydrides, halides, metal dimer and trimer chemistry was given by Langhoff and Bauschlicher.[5] Another comprehensive review of computational investigations of major organometallic reactions was given by Niu and Hall in 2000.[6] This work represents a more recent and exhaustive summary of the computational investigations for small to very large transition metal complexes, and even includes references where investigations have been made for reactions of transition metal atoms, specifically with ethene. These particular references represent the most critical for analysis of the results of the current work, and thus some exploration of these

particular results provides a good framework for understanding the experimental results in context.

One major investigation involves the activation of the prototypical C-H bond of methane with each of the transition metals of all three rows.[7] This investigation, focusing on the comparison of some computational methods, concludes that the B3LYP method is suitable in most cases for predicting systems involving transition metals. More importantly for understanding reactivity, the study rationalizes the trends in the reactivity of each of the rows in terms of factors such as: a) orbital size and orbital overlap with orbitals on an incoming reagent, b) losses in exchange stabilization energy of the atom following C-H bond insertion, and c) the energy required to promote the ground state atom to a favourable electronic configuration conducive to the reaction. Such predicted trends are in excellent agreement with experimental work by Armentrout and coworkers, for reactions of transition metal ions with H_2[8,9] and simple hydrocarbons.[10] These complementary experiments also suggested the importance of favourable electronic configuration, and orbital availability when explaining the observed reactivity.[1,2] That the calculations for the activation of the simplest C-H bond of a hydrocarbon by neutral metal atoms predict the same factors that explain metal ion reactivity strengthens all of the arguments claiming that these factors are the major contributions in metal reactivity with hydrocarbons. As a result, it is quite important to understand the predictions offered by these calculations, for the transition metals, in great detail. Such

factors can then be generalized when understanding the reactivity of the metals with other C-H containing species.

For the first row series, the insertion of the metal atoms into a C-H bond of CH_4 is predicted exothermic for all but Cr, Mn, Fe, and Co, and in the other rows the insertion is exothermic for all metals save only Mo, Re, and Os. Unlike the second- and third-row transition series, the chemistry of the first row is somewhat unique, since the size of the 3d orbitals is smaller than the valence 4s shell, and the corresponding orbital energy values are very different. As a result, these large energy differences in the 3d and 4s orbitals result in large promotion energies from ground state $3d^x4s^2$ configurations to $3d^{x+1}4s^1$. As the $4s^2$ shell is fully occupied, repulsive interactions between incoming reagents and metals having this component of their electron configuration can often be present. Thus, in order for these metals to react with incoming reagents, mixing with the $3d^{x+1}4s^1$ electronic configuration is necessary, resulting in a reduction of the repulsion from the full valence shell. Additionally, the small d-orbital size restricts the degree of orbital overlap with incoming reagents, limiting stabilization of complexes through bonding interactions. Comparing directly with the heavier metals, such disparity between the size and the energy of the corresponding d and s shells is not as large. Thus, the corresponding promotion energies necessary to reach non-repulsive electronic configurations are lower, giving rise to apparently enhanced reactivity of these species when compared to the lighter transition metals.

The importance of the promotion energy of the ground state atoms is confirmed when comparing the associated barrier heights for C-H bond activation in CH_4. All of the transition metals, excepting only Rh, require some activation energy to C-H bond insertion for methane. In general, the activation barriers show a decrease from the first to the third transition series. Additionally, within each series, the barriers decrease from Group 3 to Group 5, maximize from Group 6 to Group 8, and then decrease through to group 10. These trends correlate exactly with those elements suffering from the largest loss of exchange stabilization energy, following the pairing of electrons to form new M-H and M-C bonds, in all cases. A plot of the relative exchange stabilization energy for the first row transition series is given as Figure 3, to demonstrate the relative magnitude of exchange stabilization energy among these elements. These values have been normalized with respect to the largest stabilization energy in the period, for easy comparison. The strong correlation of loss of exchange stabilization energy with the predicted reactivity makes this an excellent starting point for understanding the reactivity of metals inserting into a C-H bond. Thus it would seem reasonable to conclude that these results could be generalized to understanding the C-H bond activation in other hydrocarbons, as well.

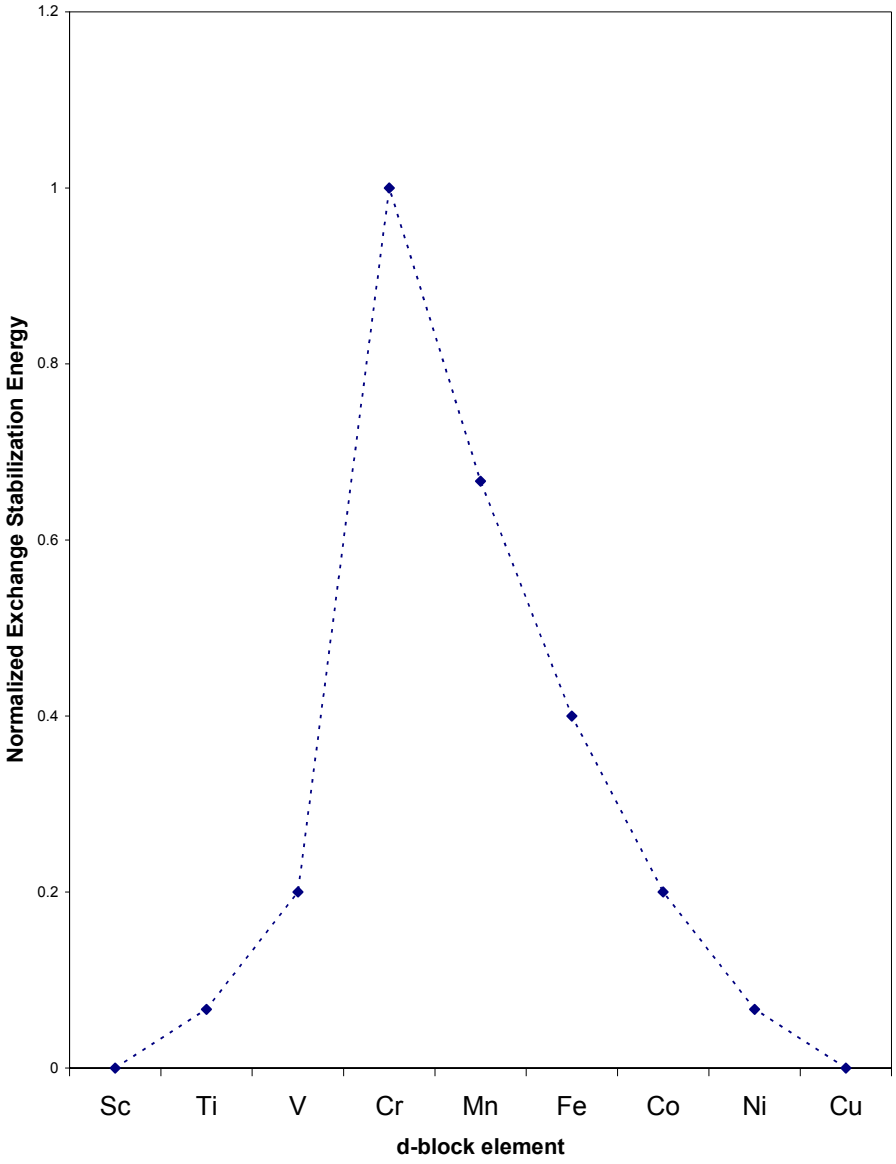

Figure 3. Plot of the relative exchange stabilization energy for the first row transition series. These values are normalized to the largest exchange stabilization energy of this series for easy comparison. The elements Cr, Mn, and Fe benefit most from the exchangeability of unpaired electrons, making these elements most resistant to bond formation, as such requires electron pairing.

An *ab initio* investigation of the insertion of second row metal atoms into the C-H bond of ethene has also been performed by Siegbahn and coworkers.[11] In this work, results are presented that give a detailed comparison with the previous C-H bond activation of methane by these metals,[11] and additionally, a previous investigation of the strengths of ethene complexation reactions (M + C_2H_4 → M(η^2-C_2H_4)) for each of the metals studied.[12] When compared to the insertion of the metal into the C-H bond of methane, each of the metals studied is predicted to be approximately 5-10 kcal.mol^{-1} more stable for insertion into the C-H bond of ethene. As was previously the case, the middle transition elements (Mo-Ru) have the least exothermic reactivity, due to losses of exchange following the pairing of electrons to form the insertion product. Additionally, each metal studied, excepting only Rh, has a corresponding barrier to C-H bond insertion by the metal. These values decrease from the left to right of the periodic table, ranging from 15 kcal.mol^{-1} to near 0 kcal.mol^{-1}. The only exceptions are the previously mentioned cases of Mo and Tc where the barriers maximize at 30 kcal.mol^{-1}, corresponding with the largest loss of exchange stabilization energy. Interestingly, in all cases excepting those where exchange energy loss is maximized, the π-complexation energy released in the reaction M + C_2H_4 → M(η^2-C_2H_4) is exothermic, in spite of the fact that no early metal complexes of this type have been observed. Furthermore, only in the case of Zr is the insertion product, H-Zr-C_2H_3 predicted to be more stable than the corresponding metal π-complex, and even in this case, the insertion product is more stable only by 1.2 kcal.mol^{-1}. Thus, unless additional impediments in the reaction following the

insertion product formation were to be present, such as the efficient removal of the H-M-C_2H_3 species by a competitive reaction, the back-reaction leading to the M(η^2-C_2H_4) complex would almost always be expected to readily occur.

The reactivity of M-H bond containing species with additional ethene molecules has also been investigated by Siegbahn. In particular, the insertion of an ethene into M-H bonds of second row metal atoms containing up to three M-H bonds,[13] and also a comparison of the relative reaction efficiency of ethene insertion into M-H and M-C bonds of prototypical organometallic species have been investigated.[14] In the former work, the reaction of MH_x, (x=1-3) with C_2H_4 is studied. Particular emphasis is placed on the energies required for π-coordination of the C_2H_4 unit to the MH_x species forming (η^2-C_2H_4)MH_x, and the subsequent barriers and reaction energies following ethene insertion into an M-H bond to form $MH_{x-1}(C_2H_5)$. In the case of MH, π-coordination of ethene is only exothermic for Y-Nb, and Rh. By comparison, for MH_2, the π-complexation reaction is exothermic for all of the metals of the second row, and in the case of Zr, Nb, Mo, Tc, and Ru for MH_3. No bound states of C_2H_4 for M = Y, Rh or Pd were found with MH_3. For the case of olefin insertion into the M-H bond of the MH_x species, barrier heights for the direct insertion reaction $MH_x + C_2H_4 \rightarrow MH_{x-1}C_2H_5$ only exist in the case of the MH species, while for MH_2, the reaction is barrierless for all metals save Mo and Tc. For the MH_3 species studied, the direct insertion is completely barrierless for all metals. If, instead, the same insertion reaction is considered following π-coordination of ethene to the MH_x species, i.e. $MH_x(\eta^2\text{-}C_2H_4) \rightarrow MH_{x-1}(C_2H_5)$, reaction barriers are predicted for the

insertion of ethene in the case of ALL metal hydride species. However, for all of these cases, the release of energy following π-complexation to the metal hydride in the gas-phase would be sufficient to overcome the reaction barrier, ultimately leading to the thermodynamically favourable alkene insertion product in all cases. Thus, in experimental cases where alkene insertion were observed, it might not be possible to determine if the mechanistic route were π-coordination of ethene, followed by alkene insertion into the M-H bond, or the alternative direct alkene insertion into the M-H bond, without a prior π-coordination step.

The reactivity of ethene with second-row transition metal complexes containing simultaneous M-H and M-C bonds has also been investigated by Siegbahn.[14] In particular, the investigation focuses on the competition between ethene insertion into the M-H bond, versus the corresponding insertion into a M-CH_3 unit. Ultimately, the calculations predict that energy barriers exist for ethene insertion in all cases, however, for the insertion into M-H bonds, the barriers are generally 10-20 kcal.mol^{-1} lower. The presented results are rationalized based on the bonding of the M-H and M-CH_3 units, for which the overlap of the CH_3 group in the M-CH_3 bond is significantly more directional than the overlap of the spherical 1s orbital of the H unit. As a result, in order to insert ethene into the M-CH_3 bond, the bond must be almost entirely broken, prior to alkene insertion. In the M-H case, such directionality factors are absent and thus, insertion into the M-H bond is kinetically more facile. However, it is worth noting that, these comparisons are made for M-CH_3 and M-H bonds on H_2M-CH_3 and MH_3 species, respectively. They are not comparisons of the relative insertion into the M-H or

M-CH_3 bonds on H_2M-CH_3 directly. However, the chemistry of the impact of an $H:^-$ or $H_3C:^-$ ligand on the metal could be considered quite similar, and thus, the same trend might be expected for an internal comparison of an alkene insertion into the M-H or M-CH_3 bond. That the $H_3C:^-$ group could be considered similar to $H:^-$ might also then predict that other similar ligands such as $HO:^-$ or $H_2C{=}HC:^-$ might merely represent other cases that function like pseudo "$H:^-$" ligands. Hence the reactivity of MH_2 and MH_3 species with respect to alkene insertion could serve as models for understanding the chemistry of H-M-OH or H-M-C_2H_3 species. Correspondingly, these computational investigations would serve as benchmarks for predicting and understanding C_2H_4 insertion for simple metal-hydride species that bear additional ionic coordinated ligands.

Throughout these comparisons Siegbahn highlights an additional point that, in spite of thermodynamically favourable bound states for both the π-coordinated ethene, and the metal vinyl hydride, equilibrium mixtures of these two species have rarely been observed experimentally.[13] Such an observation suggests that it is possible that these two species are not actually linked on the potential energy surface. This statement has also been made by George,[15] who sites a number of cases in his review of transition metal complexes activating the C-H bonds in alkenes and alkynes, where initial π-coordination of the ethene is not a likely reaction step. However, it is not entirely clear whether such sweeping statements can be made that π-coordination is, or is not, the initial step leading to C-H bond activation in every case. The only clear statement seems to

be that the thermodynamic product is the π-coordinated ethene on the metal, while the metal vinyl hydride product appears to be a kinetic product.

Subsequent to these works, most theoretical investigations in this area have been presented in combination with experimental work, instead of being presented as solely theoretical investigations. As a result, such investigations are presented later with their corresponding experimental data. However, the most recent investigation of metal atom C-H bond insertion comes from the work of Rivalta *et al*., studying the dehydrogenation reaction of ethene by Nb or Nb^+.[16] Focusing only on the Nb atom, the first step in the reaction is the π-coordination of the ethene molecule. For the ground state Nb atom, which has a ^6D configuration, π-coordination of ethene is the only thermodynamically favourable step. The subsequent C-H bond insertion has a barrier of approximately 27.9 $kcal.mol^{-1}$ on the sextet surface, which exceeds the -18.3 $kcal.mol^{-1}$ complexation energy released for ^6D Nb coordinating an ethene molecule. The ^4F Nb excited state, however, is reactive with ethene to π-coordinate, and with retention of the internal energy, the reaction can proceed through two C-H bond insertion steps spontaneously, ultimately liberating H_2 to form $Nb(\eta^2\text{-}C_2H_2)$ as the major product. By comparison of the quartet and sextet Nb atom surfaces, if the complexation energy of the sextet Nb atom and ethene were preserved, these species could also proceed through to H_2 elimination following an intersystem crossing from the sextet to quartet surfaces. Such interconversions between two-spin state surfaces of this type are possible, and have been previously explained by Armentrout.[1,2] However, experimentally, these interconversions require

substantial time to allow for the spin interconversion to the excited state surface to occur. Additionally, it is worth pointing out that, although the quartet surface represents the first excited state of the metal atom, photoexcitation to this surface requires a change in spin, which is expressly forbidden by selection rules for atomic excitation.[17] Nevertheless, if such a molecular complex were prepared on the sextet surface, and if the complex were sufficiently long-lived, spin interconversion could result in direct H_2 liberation. Whether or not such an interconversion will occur could only be determined by performing the experiment. Therefore, it is both necessary and useful to explore work in the area of gas-phase reactions that involve metal atoms and hydrocarbons.

2.3 Gas-phase transition metal reactions with hydrocarbons

Although gas-phase studies represent valuable information, still relatively few experimental studies of gas-phase transition metal atoms with hydrocarbons exist, and some only involve the study of atoms in tandem with metal atomic clusters.[18] As noted previously, the difficulty in manipulating and subsequently detecting the products of atomic metal centres inhibits their direct gas-phase study. Most recently, Parnis and coworkers have studied the reaction of Nb clusters of up to 25 constituent atoms with ethene, using a fast-flow reactor and time-of-flight mass spectrometry for indirect measurement of kinetic rate constants. In the context of their work, even the single Nb atom is shown to react spontaneously with up to six ethene molecules, leading to products consistent with loss of up to five H_2 units. Complementary DFT calculations for the first Nb/ethene reaction steps are in agreement with the loss of H_2, and predict the

formation of a coordinated acetylene molecule on the metal. As the method of detection in these experiments provides information on the mass of the products only, no further insights into the mechanistic steps was possible, other than the statement that multiple metal C-H bond insertion steps must occur.

Dehydrogenation reactions involving Y atoms and C_2H_2 have been investigated computationally by Glendening.[19] Exothermic reaction pathways are predicted for π-coordination of the acetylene group, and steps through to C-H bond insertion by the ground-state Y atom to form H-Y-CCH as a stable product, compared from Y + C_2H_2, are predicted. Based on these calculations, the only thermodynamically favourable pathway to hydrogen elimination involves the elimination of H_2 via 1,3-elimination of the H-Y-CCH product, to form YC_2 and H_2. Pathways in which multiple C-H bond insertions occur prior to elimination of H_2 are otherwise extremely endothermic. A similar computational and experimental investigation of ground state Y with ethene (C_2H_4) and propene (C_3H_8) has been conducted by Porembski and Weisshaar.[20] Their experiments involve the reaction of the metal with ethene in a fast-flow reactor system, characterized by time-of-flight mass spectrometry. The major products of the Y + C_2H_4 experiments are Y(η^2-C_2H_2) and H_2. Calculations involving stepwise C-H bond insertions, followed by H_2 elimination, have intermediate potential energy barriers above the available thermal energy at the steps leading to $H_2Y(C_2H_2)$, which suggest the reaction should not occur under their experimental conditions. That $Y(C_2H_2)$ is observed as a major product leads to the consideration of other H_2 elimination pathways. One elimination channel in which the H-Y-C_2H_3 molecule

directly eliminates H_2 by 1,3-elimination using an H from the vinyl group is shown to be possible under the experimental conditions. Thus, this pathway is rationalized as the hydrogen elimination channel, as a means of explaining the observed dehydrogenation. The elimination channel does have a very small energy barrier at the initial C-H bond insertion step, and correspondingly, when C_2D_4 is used, both $Y(C_2D_4)$ and $Y(C_2D_2)$ products are observed, reflecting the kinetic isotope effect. Thus, the conclusion that hydrogen elimination can occur via 1,3-elimination at a metal centre is quite reasonable.

A similar computational study involving Zr reactivity with ethene in the gas-phase was performed by Porembski and Weisshaar,[21] as was a complementary experimental study for Zr and Nb by Willis *et al*.[22] In the former case, the reaction of Zr with C_2H_4 parallels the reaction of Y with C_2H_4 quite well. However, H_2 elimination channels following multiple C-H bond insertions by Zr, or the direct H_2 formation via 1,3-elimination from $H\text{-}ZrC_2H_3$ are both predicted to be below the available internal energy for the system under ambient conditions. Complementary isotopic experiments are consistent with both H_2 elimination channels being active in the case of Zr + C_2H_4 in a competitive fashion. As an experimental comparison the results of Willis *et al*.[22] for Zr and Nb show experimental evidence for initial C-H bond insertion, following pickup of the C_2H_4 unit by either metal atom. For the two metals, both Zr and Nb give the same products, although, Nb is shown to be more reactive. The additional reactivity is attributed to the Nb $5s^1$ outer shell, allowing better initial coordination of the ethene, compared from that of Zr which is $5s^2$, and significantly more repulsive

for the initial coordination. In both cases, the results conclude that H_2 elimination is effected following formation of a metal ethene coordination complex, and subsequent C-H bond insertion reactions. Their calculations do not explore a 1,3-elimination channel, however, comparison of the structures of their reaction profiles with those corresponding to Zr and Y in the above works strongly suggests that 1,3-elimination channels of H_2 from H-M-C_2H_3 would be favourable in both M = Zr and Nb cases, as well.

Previously, the reaction of Zr and ZrO with sequential addition of C_2H_4 or C_3H_8 units had been studied by Wen and coworkers in the Weisshaar group.[23] In this work, the reaction of Zr + C_2H_4 yields Zr(C_2H_2), as detected by time of flight mass spectrometry, but no evidence for a Zr(C_2H_4) species is obtained. Sequential addition of C_2H_4 yields products that are consistent with additional H_2 loss, such as Zr(C_4H_4) (*i.e.* Zr(C_2H_2)$_2$). When propene (C_3H_6) is used in place of ethene, the same hydrogen liberation is observed, and Zr(C_3H_4) and masses consistent with Zr(C_3H_4)$_2$ products are observed. The only sticking point in this work surrounds the possibility that the ionization laser which ionizes the product molecules for detection in the time-of-flight mass spectrometer could result in the photoinduced elimination of H_2 from the resultant cation. However, their results suggest that there should be a mixture of the unobserved Zr(C_2H_4) and Zr(C_2H_2), while only ionized products consistent with neutral formation of Zr(C_2H_2) are observed. In light of the later postulated 1,3-elimination of H_2 by the other groups, the neutral formation of Zr(C_2H_2) is highly likely by that mechanism.

Additional experiments determining effective rate constants for the reactivity of the first,[24] second,[25,26] and part of the third row[27] of transition metal atoms with small hydrocarbons have also been explored. These experiments were performed using fast-flow tube techniques, monitored using laser induced fluorescence, and time-of-flight mass spectrometric detection of photoionized neutral products.

In the case of the first row metal atoms, none of the ground-state metal atoms were found to react significantly with ethene, with the exception of Ni. In the case of Ni, the first excited state configuration is only 200 cm^{-1} above the ground state, a level which is thermally accessible under ambient conditions. Thus, since Ni is the only element to have this low-lying excited state, the reactivity of Ni is most likely due to the excited state configuration (Ni: $^3D\ 3d^9 4s^1$) rather than the ground state configuration (Ni: $^3F\ 3d^8 4s^2$). When larger alkenes (propene, or butene isomers) were used, only the early transition metals (Sc-V) demonstrated reactivity, in addition to Ni. The metals Cr-Co and Cu were found to be unreactive with almost all of the reagents studied. In most cases, the lack of reactivity with alkenes results from the repulsive M alkene interaction at long distances, due to the closed 4s outer shell, and the inability of the alkene to reach the comparatively small, vacant d orbitals for coordination. For the particular cases of Cr-Co, combinations of 4s repulsion, and d-electron repulsion toward complexation of an incoming reagent are dominant factors, since in addition to the 4s shell, these metals all have sufficient electrons to at least partially occupy all d-orbitals. Furthermore, for bond insertion reactions, these

species suffer the most from loss in exchange stabilization energy, unlike the early metals, or the later metals. In cases where reactivity was observed, observed products following photoionization are consistent with loss of H_2 from the M + alkene reaction product. However, the nature and energy of the ionization is such that, it was possible that such products resulted from M^+ + alkene chemistry following photoionization of metal atoms, induced by multiphoton absorptions of metal products in the ionization region. Nevertheless, many of the results seem consistent with the initially formed products as metal alkene complexes, or products resulting from C-H bond insertions by the metal.

While no evidence of the exact products of metal atom reactions with hydrocarbons was determined, this postulation of the initial product as an M(η^2-C_2H_4) species is supported by the observation of an inverse kinetic isotope effect when a deuterated hydrocarbon is used. This inverse isotope effect suggests the formation of a M(alkene) complex as the initial product giving rise to M atom depletion, since products arising from direct C-H bond insertion should show significant kinetic isotope effects when C-D insertion would be the analogous step. Thus, the reaction of alkenes with the first row transition metals seems to suggest that, at least for larger alkenes, the early transition metals (and Ni) are most reactive. In all cases, these species are those that have the lowest energy differences to accessing $3d^{x+1}4s^1$ configurations, with minimized losses in exchange stabilization energy, relative to the ground state $3d^x4s^2$ configurations.

The reactions of Ni,[28] Fe,[29] and Cu[30] with ethene have also been previously investigated. In each of these cases, the major findings suggest the

presence of initially formed M(alkene) complexes, although very slowly for the case of Fe and Cu. Otherwise, no significant deviations from the chemistry observed previously are presented, with the exception that for Cu, multiple alkene units can be coordinated, leading to Cu(alkene)$_n$ [n>1] species.

By comparison, the second row transition metals show dramatically increased reactivity with ethene, compared from the first row.[25] With the exception of Mo and Ag, the entire second row reacts with C_2H_4, while Nb is the most reactive. However, slow reactivity of Mo with C_2H_4, likely producing an a weakly bound Mo(η^2-C_2H_4) complex has been previously observed in kinetics measurements by Lian and coworkers.[31] Such work, which also studied the reactivity of Mo_2, showed the dimer to be inert to C_2H_4 reactivity. Zr, Nb, Ta, their corresponding diatomic oxides, and MoO have also been studied for reactivity with C_2H_4 using flow tube kinetics analysis by Parnis and coworkers.[32] In this work, surprisingly similar reactivity between M and MO is observed in most cases. The results also conclude that the initially formed products are those involving π-coordination of ethene to the metal atom or oxide, which may be followed by one or more C-H bond insertions, and subsequent H_2 elimination, analogous to results observed for reactivity with alkanes.

The calculations performed in the Weisshaar[25] work do suggest exothermic π-coordination of ethene for all of the second row metals, although some metals require spin interconversions to reach bound M-alkene complexes. In contrast with the first row metals, many of the ground state second row metals have outer $5s^1$ configurations, excepting only Y and Zr ($5s^2$), and Pd, which has a

$5s^0$ configuration. Additionally, the energies and sizes of these orbitals are much closer than in the first row, and thus, the enhanced reactivity of these species with ethene is likely due to combinations of these factors. Following complexation, Nb, and Rb-Pd are all predicted to be barrierless to the insertion of the metal into the C-H bond of ethene, forming H-M-C_2H_3 species, and for the other early metals the barriers are only predicted around 2 kcal.mol^{-1}. Mo and Tc show significant C-H insertion barriers, again, due to losses in exchange stabilization energy upon forming the two new M-H and M-C bonds. Nevertheless, for those species in which C-H bond insertion is favourable, continued insertion and resultant H_2 elimination is predicted to be spontaneous, although some species may not be able to proceed to H_2 elimination from an $H_2M(\eta^2\text{-}C_2H_2)$ species directly. However, the calculations do not include direct 1,3-elmination of H_2 from the H-M-C_2H_3 species, and since other works have strongly suggested this as a highly active elimination pathway, such conclusions may be false.

Finally, in the case of the third row, the reactivity with Hf, Ta, Ir, Pt and Au with ethene has been studied in fast flow kinetics measurements by Carroll and Weisshaar.[27] In these particular experiments, no information concerning the products are given, however, some results are consistent with metal atom and ethene π-coordination and C-H bond insertion products. More detailed analysis is required in these systems, in order to make further conclusions. However, the general results agree with the reactivity of metals in the second row, and each of these third row metals react with ethene under ambient conditions, excepting

only Au. As the interplay of the 5d, 6s, 6p orbitals is significantly more complicated in these systems, compared from the first row systems presented in this work, no further analysis beyond the comparison of alkene coordination and C-H bond insertion will be considered in these cases.

Returning to the chemistry of the first row, that these metals show reactivity only for cases where the electronic configuration of the metal species matches an excited state with $3d^{x+1}4s^1$, suggests that excited state metal atoms should spontaneously react in the gas phase. Relatively few examples of directly prepared excited state atom reactions with ethene are available. However, reactions of the first excited states of Ti (Ti: a^5F, $3d^34s^{1)}$ and V (V: a^6D, $3d^44s^1$) with ethene have been investigated.[33] In both cases, the high spin excited state atoms are quite reactive with C_2H_4, compared from the ground state atom. The rate constants measured in the study compare the hard sphere rate constant with the experimental rate constant for M + C_2H_4 reaction, i.e. $k_{hardsphere}/k_{exp}$, yielding ratios of 1 for excited state Ti and 4 for excited state V. This suggests that for Ti, the excited state would be reactive with C_2H_4 in every collision, while, for V, every fourth collision of ethene with the excited state V atom would result in reactivity. Using the obtained rate constants, the activation energy is calculated assuming Arrhenius behavior for the corresponding reaction, yielding E_{max} values of <0.2 kcal for Ti, and 0.8 kcal for V. Although no specific evidence of the products is given, the depletion of population from the $4s^2$ orbital in the excited state atoms opens the possibility of M(alkene) adduct formation, which may result in further chemistry, such as C-H bond activation as observed in other studies.

A further investigation of the V: $3d^4 4s^1$, a^4D state with C_2H_4 has been investigated by the Weisshaar group.[34] Excited state V atoms were efficiently prepared by stimulated emission of an initially photoexcited V atom. The resulting state is approximately 8500 cm^{-1} above the ground state, and cannot be directly accessed by photoexcitation due to parity restrictions, nor can the state relax to the ground state. When ethene is reacted with the excited state V atom, the rate constant for the reaction is approximately five times the rate constant for the previously investigated high spin excited state V atom. Thus, for this excited quartet state, the rate of reaction with ethene is approximately the expected hard sphere collision rate. However, the nature of the measurement on the excited state cannot distinguish between those collisions with ethene that lead to reactivity, and those which simply induce collisional deactivation of the excited state metal species. Similarly, no information about the excited state V and ethene reaction products is obtained in the study, however, a detailed description of the possible potential energy surfaces for these systems suggests that π-coordination of ethene, followed by C-H bond insertion is most likely.

Thus, the reactivity of ethene with transition metal atoms has been reasonably well characterized in the gas-phase, in spite of the paucity of experimental results. As most of the results which have been performed show only depletion of metal atoms, or give elementary information regarding the mass of the products, further analysis is required in all cases to understand the mechanistic aspects of the associated reactions. In response to this, additional studies employing the technique of matrix isolation infrared spectroscopy aimed

at characterizing the reaction products of metal atoms with ethene have been performed. These studies complement the gas-phase work, in many cases, providing useful insights into the reactivity of ethene with transition metal species.

2.4 Transition metal reactions with hydrocarbons in cryogenic matrices

Given the significance and importance of metal hydrocarbon reactions in areas such as catalysis, understanding mechanistic aspects of the reactivity of transition metal species with hydrocarbons has been of considerable interest. As a result, a variety of matrix isolation UV-visible and infrared studies have been performed in order to identify initially formed intermediates, and subsequently formed products. However, it is important to recognize that the matrix isolation technique is significantly different than studies which occur in the gas-phase, and thus, considerable efforts have been made to study the effects of the matrix isolation technique on the reagents under study. A detailed account of the chemistry and physics of matrix isolated species has been previously published by Andrews and Moskovits,[35] and represents an excellent starting point for understanding a number of effects associated with matrix-isolation. In any event, before considering the reactions of metal atoms with hydrocarbons under matrix isolation conditions, a brief review of the impact of matrix isolation of the reagents used in this work is important.

2.5 Water in inert gas matrices

By far, the most persistent molecule present as an impurity in matrices is water. The infrared spectrum of water isolated in inert matrices was first reported by Reddington and Milligan in 1962.[36] In this work, the infrared spectrum of H_2O,

D_2O, and HOD isolated in Ar from 4-27 K is presented, with all of the major fundamental absorption bands observed for each isotopomer correlating very well with the gas-phase rovibrational spectrum of water isotopomers.[37] Surprisingly, increasing the temperature of the matrix in which water molecules are isolated gives rise to new absorptions, with regular spacing consistent with rotational transitions of the lowest J rotational levels. Thus, when water is isolated in Ar, the water molecule is able to undergo essentially unrestricted rotation. A comparison infrared absorption study of a similar concentration of water in nitrogen, however, gives rise only to non-rotating matrix isolated water.[38] In either case, warming of the matrix from the lowest achievable temperatures causes losses in infrared features, while a secondary set of features grows. The growth and decay behaviour of the observed spectral features is consistent with the loss of monomeric water, to form water aggregates such as the water dimer, $(H_2O)_2$ and trimer, $(H_2O)_3$.[36,38] That water is so easily able to form complexes within the matrix isolation environment, even with other water molecules, has made water a very annoying matrix impurity, and as a result significant efforts have been made to understand water in matrices.

The low temperatures of the matrix isolation environment, and the highly polar nature of the O-H bond, make H_2O ideally suited for complexation with other species, even if the secondary species has only slight polarity. As a result, infrared spectra of matrix isolated species can often include spectral features due to water complexation. In order to understand water within the matrix isolation environment, a detailed study of matrix-isolated water was conducted by Ayers

and Pullin.[39-43] In the first of their work, reassignments of the infrared spectrum of H_2O and HOD isolated in Ar were presented,[39] along with an in depth concentration study of water in matrices to properly identify $(H_2O)_n$, n = 1-4.[39,40,41] Furthermore, the addition of small amounts of Xe atoms, species which are significantly more polarizable than Ar,[44] resulted in the efficient quenching of rotation of H_2O within matrices.[40] Such detailed analyses provided significant insight into concentration ranges where monomeric H_2O is expected in matrices. Following these initial studies, complexation studies of water with electron donors such as dimethyl ether and hydrogen bond donors such as HCl have demonstrated the impact of fundamental infrared absorption positions of the H_2O molecule in the complex when complexation arises from either $M^{\delta-\cdots\ \delta+}$H-OH or $M^{\delta+\cdots\delta-}$:OH_2 interactions.[40] As a result, these works have become pivotal in understanding all further studies involving water complexation in matrices, and that water is such a successful complexation agent requires that all investigations under matrix isolation conditions must consider possible impacts of water impurities. Unsurprisingly, aspects of this, and other molecular complexations, are covered in detail by Moskovits and Andrews.[35]

2.6 Ethene in inert gas matrices

The molecule ethene, $H_2C{=}CH_2$, is the simplest alkene, and as a result, represents the best choice for studying fundamental interactions with molecular π clouds. As a result, it is not surprising that significant study of ethene in rare-gas matrices has been performed.[45] The most important of these studies for this

work are those which are concerned with the vibrational spectra of ethene isolated in matrices.

The first reported matrix isolated spectrum of ethene in an Ar matrix was reported by Barnes *et al*.[46] This work, which also reported the spectra of the next larger alkenes up to the butene isomers, characterized each of the fundamental absorptions of ethene. Additionally, their spectra give evidence of several infrared-inactive absorptions appearing in the matrix isolated spectra that are not evident in the gas-phase spectra of ethene. Initially, the observation of these fundamentals was attributed to interactions of ethene with the matrix environment, which distort the molecule sufficiently to allow the forbidden absorptions to be observed. However, an alternative explanation is the potential for aggregation of ethene under their experimental conditions.

Later, Rytter and Gruen performed a series of matrix isolation experiments in which the concentration of ethene was varied from pure argon or xenon to pure ethene samples.[47] Both infrared and Raman spectra of the matrices, prepared at 15K, were recorded. As the concentration of ethene in the matrix sample was increased, infrared absorptions associated with matrix isolated ethene monomers diminish, yielding shifts consistent with ethene dimerization, and ultimately absorptions due to crystalline ethylene. These absorption bands were characterized by systematic increases in ethene concentration, and the formation of each at the expense of the smaller ethene molecule can be reasonably fit by growth-and-decay models. From analysis of these results, the ethene dimer is inferred to be a very weak van der Waals molecule, with D_{2d}

symmetry. The specific structure has one planar ethene with a second ethene molecule perpendicular to the first, between the two CH_2 units. This structure was, however, re-evaluated by Cowieson *et al*. some years later, while reinvestigating the Raman spectra of ethene dimers in Ar.[48] Instead, the more likely structure of the dimer, according to their spectra and *ab initio* calculations, is a T-shaped complex where the CH_2 unit of one ethene interacts with the π-cloud of the second ethene molecule.

According to the models calculated by Rytter and Gruen,[47] the matrix isolated ethene dimer should maximize at concentrations near 8% by mole of ethene in rare gas, although, even by this concentration significant formation of ethene monomer is expected to be present. These observations suggest that, for matrix isolation work involving ethene, single ethene monomers would only be expected to be isolated well below 2% by mole ethene in an inert gas matrix.

Finally, Collins *et al*. isolated several isotopomers of C_2H_4 in Xe.[49] Their results confirm the previous studies, but also give evidence for multiple trapping environments in the Xe host. Although no firm conclusions can be made in their work on the exact nature of new observations of C_2H_4 in Xe, several possible factors are given, including the postulation that C_2H_4 can exhibit slight rotation in the large lattice sites of Xe.

The persistent presence of H_2O in matrix isolation vacuum systems has required a number of groups to consider the complexation of H_2O with other guests within the matrix isolation environment. Water molecules hydrogen bond very readily, and when ethene and water are co-condensed in rare-gas matrices,

the formation of ethene water complexes arise. Engdahl and Nelander studied the infrared spectra of ethene-water complexes,[50] and complexes of water with a variety of other π-containing species.[51,52,53] In their work, systematic increases in the concentration of ethene, while holding the concentration of water constant, showed evidence for the decrease in the concentration of matrix isolated water, with an increase in several new features in the infrared spectra. The new infrared features grew simultaneously with increases in ethene concentration, at the expense of freely isolated water features. As a result, these features were assigned to a T-shaped 1:1 complex of ethene:water, with the O-H bond of water hydrogen bonded to the π-cloud of ethene. Isotopic measurements involving HOD, and D_2O were consistent with this assignment. Later, gas-phase rotational spectra of ethene:water mixtures were recorded,[54,55] and the formation of a gas-phase ethene:water 1:1 complex having a similar structure to that proposed by Engdahl and Nelander was also observed. As a result, these works have clearly demonstrated the viability of matrix isolation for investigation of complexed species, and many molecular complexes have been prepared using similar techniques.

2.7 Metal atoms in inert gas matrices

For the transition metals, the availability of low-lying vacant orbitals, along with unpaired electrons in the valency makes these species quite reactive. As a result, many matrix studies involving transition metals exist.[45] Since the matrix isolation technique requires that reagents be in the gas phase prior to condensation in the matrix, the vaporization of metal atoms in matrix isolation

experiments is generally the most difficult step. However, the steps to facilitate metal atom deposition are fairly straightforward.[56] As a means of characterizing techniques for depositing metal atoms in matrices, the UV-visible spectrum of metal atoms have been recorded and compared with gas-phase values. The entire first row of transition metals, and many second row metals have been characterized in this way,[57] although comparatively less is known about the heavy transition metals in matrices.

The three most common methods of generating metal atoms for deposition into matrices are: hollow cathode discharge sources, laser ablation, and thermal vaporization by resistively heating pure metal under vacuum. Each of these has been used with matrix isolation, in each case providing strengths and weaknesses.

The hollow cathode source for metal atom deposition is the least used of the previously mentioned methods, but bears mention briefly for completion of the topic. A description of the apparatus and its uses was originally given by Carstens *et al*.[58] Briefly, this source employs a removable cathode which can be formed from any machineable material. During the discharge event, metal atoms and atomic ions are expelled from the surface of the cathode. These metal species are entrained in a flow of rare-gas and reagent which passes over the cathode surface. Consequently, the rare-gas mixture containing the reagents can undergo reactions with metal atoms or metal ions, with the resultant species trapped on a cold surface as with all matrix isolation experiments. Since metal atoms and atomic ions can induce the observed chemistry, results obtained from

these studies are difficult to interpret clearly, and thus this method is best suited for spectroscopic characterization of unknown species. One benefit of this method is the high yield of metallic particles that can be generated, when the apparatus is in working order. However, the technique requires significant power and reagent in order to be effective, making it a comparatively costly experimental choice.

The laser ablation technique is a second technique used in the generation of metal atoms that is similar to the hollow cathode, but eliminates many of the disadvantages. Of the three metal atom deposition techniques, the laser ablation technique is the newest method, and can be used to vaporize even the most difficult metal substrates. The technique was first employed by Knight *et al*. for preparing B_2,[59] and subsequently has been adopted for use with metals by Andrews,[60] and by Zhou[61] for characterizing reaction products of metallic species. The simplicity of the laser ablation technique for use with matrix isolation, and the high yields of metallic species that can be produced have made this method popular for characterizing new organometallic species. In general, the technique involves focusing light from a laser source onto the surface of a metallic target. The focused energy results in a plume of metal vapour, containing metal atoms, atomic ions, and many electrons. Although the majority of these resultant species are in their electronic ground state following vaporization, this method does yield excited state species, providing additional complications when studying associated reactivity. Additionally, metal ion neutralization frequently occurs, resulting in the formation of excited state neutral

metal atomic species. Relaxation of these excited species to ground state metal atoms by resonant emission ensures that the reaction environment is bathed in light which corresponds exactly to atomic transitions for the reagents under investigation. Furthermore, the presence of electrons in the plume can result in negatively charged species. As a result, the laser ablation technique is excellent for generating new organometallic species, but is somewhat complicated for mechanistic investigations.

Unlike the previous two techniques, the technique of thermal vaporization is best suited for mechanistic investigations of the reactivity of metallic atoms. Consequently, this technique has been widely used for studying metal atom chemistry, and many of these investigations have been summarized in books involving the subject.[35,57] The thermal vaporization technique involves the resistive heating of a source of metal to the vacuum vaporization temperature, at which point metal atoms begin to vaporize from the metal substrate. Under thermal energy, all vaporized species are neutral, and in the electronic ground state, which simplifies many of the downsides associated with either the hollow cathode or laser ablation techniques. However, the temperatures required to vaporize transition metals by thermal vaporization result in a distribution of light from the metal source that can be described by blackbody emission. Thus, matrix samples prepared in this way are continuously bathed in light, meaning that photoexcitation of isolated species can result, leading to photochemical reactions.

When using any of these metal atom generation methods, it is important to introduce enough metal into the system to generate sufficient products for spectroscopic observation, and characterization. Methods for characterization of metal yield do exist,[57] and studies characterizing metal behaviour in various matrices, under various experimental conditions have been performed. One of the most common side reactions of metals is the formation of metallic dimers, M_2.[35,57] The dimer species in matrices are believed to form during the matrix condensation process, rather than directly in the gas-phase, and represent a deactivation pathway of the metal atom. Other than simple association reactions,[35] very little reaction chemistry with the dimer has been studied, since the formation of these species is somewhat irreproducible. The inhibition of dimers has been studied in some matrix systems, and in general, the use of the heavier inert gases can inhibit dimer formation. Combinations of higher freezing temperatures, and the formation of metal-rare gas van der Waals complexes are cited as the major factors immobilizing metal atoms during matrix condensation, thereby inhibiting dimer formation on deposition.[57] In some cases, where reactivity is observed when the dimer is present, the chemistry is explained in terms of dimer dissociation. Photoexcitation of the dimer yields an excited species, which dissociates into two metal atoms. In some cases, this dissociation results in a source of excited state metal atoms which lead to subsequent chemistry. One example of such chemistry is the observed reactivity of Co_2 with ethene under matrix isolation conditions, which was observed by Ozin

et al.[62] However, no other major studies characterizing photo-dissociation of metallic dimers have been performed.

One of the other major loss mechanisms of metal atoms under matrix isolation conditions comes from the persistent presence of water. Although the transition metals have a repulsive 4s outer shell, many metal atoms react directly with water. This reactivity is partially explained by the dense, unpolarizable electron pairs on the O atom of H_2O, which can penetrate the outer shell of the metal atom. In fact, under matrix isolation conditions all of the first row metal atoms react spontaneously with water, either inserting the metal atom into the O-H bond,[63] or forming adducts of the form M-OH_2.[64] Such adducts have also been observed in the gas-phase by Mitchell and coworkers.[65] In this specific case, the reaction of Ni is studied with H_2O, and both the Ni-OH_2 and H-Ni-OH products are observed. The further observation of dual chemistry with neutral nickel atoms provides insight into the nature of these two competitive reactions. As was previously the case in other gas-phase studies, the low lying first excited state of nickel (having a $3d^9 4s^1$ configuration) is believed to result in the Ni/H_2O insertion product, H-Ni-OH. By comparison, the ground state Ni $3d^8 4s^2$ configuration is believed to be responsible for the formation of the Ni-OH_2 product. Theoretical calculations in the same work support such observations, suggesting further that metal atom bond insertions result from partially filled $3d^x 4s^1$ configurations when they occur.

The reaction of the metal atoms with water has been investigated by matrix isolation in great detail. The early transition metals, Sc-V react

spontaneously with water,[63] forming H-M-OH species directly, while the later species (Cr-Cu) form M-OH_2 adducts.[64] Irradiation of these adducts results in the metal atoms inserting into the O-H bond of water, forming H-M-OH similarly to the case of the early transition metals. The nature of the H-M-OH species is drastically different dependent on the identity of the metal atom. Common reactions involve H atom loss, or subsequent insertions into the other O-H bond, ultimately leading to H_2 elimination. The nature of the reactivity is quite specific to the metal atom involved in the reaction, and the most interesting results occur for the early transition metals.

Kauffman and coworkers[63] performed the original study of the reaction products of thermally vaporized Sc-V with water, where H-M-OH is observed spontaneously in all cases. Irradiation of these samples with 300-400 nm light causes elimination to occur from this product, yielding MO + H_2 in all cases. However only in the case of Sc was H atom loss observed, to form Sc-OH as a major photodecomposition product. Additionally, the metal atoms demonstrate reactivity with multiple water molecules, under higher H_2O/Ar concentration, giving rise to $H_xM(OH)_x$ species. Later, Zhou *et al*. reexamined the reaction of laser ablated Group IIIB,[66,67] IVB,[61] and Group VB[68] metal atoms with H_2O. For Sc,[66] H-Sc-OH and ScO were observed as major products. Irradiation of matrices in this case led to formation of Sc-OH, which undergoes a further photoinduced rearrangement to HScO. Similar results are obtained for Y and La,[67] in which H-Y-OH, YO and H-La-OH, LaO are major products.

In comparison, the reaction of the Group IV metals Ti, Zr and Hf and group V metals, V, Nb, and Ta with H_2O show similar products of O-H insertion by the metal atoms. However, the higher valency of these species also permits the formation of H_2MO species in all cases, for which similar species have never been observed with the Group III atoms. The simplest explanation is the availability of a formally M^{4+} oxidation state, unavailable to the d^3-metals of Group III. Many of the products are present immediately following deposition of the matrix, and irradiation of the matrices can increase the various O-H insertion products, which can also be increased by annealing the matrix. Computational investigations suggest that it is mechanistically possible for the formation of the H_2MO to proceed sequentially, as $M + H_2O \rightarrow H\text{-}M\text{-}OH \rightarrow H_2MO$ in the gas-phase during deposition. Similar results also suggest that H_2 elimination to form MO and H_2 should also occur during deposition conditions. No investigation of a direct 1,3-H_2 elimination pathway from H-M-OH has been considered, although this would be analogous to the loss that is observed for certain H-M-C_2H_3 species, as described above.[21] The observation of H_2MO following annealing of their matrices suggests that $^{n}MO + H_2 \rightarrow {}^{n-2}H_2MO$ may be a competitive route to the H_2MO product, instead of the stepwise formation from the H-M-OH species. The observation of additional formation of H_2MO following annealing, in the absence of H-M-OH as a source is consistent with this idea, although it does not exclude the spontaneous formation during deposition. Intuitive analysis of the presented computational calculations suggests that the barrier to formation of H_2MO from $MO + H_2$ is much smaller than a second insertion from H-M-OH. As

the formation is observed spontaneously under matrix isolation conditions near 10K, the observed H_2MO species following annealing are likely to result from MO reaction with available H_2 that is present in their work due to hydrogen elimination during deposition.

2.8 Reactions of metal atoms with ethene in inert matrices

The chemistry of metal atoms with ethene parallels the chemistry of transition metal atoms with water quite well. In general, metal atoms fall into two categories: those which have been observed to form metal-ethene coordination complexes, and those metals which can be made to insert into the C-H bond of ethene. Since ethene is the simplest of the alkenes, this fact has opened up the study of ethene reacting with transition metals in inert gas matrices multiple times, in order to investigate fundamental metal-ethene interactions. A brief summary of much of the early work in this area has been reviewed by Moskovits and Andrews.[35] To date, no evidence of a single ethene π-coordinated to an early transition metal atom has been observed under matrix isolation conditions. The later transition metals, however, can complex ethene quite efficiently.

The first observation of a matrix isolated M-(η^2-C_2H_4) complex was observed in a letter by Kasai and McLeod.[69] Their work reported the electron spin resonance (ESR) spectrum of a silver atom ethene complex, isolated in Ne. From their first observations, complexation of the species was accompanied with a change in the matrix from white (when Ag is present, without C_2H_4), to a red-matrix when C_2H_4 and Ag were codeposited. Similar results were presented for Cu in the letter, but Au was mentioned to be unreactive with respect to C_2H_4

complexation. Their letter was followed up by a companion study of Cu and Ag in matrices containing up to 10% ethene by mole fraction. In matrices with concentrations of as low as 2% by mole ethene prepared containing either Cu or Ag, their spectra gave clear evidence for the formation of $M(C_2H_4)_n$, M=Cu,Ag, n = 1,2. Again, no evidence of a similar complex for Au was observed. In 1976, McIntosh and Ozin reported an $Au(C_2H_4)$ complex characterized by infrared and ultraviolet visible spectroscopy. Again, the observation of a colour change in the matrix following codeposition of Au with C_2H_4 in Ar suggested reactivity of the two species. In the UV-visible spectra, several blue-shifts in the spectra of Au atoms isolated in Ar were observed, when C_2H_4 was present in as much as 10%. The shifting in these bands was proposed to arise from metal to π^* charge transfer in the $Au(C_2H_4)$ complex. When similar experiments were examined using infrared spectroscopy, a number of new features in the infrared spectrum appear, corresponding to shifts in the matrix isolated spectrum of C_2H_4. Such shifts, which are consistent with complexation, also shift upon isotopic substitution, consistent with an $Au(C_2H_4)$ complex. Additional experiments with a 50/50 mixture of isotopic ^{12}C and ^{13}C ethene do not show evidence for mixed $Au(C_2H_4)$ spectra, suggesting that Au undergoes only a primary complexation, unlike the Cu and Ag metals. In 1983, ESR experiments by Kasai[70] confirmed the presence of $Au(C_2H_4)$, and also the presence of $Au(C_2H_4)_2$ under the conditions used by the previous authors. Additional investigations with Cu, Ag, and Au showed that these species could complex up to 3 ethene molecules in some cases, and that dimers and trimers of the metal species could uptake even more

C_2H_4.[71] A final study on these systems, which incorporated an SCF-Xα study of the bonding of M(C_2H_4), M = Cu, Ag, Au was able to qualitatively describe the bonding in the complexes, with a reasonable correlation of the optical spectrum of the species, as well.[72]

Following the work with coinage metals, similar olefin coordination complexes were observed for the Ni and Pd.[57,73] Under conditions of ethene to Ar from 1 to 50 through to pure ethene, Ni atoms co-condensed with the gas-mixture gave infrared evidence for Ni$(C_2H_4)_n$, n=1, 2, 3.[74] The identification of these species was performed on the basis of concentration variation of C_2H_4 in Ar. Surprisingly, in pure C_2H_4, both Ni$(C_2H_4)_2$ and Ni$(C_2H_4)_3$ were produced, in spite of the expectation that Ni$(C_2H_4)_3$ would be the dominant product. However, many of the vibrational modes associated with the Ni$(C_2H_4)_2$ species were later believed to be due to ethane (C_2H_6) formation via metal catalyzed sacrificial hydrogenation, as is discussed in Chapter 6. Similar experiments were performed with Pd, providing similar infrared spectroscopic evidence for Pd$(C_2H_4)_n$, n = 1-3 species. The presence of multiple ethene molecules within various complexes give consistent shifts in the infrared spectra for experiments performed using ^{12}C and ^{13}C ethene mixtures. In particular, infrared absorption bands due to multiple ethene molecules split as might be expected when Pd$(^{12}C_2H_4)_{3-x}(^{13}C_2H_4)_x$, x=0-3 mixed isotopomers are formed. However, in these experiments, a number of features assigned to Pd$(C_2H_4)_2$ appear in the infrared spectra at practically identical wavenumber positions to Ni$(C_2H_4)_2$. Although these absorptions are rationalized as the Pd$(C_2H_4)_2$ species, the formation of

C_2H_6, analogous to that in the case of Ni, is also likely under the extremely high concentration of ethene employed in both of the studies. Finally, owing primarily to the ease with which these $M(C_2H_4)_n$ complexes formed, additional investigations were performed in the Ozin group to form $Ni_n(C_2H_4)_m$ complexes. These species extend the olefin coordination to clusters, and generalized surfaces.[75] Naturally, this chemistry is extremely complicated, and is mentioned here only for completion.

The peculiar formation of $Ni(C_2H_4)_n$ species under conditions where only $Ni(C_2H_4)_3$ would be expected in the work of the Ozin group, along with the fundamental nature of the M-(C_2H_4) interaction, prompted the reinvestigation of the formation of these species by Merle-Mejean and coworkers in 1992.[76] Their investigation included infrared, UV-visible and Raman analysis of matrices containing products of Ni vapour co-condensed with ethene isotopomers in Ar at concentrations from 1:100 to 1:10 ethene:Ar, or in pure ethene. In their investigation, the $Ni(C_2H_4)_3$ compound was conclusively identified by depositing metal into neat ethene matrices. Following this identification, the systematic dilution of ethene in Ar was performed, in order to conclusively identify the lower $Ni(C_2H_4)_n$ species. At a concentration of 1:10 ethene:Ar, all of the $Ni(C_2H_4)_3$ bands were still present, while two additional products, B and C were observed in their experimental spectra. Annealing of the matrix at 1:10 ethene:Ar caused species B to grow, at the expense of species C, and further annealing to higher temperatures resulted in the formation of species A with no further observation of either B or C. The sequential behaviour of these species upon annealing

suggests that the three species are a series of linked reaction products, in which C → B → A = $Ni(C_2H_4)_3$. Surprisingly, a further 10 fold dilution of the matrix sample to 1:100 C_2H_4:Ar gave continued presence of A = $Ni(C_2H_4)_3$ on deposition of the matrix. Following a gentle annealing of this dilute matrix, significant growth of species C in the vibrational spectra was observed. However, the authors note the absence of several bands previously assigned to $Ni(C_2H_4)_2$,[74] under virtually identical conditions. The set of unobserved bands, with the major peak at 1465 cm^{-1} correspond to C_2H_6, which does not form in the experiments by Merle-Mejean.[76] The lack of C_2H_6 production in these complementary experiments suggests that some difference of the two apparatus designs may be responsible for C_2H_6 formation in the experiments by Huber *et al*.,[74] for which photoexcitation from the furnace in the Huber experiments is believed to be one major difference. Nevertheless, on the basis of the annealing experiments, and isotopic substitution of the ethene molecule in Ar, major bands in the infrared and Raman spectra of A = $Ni(C_2H_4)_3$, B = $Ni(C_2H_4)_2$ and C = $Ni(C_2H_4)$ were observed. The infrared and Raman spectrum of the $Ni(C_2H_4)$ species was only weakly observed in the experiments by Merle-Mejean,[76] due to the high dilution of the C_2H_4 required to conclusively identify the product. However, the spectrum of this molecule was later confirmed in complementary experiments by Lee *et al*.[77]

More recently, Pd and Pt have been reinvestigated in Ar containing C_2H_4 by Cho and Andrews.[78] These experiments produce atomic Pd or Pt by laser ablation, and condense in Ar containing a low concentration of ethene isotopomers, near 7K. In the case of Pd, only a $Pd(C_2H_4)$ complex is formed,

similar to the results described above. On the other hand, Pt inserts into the C-H bond, forming an H-Pt-C_2H_3 species. However, in the case of either metal, C_2H_2 is observed in the infrared spectra, suggesting metal atoms react with C_2H_4 to eliminate H_2 efficiently. Additionally, when CH_2=CD_2 is used, C_2H_2, C_2D_2, and CHCD are observed in the spectra. Although only HD elimination was expected, yielding only CHCD as the expected dehydrogenation product – the appearance of all three acetylene isotopomers suggests a significant C-H rearrangement at the metal. The authors propose the high energy of the metal atoms generated by laser ablation as one factor which accounts for the significant C-H(D) rearrangement in their experiments.

Returning to the pioneering work performed by the Ozin group for ethene coordination on Ni clusters isolated in matrices,[75] similar reactivity for ethene with Co was investigated.[79] The formation of $Co(C_2H_4)_n$ species is present in the experimental spectra, however, Co aggregates quite aggressively within inert matrices, forming higher Co_n species. The same is also true for the $Co(C_2H_4)_n$ species, forming $Co_n(C_2H_4)_m$ species as well. However, one interesting result in which Co_2 photodissociation leading to Co + Co*,[80] which subsequently leads to the increased formation of $Co(C_2H_4)$, was observed in the context of this work. No additional chemistry from irradiation of the matrix was observed. Of course, the chemistry of Co with C_2H_4 is otherwise extremely complicated, and has only been investigated in this preliminary study, which is likely to contain misidentifications. Nevertheless, through the context of this work, the

observation of Co_2 reacting with ethene, representing the only M_2 reaction with C_2H_4 is an important observation.

Only one other investigation of Co cocondensed with C_2H_4 under matrix isolation conditions has been performed, by Locke and Shevlin.[81] In these experiments, thermally vaporized Co was trapped in pure ethene matrices at 77K, with trace amounts of ethanal (acetaldehyde, CH_3CHO) or methanal (formaldehyde, H_2CO) present in infrared absorption spectra. In cases where Co is cocondensed with CH_3CHO alone, CH_4 is generated as a major product. The formation of this product is believed to result from insertion of the Co into the aldehydic C-H bond, followed by steps leading to H,CH_3 elimination from the metal, and resultant Co-CO formation. When the same reaction is performed in C_2H_4 matrices, 2-butanone, 2-butanol, ethanol, ethyl acetate, and methane are all formed as major products. These specific products can be formed only via the insertion of a C_2H_4 or additional acetaldehyde units into the Co-H bond, followed by reductive elimination steps. As a means of identifying mechanistic aspects of the product formation, selected isotopomers of acetaldehyde and ethene have been used. For example, the reaction of Co + C_2H_4 + CD_3CHO gives rise to CD_3H, CD_3CH_2OH, $CD_3(C=O)CH_2CH_3$, and $CD_3COOCH_2CD_3$. The formation of $CD_3(C=O)CH_2CH_3$ can occur only via C_2H_4 insertion into an M-C or M-H bond, followed by reductive elimination. This study represents one of the few examples of such ethene insertions into organometallic intermediates, under conditions of matrix isolation. Furthermore, the relatively complicated restructuring of initial reagents by the metal atom, reflected in the remaining products, indicates the

facility with which a number of steps can be undertaken, even under matrix isolation conditions. This latter point demonstrates the utility of the matrix isolation technique for studying the reaction chemistry of organometallic intermediates.

Similar reactions were performed by Cardenas and Shevlin with iron atoms in neat ethene matrices at 77K, again characterized by infrared absorption spectroscopy.[82] Under these conditions, the reaction of Fe with C_2H_4, following warming and recooling to 77K are ethane (major product) and butane, with trace amounts of the three butene isomers. A 50/50 mixture of C_2H_4/C_2D_4 results in an expected statistical isotopic distribution of products, which must implicate the insertion of the metal into the C-H(D) bond of ethene in order to form the product. Subsequent ethene insertion into the Fe-H bond, followed by reductive elimination would lead to the observed hydrocarbon products. Additional experiments involving Fe atoms with trace amounts of h_6-propene (CH_3-CH=CH_2) and other alkenes in pure C_2D_4 resulted in exchange of D atoms for H atoms.[83] Again, these results can only be rationalized if a C-H bond activation step occurs involving the metal atom, with a subsequent alkene insertion, and reductive elimination steps. That a number of these exchanges occur suggests these steps to be relatively rapid. Interestingly, when C_2H_4 and iron atoms generated by reduction of $FeCl_2$ are cocondensed, no hydrogenation or aggregation of ethene is observed, in contrast to the results obtained when Fe atoms are thermally generated.[82] Since the reduction method involves no blackbody irradiation, while the thermal vaporization would bathe the matrix system with

light, this may suggest that the steps in the Fe/C_2H_4 reactions require photoexcitation.

Iron atoms were co-deposited with ethene in Ar at concentrations of 1:200, by Kafafi and coworkers,[84] and later reinvestigated by Yamada.[85] In these experiments, the yield of metal into the matrix was quite high, and co-deposition of the metal with the matrix sample led to the observation of several new products in the corresponding infrared spectra, including products of Fe_n (n>1) chemistry. However, under sample preparation conditions where the amount of metal was greatly reduced, new features in the infrared spectrum consistent with $Fe(C_2H_4)$ and $Fe(C_2H_4)_2$ were observed. In the specific case of $Fe(C_2H_4)$, the molecular complex was believed to be an $Fe^{\delta-\ldots\delta+}H_2C{=}CH_2$ complex, rather than a $Fe(\eta^2\text{-}C_2H_4)$ complex as observed for the later transition metals. However, the results of Yamada and coworkers later confirmed the more traditional $Fe(\eta^2\text{-}C_2H_4)$ structure to be the more likely geometry. By comparison, the infrared absorption spectrum of $Fe(C_2H_4)_2$ is also consistent with two π-coordinated ethene molecules, on the metal centre. Additional characterization of these species using isotopomers of ethene was also performed, confirming these geometries for the two species. Interestingly, irradiation of the matrix samples containing these two molecules with $280 < \lambda < 360$ nm light caused the decrease in the intensity of features associated with $Fe(C_2H_4)$, and new features associated with $H\text{-}Fe\text{-}CH{=}CH_2$. Irradiation with >400 nm of the $H\text{-}Fe\text{-}CH{=}CH_2$ molecule caused a decrease in absorption features due to this species, with reappearance of features associated with the $Fe(C_2H_4)$ molecule. The series of

irradiations could be repeated, interconverting the two species, indefinitely. Additionally, annealing of matrices in which the H-Fe-C_2H_3 absorptions were present resulted in sharpening of features attributed to this species, indicative of the interconversion of conformational isomers of the molecule to the thermodynamically favourable conformation within the matrix. One additional finding of this study was that prolonged irradiation of the matrices in which $Fe(C_2H_4)_2$ was present caused the destruction of this species, with growth of features associated with C_2H_6 and CH_4. The photoproduction of C_2H_6 and CH_4 in this process was believed to result from a disproportionation of one C_2H_4 on Fe, leading to the products of ethene hydrogenation, and an IR-invisible iron carbide product. Although no iron carbide product was observed, this mechanistic insight was the best that could be proposed given the information available. No additional investigations with Fe, or other elements from the Fe group have been performed under matrix isolation conditions with C_2H_4. Similarly, no such investigations with Cr or Mn have been performed.

Although a wealth of results for later transition metals with ethene in matrices exist, comparatively few studies involving the early transition metals have been performed. The earliest case of early transition metal reactions with ethene under matrix isolation conditions was performed by Lee *et al*., in which infrared absorption spectra of Ti atoms codeposited with 1:200 ethene:Ar, near 10K were obtained.[86] Similar to the results of Ritter and coworkers,[24] deposition of ground state Ti atoms with ethene in Ar yielded no new significant products. By contrast, theoretical calculations presented in the work of Lee *et al*. predict a

strongly bound Ti(C_2H_4) species,[86] although, the species is never observed in any of the work. Following irradiation of the matrices with visible light >400 nm, corresponding to Ti atom excitations, two new sets of infrared absorption bands corresponding to H-Ti-C_2H_3, and $H_2Ti(\eta^2\text{-}C_2H_2)$ were observed. Further irradiation of samples containing either isomer resulted in their photo-interconversion, and prolonged irradiations with visible light resulted in their eventual destruction. In all cases, the expected major photodecomposition products were believed to be Ti(C_2H_2) and H_2, or even further dehydrogenated samples. However, spectral features corresponding to these species were never observed. Additional insight into the formation of the dihydro- isomer was obtained by investigating the conversion of the H-Ti-C_2H_3 product into H_2Ti(C_2H_2). Following irradiation of the matrix containing Ti and $H_2C{=}CD_2$, both H-Ti-$CHCD_2$ and D-Ti-$CDCH_2$ were formed. Further irradiation of these samples produced only one product, at the expense of either precursor: HDTi(CHCD). This species can only result from migration of an H/D from the methylene ($=CH_2$) side of the vinyl group, in either case. The thorough investigation of the Ti/C_2H_4 system by Lee and coworkers represents a benchmark for investigations of early transition metals reacting with ethene.

Following from this investigation, similar matrix experiments with laser ablated Zr[87] and Hf[88] deposited in Ar with ethene were performed. As the reactivity of Zr with C_2H_4 has been extensively studied in gas-phase work,[21,22] as evidenced by the results presented above, this matrix study provides excellent complementary support for understanding mechanistic aspects of the observed

gas-phase dehydrogenation reactions. For each of Zr[87] and Hf,[88] the two cases parallel extremely well with respect to their reactivity toward ethene. Following deposition of metal atoms in the matrices containing ethene, three distinct groups of product features are evident in the infrared absorption spectra. On the basis of isotopic substitution and computational investigations, the first set of product absorptions belong to H-M-C_2H_3, M = Zr, Hf. These features can be increased by irradiation of the matrix with visible light, or by annealing of the matrix after irradiation has been performed. The second group of features belong to an $H_2M(C_2H_2)$ species, and these features are also increased following irradiation of the matrix with light, or thermal annealing of the resultant matrices. On the basis of irradiation and annealing experiments, it is proposed that this isomer is the most stable of the three, although this is in direct contrast with calculations presented in previous works.[22] Additionally, the $H_2M(C_2H_2)$ is proposed as the direct precursor to H_2 elimination. However, this ignores the proposed 1,3 elimination mechanism where H_2 elimination could proceed by elimination from the H-M and one of the C-H bonds of the $=CH_2$ of the vinyl group in H-M-$CH=CH_2$ in all cases. Evidence in the spectra for C_2H_2 and H_2 formation is present, under all conditions. Additionally, as was the case with Pt above,[78] the use of $CH_2=CD_2$ as the ethene source gives CHCD, C_2H_2, and C_2D_2, suggesting that scrambling of the ethene must occur on the metal centre, although the exact mechanism by which any of the products is formed is not certain. Finally, the third set of product features is attributed to an H_3M-CCH species, which has never before been observed in any earlier matrix work with ethene. Additionally,

the earlier work with Zr and C_2H_4 in the gas-phase does not give products that are consistent with this isomer,[21,22] which may suggest that its formation is unique to the matrix isolation environment. As an additional surprise, no evidence for the formation of H-M-CCH is observed, suggesting that H_2 elimination from the ternary hydride species is not favourable, nor is the reaction of free M with liberated C_2H_2. This latter point may support the idea that H_2 elimination occurs via 1,3-elimination from the H-M-C_2H_3 species, rather than from the binary or ternary metal hydride species. Nevertheless, the observation of more C-H bond insertion species following irradiation of matrices containing early transition metal atoms and ethene suggests that this mechanism is a general reaction for some excited state early transition metal species.

The last and most recent investigation of early transition metal reactivity with ethene was very recently published by Cho and Andrews.[89] Their work investigated the codeposition of the group V metals, V, Nb, and Ta generated by laser ablation with isotopomers of ethene in Ar, at 8 K. As with the works presented above, all three of the metals can be made to react with isotopomers of ethene. While V is unreactive following deposition, Nb and Ta give rise to products of C-H bond insertion. All of the metals become further reactive following irradiation of the matrix with light corresponding to electronic transitions of the metal atomic species. Interestingly, V atoms form a stable H-V-C_2H_3 product in high yield, while only trace amounts of this product are observed for Nb, and no such product is observed with Ta. All three metals react with ethene to form $H_2M(C_2H_2)$ species, which is once again proposed as the direct precursor

to hydrogen elimination in dehydrogenation mechanisms. Hydrocarbon products such as acetylene are also observed in the spectra of all matrices. Additional experiments with V and isotopomers of ethene demonstrate that the $H_2M(C_2H_2)$ species is produced sequentially from the H-M-C_2H_3 species, which is expected to be the same mechanism in the cases of Nb and Ta. Corresponding computational investigations suggest that, for V, the $H_2V(C_2H_2)$ species is higher in energy than the H-V-C_2H_3 species, while for Nb and Ta, the $H_2M(C_2H_2)$ species is the thermodynamically favoured product. Thus, the barrier to formation in the heavier metals is significantly lower, and the lack of observation of significant H-M-C_2H_3, M = Nb, Ta is likely due to the inability of these species to be appreciably stabilized under matrix isolation conditions.

These last results with the group V metals are of the most direct relevance to the current work, and the unique reactivity even among these three metals underscores the need for further investigations. In the remaining chapters, factors affecting the formation of initial products in the reactions of early transition metals with ethene will be presented, followed by investigations of the reactivity of these species with water, and with additional ethene.

2.9 References for Chapter 2

[1] Armentrout, P.B.; *Science*, **1991**, 251, 175.

[2] Armentrout, P.B.; *Ann. Rev.*, **1990**, 41, 313.

[3] a) See for example: *The Organometallic Chemistry of the Transition Metals*, 4th Ed, Crabtree, R.; John Wiley & Sons, Inc.: Hoboken, NJ, **2005**. b) Cotton, F.A.; Wilkinson, G.; *Advanced Inorganic Chemistry,* 5th Ed.; Wiley, New York, **1988.**

[4] Weisshaar, J. C.; *Acc. Chem. Res.*, **1993**, 26, 213.

[5] Langhoff, S.R.; Bauschlicher, C.W. Jr.; *Ann. Rev. Phys.Chem.*, **1988**, 39, 181.

[6] Niu, S.; and Hall, M.B.; *Chem. Rev.*, **2000**, 100, 353.

[7] Wittborn, A.M.C.; Costas, M.; Blomberg, M.R.A.; Siegbahn, P.E.M.; *J. Chem. Phys.*, **1997**, 107, 4318.

[8] Elkind, J.L.; Armentrout, P.B.; *J. Phys. Chem.*, **1987**, 91, 2037.

[9] Elkind, J.L.; Armentrout, P.B.; *J. Phys. Chem.*, **1986**, 90, 6576.

[10] Armentrout, P.B.; Beauchamp, J.L.; *Acc. Chem. Res.*, **1989**, 22, 315.

[11] Siegbahn, P.E.M.; Blomberg, M. R. A.; Svensson, M.; *J. Am. Chem. Soc.*, **1993**, 115, 1952.

[12] Blomberg, M.R.A.; Siegbahn, P.E.M.; Svensson, M.; *J. Phys. Chem.*, **1992,** 96, 9794.

[13] Siegbahn, P.E.M. *J. Am. Chem. Soc.,* **1993**, 115, 5803.

[14] Siegbahn, P.E.M.; *Chem. Phys. Lett*. **1993**, 205, 290.

[15] George, A.V; *Trends in Organomet. Chem.,* **1997**, 2, 39.

[16] Rivalta, I.; Russo, N.; Sicilia, E. *J. Mol. Struc. THEOCHEM,* **2006**, 762, 25.

[17] See, for example: Herzberg, G.; *Atomic Spectra and Atomic Structure,* 2nd Ed., Dover, New York, 1944.

[18] See for example: Parnis, J.M.; Escobar-Cabrera, E.;, Thompson, M.G.K.; Jacula, J.P; Lafleur, R.D.; Guevara-Garcia, A.; Martinez, A.; Rayner, D.M.; *J. Phys. Chem.,* **2005**, 109, 7046.

[19] Glendening, E.D.; *J. Phys. Chem. A.*, **2004**, 108, 10165.

[20] Porembski, M.; Weisshaar, J.C.; *J. Phys. Chem. A.,* **2001**, 105, 6655.

[21] Porembski, M.; Weisssshaar, J.C.; *J. Phys. Chem. A.,* **2001,** 105, 4851.

[22] Willis, P.A.; Stauffer, H.U.; Hinrichs, R. Z.; Davis, H.F.; *J. Phys. Chem. A.*, **1999**, 103, 3706.

[23] Wen, Y.; Porembski, M.; Ferrett, T.A.; Weishaar, J.C.; *J. Phys. Chem. A.*, **1998**, 102, 8362.

[24] Ritter, D.; Carroll, J.J.; Weisshaar, J.C.; *J. Phys. Chem.,* **1992**, 96, 10636.

[25] Carroll, J.J.; Haug, K.L.; Weisshaar, J.C.; Blomberg, M.R.A.; Siegbahn, P.E.M.; Svensson, M.; *J. Phys. Chem.*, **1995**, 99, 13955.

[26] Carroll, J.J.; Haug, K.L.; Weisshaar, J.C.; *J. Am. Chem. Soc.,* **1993**, 115, 6962.

[27] Carroll, J.J.; Weisshaar, J.C.; *J. Phys. Chem.,* **1996**, 100, 12355.

[28] Brown, C.E.; Mitchell, S.A.; Hacket, P.A.; *Chem. Phys. Lett*., **1992**, 191, 175.

[29] Mitchell, S.A.; Hackett, P.A.; *J. Chem. Phys.*, **1990**, 93, 7822.

[30] Blitz, M.A.; Mitchell, S.A.; Hackett, P.A.; *J. Phys. Chem.*, **1991,** 95, 8719.

[31] Lian, L, Mitchell, S.A.; Rayner, D.M.; *J. Phys. Chem.*, **1994,** 98, 11637.

[32] Parnis, J.M.; Lafleur, R.D.; Rayner, D.M.; *J. Phys. Chem.*, **1995**, 99, 673.

[33] Senba, K.; Matsui, R.; Honma, K.; *J. Phys. Chem.*, **1995**, 99, 13992.

[34] Wen, Y.; Yethiraj, A.; Weisshaar, J.C.; *J. Chem. Phys.,* **1996**, 106, 1, 5509.

[35] See, for example: Moskovits, M.; Andrews, L.; *Chemistry and Physics of Matrix Isolated Species,* Elsevier, New York, **1989**.

[36] Reddington, R.L.; Milligan, D.E.; *J. Chem. Phys.*, **1962**, 37, 2162.

[37] Benedict, W.S.; Gailar, N.; Plyler, E.K.; *J. Chem. Phys.*, **1956**, 24, 1139.

[38] Tursi, A.J.; Nixon, E.R.; *J. Chem. Phys.*, **1970**, 52, 1521.

[39] Ayers, G.P.; Pullin, A.D.E.; *Chem. Phys. Lett.*, **1974**, 29, 604.

[40] Ayers, G.P.; Pullin, A.D.E.; *Spectrochim. Acta*, **1976**, 32A, 1629.

[41] Ayers, G.P.; Pullin, A.D.E.;*Spectrochim. Acta,* **1976**, 32A, 1641.

[42] Ayers, G.P.; Pullin, A.D.E.; *Spectrochim. Acta*, **1976**, 32A, 1689.

[43] Ayers, G.P.; Pullin, A.D.E.; *Spectrochim. Acta*, **1976**, 32A, 1695.

[44] See, for example: Weast, R.C; Lide, D. R. (eds); *CRC Handbook of Chemistry and Physics,* 70th ed., CRC Press, Boca Raton, **1989**.

[45] See, for example: Ball, D.W.; Kafafi, Z.H.; Fredin, L.; Hauge, R.H.; Margrave, J.L. (eds); *A Bibliography of Matrix Isolation Spectroscopy, 1954-1985.* Rice University Press, Texas, **1985**.

[46] Barnes, A.J.; Howells, J.D.R.; *J. Chem. Soc. Farad. Trans II*., **1973**, 69, 532.

[47] Rytter, E.; Gruen, D.M.; *Spectrochim. Acta A.*, **1979**, 35A, 199.

[48] Cowieson, D.R.; Barnes, A.J.; Orville-Thomas, W.J.; *J. Raman Spec.*, **1981**, 10, 224.

[49] Collins, S.T.; Casey, P.A.; Pimentel, G.C.; *J. Chem. Phys.*, **1988**, 12, 7307.

[50] Engdahl, A.; Nelander, B.; *Chem. Phys. Lett.*, **1985**, 113, 49.

[51] Engdahl, A.; Nelander, B.; *J. Phys. Chem.*, **1986**, 90, 4982.

[52] Nelander, B.; *J. Phys. Chem.*, **1988**, 92, 5642.

[53] Nelander, B.; *J. Mol. Struc*, **1990**, 222, 121.

[54] Peterson, K.I.; Klemperer, W.; *J. Chem. Phys.*, **1986**, 85, 725.

[55] Andrews, A.M.; Kuczkowski, R.L.; *J. Chem. Phys.*, **1993**, 98, 791.

[56] See for example: Dunkin, I.R.; *Matrix Isolation Techniques*, Oxford University Press, New York, **1998**.

[57] See, for example: Moskovits, M.; Ozin, G.A.; *Cryochemistry*, Wiley, New York, **1976**.

[58] Carstens, D.H.W.; Kozlowski, J.F.; Gruen, D.M.; *High Temp. Sci.*, **1972**, 4, 301.

[59] Knight, L.B. Jr; Gregory, B.W.; Cobranchi, S.T.; Feller, D.; Davidson, E.R.; *J. Am. Chem. Soc.*, **1987**, 109, 3521.

[60] Chertihin, G.V.; Andrews, L.; *J. Am. Chem. Soc.*, **1994**, 116, 8322.

[61] Zhou, M.; Zhang, L.; Dong, J.; Qin, Q.; *J. Am. Chem. Soc.*, **2000**, 122, 10680.

[62] Hanlan, A.J.L.; Ozin, G.A.; Power, W.J.; *Inorg. Chem.*, **1978,** 17, 3648.

[63] Kauffman, J.W.; Hauge, R.H.; Margrave, J.L.; *J. Phys. Chem.*, **1985**, 89, 3457.

[64] Kauffman, J.W.; Hauge, R.H.; Margrave, J.L.; *J. Phys. Chem.*, **1985**, 89, 3541.

[65] See, for example: Mitchell, S.A.; Blitz, M.A.; Siegbahn, P.E.M.; Svensson, M.; *J. Chem. Phys.*, **1994**, 100, 423.

[66] Zhang, L; Dong, J.; Zhou, M.; *J. Phys. Chem. A*, **2000**, 104, 8882.

[67] Zhang, L.; Shao, L.; Zhou, M.; *Chem. Phys.*, **2001**, 272, 27.

[68] Zhou, M.; Dong, J.; Zhang, L.; Qin, Q.; *J. Am. Chem. Soc.*, **2001**, 123, 135.

[69] Kasai, P.H.; McLeod, D. Jr.; *J. Am. Chem. Soc.*, **1975**, 97, 6602.

[70] Kasai, P.H.; *J. Am. Chem. Soc.*, **1983**, 105, 6704.

[71] Ozin, G.A.; Huber, H.; McIntosh, D.; *Inorg. Chem.*, **1977**, 16, 3070.

[72] McIntosh, D.F.; Ozin, G.A.; Messmer, R.P.; *Inorg. Chem.*, **1980**, 19, 3321.

[73] Ozin, G.A.; Power, W.J.; *Inorg. Chem.*, **1977**, 16, 212.

[74] Huber, H.; Ozing, G.A.; Power, W.J.; *J. Am. Chem. Soc.*, **1976**, 98, 6508.

[75] Ozin, G.A.; Power, W.J.; upton, T.H.; Goddard, W.A. III.; *J. Am. Chem. Soc.*, **1978**, 100, 4750.

[76] Merle-Mejean, T.; Cosse-Mertens, C.; Bouchareb, S.; Galan, F.; Mascetti,J.; Tranquille, M.; *J. Phys. Chem.*, **1992**, 96, 9148.

[77] Lee, Y.K.; Hannachi, Y.; Xu, C.; Andrews, L.; Manceron, L.; *J. Phys. Chem.*, **1996**, 100, 11228.

[78] Cho, H.G.; Andrews, L.; *J. Phys. Chem. A.,* **2004**, 108, 6272.

[79] Hanlan, A.J. L.; Ozin, G.A.; Power. W.J.; *Inorg. Chem.*, **1978**, 17, 3648.

[80] Ozin, G.A.; Hanlan, A.J.L.; *Inorg. Chem.*, **1979**, 18, 1781.

[81] Locke, S.A.; Shevlin, P.B.; *Organometallics*, **1984**, 3, 217.

[82] Cardenas, T.G.; Shevlin, P.B.; *J. Org. Chem.*, **1984**, 49, 4726.

[83] Cardenas, T.G.; Shevlin, P.B.; *Organometallics*, **1986**, 5, 784.

[84] Kafafi, Z.H.; Hauge, R.H.; Margrave, J.L.; *J. Am. Chem. Soc.*, **1985**, 107, 7550.

[85] Yamada, Y.; Katsumata, K.; Ono, Y.; Yamaguchi, K.; *J. Radio. Nuc. Chem.*, **2003**, 255, 419.

[86] Lee, Y.K.; Manceron, L.; Papai, I.; *J. Phys. Chem. A.*, **1997**, 101, 9650.

[87] Cho, H.G.; Andrews, L.; *J. Phys. Chem. A.*, **2004**, 108, 3965.

[88] Cho, H.G.; Andrews, L.; *J. Phys. Chem. A.*, **2004**, 108, 10441.

[89] Cho, H.G.; Andrews, L.; *J. Phys. Chem. A.*, **2007**, 111, 5201.

Chapter 3

Experimental and theoretical methods used for the analysis of reactions involving transition metal centres with organic substrates

3.0 Overview of Technical Section

The following sections represent a general overview explaining a typical experiment using matrix isolation spectroscopic techniques for the study of transition metal centres reacting with small molecules. Included is a general outline describing the experimental system used to generate the results presented in the following chapters, and some of the necessary aspects (such as theoretical methods) involved in analyzing and interpreting the results. As these experimental and theoretical details are presented as a general contextual overview, the introduction of additional aspects specific to a reported set of results will be presented in sections of the results chapters that follow.

3.1 Basic Experiments in the Matrix Isolation System

The basic experimental procedure that is used throughout this work for studying the reaction of transition metal atoms with hydrocarbons is relatively

simple: Gas-phase metal atoms are generated by resistively heating a thin strip of pure metal to the vacuum vaporization point of the particular metal in question. Metal atoms vaporize from the filament and, once formed, these metal atoms are mixed with a flow of excess rare gas which contains a fixed concentration of a hydrocarbon of interest. The rare gas, containing the metal atoms and hydrocarbon, is then directed toward the surface of a spectroscopic window maintained below the freezing point of the rare gas being used. As this mixture encounters the surface of the cold window, the excess of rare gas atoms begin to condense. As a result, the metal atoms, hydrocarbons, and any intermediate reaction products are subjected to repeated collisions with the rare gas. When collisions of metal atoms with the hydrocarbon reagent lead to intermediate reaction products, energy released during the chemical reaction is retained within the chemical system as internal energy. This conserved internal energy is stored in vibrational, rotational, and translational modes of the excited intermediate(s). As these energized intermediates are in the presence of the relatively high pressure of the excess rare-gas during condensation, repeated collisions of the energized species with the rare gas results in dissipation of the excess energy to the bath of rare gas-atoms. Following complete condensation of the gas-mixture, excess reagents, reaction products, and stabilized intermediates are trapped inside a cage of rare gas atoms referred to as the matrix. Since the composition of the matrix is primarily the rare gas atoms in most cases, this allows various forms of spectroscopy to be used. For example infrared and ultraviolet visible spectroscopic methods allow for the investigation of the species trapped with the

matrix. The analysis of these spectra can provide vital information about mechanistic aspects of reactions under study. Additional techniques in which energy can be introduced into the system either thermally, or through introduction of photons, can further the reaction allowing for the characterization of additional products and reaction processes. Furthermore, variation in concentration of any of the reagents codeposited with the rare gas can also provide additional information on the overall reactivity and mechanistic steps involved in a particular chemical reaction. In order to further understand the specifics of matrix isolation experiments it is first necessary to understand the nature of the matrix equipment used, which can be very particular to the type of reactions under study. In the following sections, a general experimental matrix isolation apparatus is described, with additional details for the particular furnace assembly necessary for studying reactivity of transition metal centres in matrices.

3.1.1 Experimental system for studying transition metal reactions

A variety of different experiments can benefit from employing the technique of matrix isolation, and a brief discussion of these has been summarized previously by Dunkin.[1] Examples directly relevant to this work include the generation and reaction of metal atoms by direct thermal vaporization, by laser ablation of solid metal targets, or by sputtering metal target sources. In general, the technique is suitable for the stabilization and isolation of high energy intermediates in overall reaction processes, and as such the differences in specific matrix isolation apparatus arise due to the nature of the specific type of chemistry under study. In the three listed examples, the nature of

metal atom generation is very different, however, the general design of the matrix isolation systems used in each case is qualitatively similar. In this section, an outline of the key components necessary to perform successful matrix isolation experiments is presented. In the context of this description, the key components which will be used to generate subsequent results will be highlighted. In this manner, it will be possible to outline those parameters which can be tuned in order to produce the different experimental techniques implemented throughout the course of this work.

3.1.2 The vacuum system used for matrix isolation experiments

The vacuum system used for all portions of this work consists of three main regions: 1) Vacuum pumps for maintaining the low pressure environment of the system, to eliminate experimental impurities and help maintain cryogenic temperatures, 2) a gas-sample introduction area used as a reservoir of source gas for preparation of the matrix, and 3) the cold tip and associated refrigeration unit to achieve cryogenic temperatures, on which matrix formation and spectroscopic analysis occurs. A simplified schematic diagram of the overall matrix system is given as Figure 4. In the following sections, the individual components will be described, to explicate their use in the overall experiments.

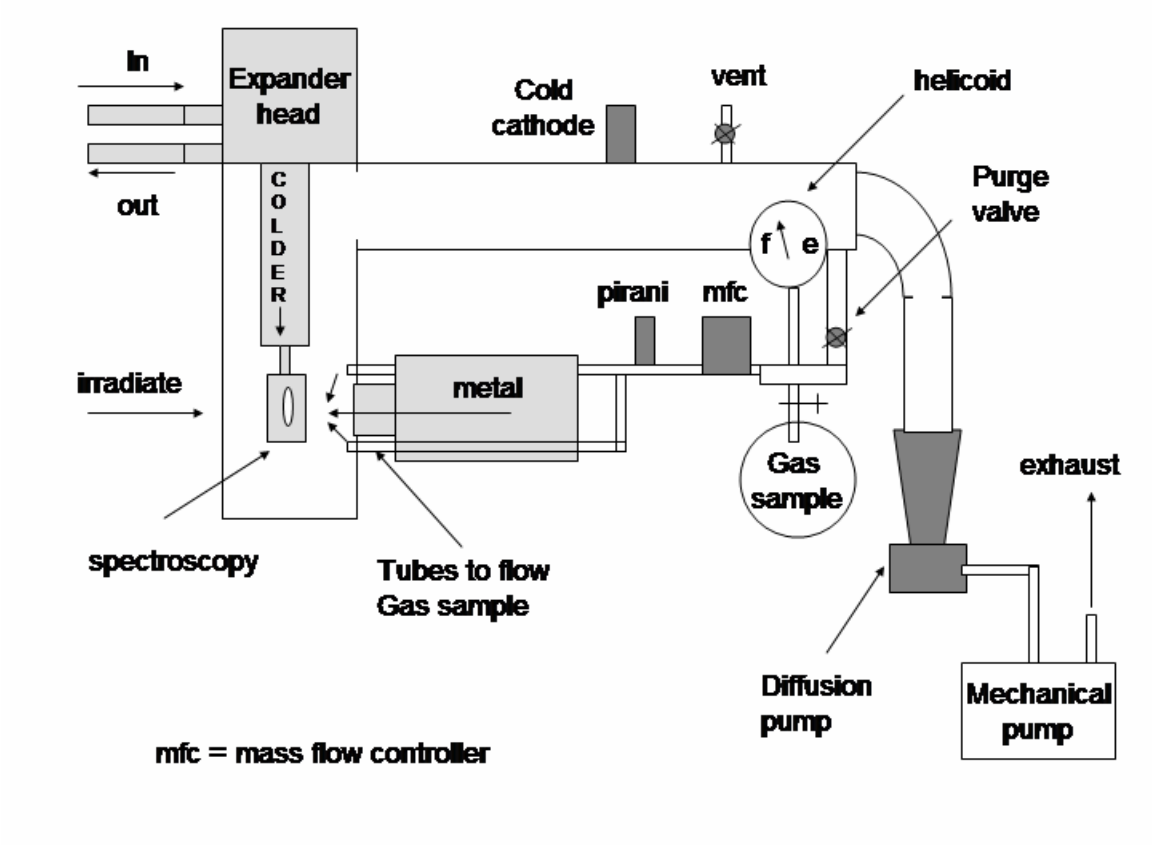

Figure 4: Schematic diagram of the general matrix isolation experimental apparatus used for studying transition metal centres reacting with hydrocarbons. The orientation of the bottom tip of the expander head can be rotated to deposit a sample on the flat surface, for acquiring spectra, or for irradiation of the matrix.

3.1.2.1 Achieving vacuum conditions: pumps

Vacuum conditions are achieved using two stages of pumping. The first stage, a mechanical rotary pump (model Edwards E2M2), provides the basic pumping necessary to achieve low vacuum conditions. Using this pump to evacuate the system only, typical pressures of 10^{-2} to 10^{-3} Torr[3] can be achieved. The pressures in this range are measured using a pirani guage, located near the outlet where gas flows to the matrix (labeled "pirani" in Figure 4). The position of this gauge is convenient, since the gauge can monitor the flow of gas passing by the pirani during matrix deposition. Alternatively, when cleaning the system, this gauge indicates the pressure within the system, and can be monitored during re-evacuation to ensure no major leaks are present in the vacuum system. When additional pumps are used, this gauge is read to ensure the system has reached a threshold pressure prior to activating the second stage of pumping. Although five orders of magnitude lower in pressure than atmospheric pressure, these pressures are not low enough to generate conditions that give successful matrix isolation experiments. If an experiment is performed under these conditions, the sample region is inundated with the trace amounts of atmospheric gas, and vapours which stream back from the oils used to lubricate and seal the mechanical pump. These contaminants ultimately end up in the spectroscopic region, and interfere strongly, either through parallel reaction processes, or

[3] The pressure gauges in all systems are measured in units of Torr, and as such measured pressures are in these units. Thus, all pressure units quoted in this thesis will be in Torr units.

congestion in spectroscopic results. As well, the high pressures within the system result in significant numbers of collisions of molecules with the interior of the matrix system. When the matrix isolation system is cooling, the high number of collisions, even at 10^{-3} Torr, results in significant thermal transfer to the matrix tip, making cryogenic temperatures much more difficult to achieve. Thus, it is imperative when using this type of design to introduce a second stage of pumping to further reduce the pressure of the vacuum system, and minimize these interferences.

In the particular system used for these experiments, a diffusion pump is used as the secondary pump, connected between the main vacuum chamber and the mechanical pump (see Figure 4). A basic diffusion pump consists of a pan at the bottom of the unit that, in our experiments, contains silicon-based oil. The pan is heated to vaporize the oil, and the resultant vapor is streamed through jets at the top of the pump assembly. The pump is cooled via a water-assembly that ensures the top of the pump wall is very cold, with a decreasing thermal gradient leading down toward the oil pan. As a result, the aerosol of sprayed oil is instantly cooled at the top of the pump, and the oil vapor rapidly condenses, returning to the oil pan. This process cycles as long as the heat to the diffusion pump oil pan is maintained. Since there are no mechanical parts on the interior of the pump, this class of pump is extremely robust, simple, and requires relatively little maintenance once operable.

Under normal operation, the top of the diffusion pump is open to the main vacuum system. A gate valve connecting the main vacuum system and the

diffusion pump is often used to isolate the system from the pump, when maintenance in the vacuum chamber is performed. When the gate-valve is in the open position, molecules leaving the vacuum system and entering the diffusion pump region are pushed toward the cold wall by momentum transfer, and become trapped in the condensing oil, and removed down to the oil pan. From the oil pan, the simplest route out of the vacuum system is the connection leading to the mechanical pump, which is ultimately exhausted to atmosphere. Using this method of pumping, the 10^{-2} to 10^{-3} Torr pressures which can be maintained by pumping with the mechanical pump only, can be significantly reduced to 10^{-7} to 10^{-8} Torr, fairly easily. These pressure conditions are monitored using a cold cathode ion gauge, which can measure pressures down to 10^{-9} Torr. Normally, this sensitive gauge is only active when the system is below 10^{-4} Torr, and is otherwise turned off, when the pressures inside the system are beyond this threshold.

One major downside to the diffusion pump is the increased temperatures at the oil pan, and that the silicon based oil can be reactive with gas-sample impurities. These factors make the pump region quite sensitive to oil decomposition, especially to molecules which contain oxygen. Significant introduction of oxygen directly into the pump can result in the catastrophic destruction of the pump oil, leading to silicon dioxide based products, and requiring significant maintenance to restore pump operation. To avoid this maintenance, whenever significant pressures ($> 5 \times 10^{-2}$ Torr) of gas are introduced into the main vacuum system, the diffusion pump can be bypassed by

connecting the main vacuum system directly to the mechanical pump. Evacuating the system with the mechanical pump until a base pressure lower than the threshold pressure is attained is thus a general precautionary measure. Once this threshold pressure is achieved, the diffusion pump can be opened to the main vacuum chamber once again, returning to normal operation.

Other means of pumping the system, and of monitoring the pressure do exist. In some cases, turbo molecular pumps are used in place of the diffusion pump, although these pumps provide similar pumping efficiency, but lack some of the simplicity of the diffusion based pumps, and require more care and maintenance. The major benefit of diffusion pumps is the lack of mechanical parts, unlike the comparatively complicated turbo molecular pumps. This means that diffusion pump based systems can be left unmonitored for prolonged periods, allowing the system to achieve much higher quality vacuum conditions. As well, there exist many other forms of gauge for measuring pressures, however, these provide similar monitoring capacity to the gauges employed here, and will therefore not be dealt with directly in this work. Excellent summaries of both the pumps and gauges used in various applications are given in Dunkin's book.[1]

3.1.3 Gas-sample introduction region

Gas-samples used in these experiments are prepared on a standard gas handling line, using protocols described below. Once prepared, a gas sample is connected to the matrix system at the marked position in Figure 4. A valve isolating the vacuum system from the entry point of the gas-sample protects the

vacuum system from introduction of significant atmospheric gas during the exchange of various gas-samples. Similarly, a second valve in the gas-sample region provides a channel for gas to flow to the pump. This channel is used when purging the system of gas-samples, between experiments. During an experiment, this purge valve is closed, to ensure that the gas-sample under study is not immediately lost by evacuation through the pump. The total pressure remaining in the gas-sample bulb can be measured, quantitatively, with a Helicoid gauge, indicated in Figure 4. As the gas-sample is depleted, the reading of this gauge decreases, and thus measuring the pressure of this gauge before and after an experimental run provides one estimate of the total gas deposited on the matrix tip.

The flow of matrix gas-sample to the cold tip is maintained with an MKS 1100 series mass-flow controller. This electronic valve can be tuned to a fixed set point of gas-delivery, and will flow gas at the fixed rate while engaged, or until the pressure in the gas-sample bulb depletes below a threshold value (~200 Torr). The duration of flow and the flow-rate set-point provide a second estimate of the total gas flowed during a matrix experiment. The set point for the mass flow controller is based upon a calibration factor for a reference gas. Since the majority of our matrices are prepared using argon, the electronics are generally calibrated to flow Ar gas, unless otherwise specified. However, as our samples contain reagent gases diluted in Ar, the proper calibration factor that would need to be employed does deviate from the calibration factor for pure Ar. This deviation increases with higher partial pressures of the reagent in our samples.

Thus, in quantitative estimates of the matrix sample deposited, calculations based on the mass-flow controller set point can contain small errors. However, for qualitative experiments involving the same matrix gas-composition, replicate depositions are effectively similar. Since the majority of experiments performed in this work are qualitative in nature, the errors associated with small deviations in calibration factor have been generally ignored.

When the mass-flow controller is activated, the gas-sample flows through copper pipe, past the pirani gauge, toward the matrix tip. When the compressor cooling the matrix tip is active, and the matrix tip is at its coldest temperatures, the gas-sample condenses on the surface of the matrix tip, and spectroscopic analysis can be performed. Additionally, under conditions where metal atoms are deposited simultaneously with the matrix gas-sample, the metal atoms and matrix gas are mixed in the region immediately prior to condensing on the matrix tip surface. Although the majority of the gas that enters the matrix system in this region is expected to condense on the matrix tip, there is always some evidence on the pressure gauges indicating that a very small fraction of the gas is able to escape toward the pump. However, this fraction is negligible compared from the faction that condenses on the tip, and thus, any calculations involving the amount of material deposited on the matrix surface assume a unit efficiency for gas sticking on the matrix tip. Once a sample is prepared on the surface of the matrix tip, it is possible to rotate the matrix expander head 90^{o} or 180^{o} from the matrix deposition position, to perform spectroscopic analysis, or to irradiate the sample with light from an external light source, as described below.

3.1.4 Achieving cryogenic temperatures at the matrix tip

Many of the original matrix isolation experiments employed cooling systems which were very simple mechanically, such as the use of liquid nitrogen, or liquid helium to cool the matrix tip. Although these cryogenic fluids were very simple to use, the rapid boil off allows experiments to be performed only on a matter of hours. Also the chronic need for additional cryogenic fluids becomes expensive, particularly in the case of using He, when extremely low temperatures are required. Even with methods of recovery of the boiled gas, these cryogenic fluid based systems require extensive work. As a result, closed cycle refrigeration units have been developed which can achieve cryogenic temperatures with very minimal loss of fluids used to maintain cooling.

In Figure 4, the expander head region is connected to a helium compressor at the indicated in/out ports. While operating, the helium compressor forces high pressure helium into the expander head system. Once the helium is in the reduced pressure of the expander head, the controlled expansion of the gas throughout the expander assembly results in the cooling of the expander head as a first step. A rotating valve controls the direction of gas-expansion, through two stages. In the first stage, gas is allowed to expand throughout the expander head assembly as explained in detail by Dunkin.[1] Once complete, the rotating value is moved to a second position, where the gas is free to flow back into the compressor unit, recycling the gas for continued use. As a result, the entire expander head unit is slowly cooled to the working temperature of the apparatus. Complete cooling from room temperature requires approximately one

hour for a standard unit. Additionally, once cooled, this type of cooling can be maintained for as long as the compressor is engaged, and thus experiments can be performed over many hours or even days. The only downside of these compressors, compared with the use of cryogenic fluids to maintain temperatures, is the loud noise associated with the compressor during operation. However, the conveniences of low maintenance overwhelm this disadvantage dramatically.

As the compressor and expander head age, the components on the interior of the expander head undergo associated wear, and the minimum working temperature of the system will slowly increase. These components can be maintained or replaced, allowing the system to once again achieve lowered temperatures. Compressors based on this design exist that can reach temperatures as low as 4 K, although, the specific refrigeration units used in this work achieve temperatures near 13-18 K. These temperatures are low enough to condense Ar, the matrix host predominantly used throughout these experiments, and cooling below this temperature has only moderate advantages. Some analysis of the impact of sample deposition temperature is given in the results sections, when important.

3.2 Spectroscopic analysis of formed matrices

One of the major advantages to the matrix isolation technique lies in the fact that, once formed, the rare-gas matrices can be maintained for relatively long times, and can be interrogated with a variety of forms of spectroscopy. In this work, matrices contain transition metal atoms, which are ideally suited for

observation using ultraviolet-visible spectroscopy. Understanding the transitions associated with atoms isolated in matrices allows for irradiation of the matrix with wavelengths corresponding to absorptions of the isolated transition metal centres. By this technique, energy can be introduced into the system, allowing the possibility of observation of reactivity of excited state species.

In order to further understand the reaction of transition metal centres with hydrocarbons, infrared spectroscopy is used as a complementary technique. Since the hydrocarbons under study undergo metal-mediated transformations from one structural form to another, the structural characterization aspects of infrared spectroscopy become very valuable. In the following sections, the use of these techniques in specific matrix isolation experiments will be described, and technical aspects required to facilitate the coupling of matrix preparation, matrix irradiations, and spectroscopic analyses will be considered.

3.2.1 Apparatus considerations for use of spectroscopy and irradiation

In order to perform spectroscopic measurements in a typical matrix isolation experiment, two factors must be considered: 1) The composition of the spectroscopic window on which the matrix is deposited, and 2) the composition of the outer windows on the matrix isolation apparatus. Ideally, these three materials will be identical to each other, and identically matched to any optics used in the associated spectrometers, to minimize losses due to scattering of light. Additionally, these windows must be made of materials that will be free of absorptions in the range of light used in the type of spectroscopic measurement for a given experiment, in order for results in that range to be obtained. In the

sections below, two main types of spectroscopy will be described, specifically ultraviolet visible (UV-visible) and infrared (IR) spectroscopy.

For UV-visible spectroscopic analysis, one of the best choices of window is high quality UV-quartz, which has full transparency throughout the UV and visible regions. This material is also quite durable, making for a very robust spectroscopic window. However, UV quartz is composed of silicon dioxide and thus simultaneous measurements through these windows with IR spectroscopy is practically impossible due to large absorption bands associated with quartz throughout the mid IR (1500-500 cm^{-1}). An alternative to quartz is the use of potassium bromide (KBr) windows. KBr windows have the advantage of being transparent in the UV-visible range, and additionally, they have an infrared transparency from 4000 cm^{-1} to 400 cm^{-1}, the major mid-IR range used for structural determination. As a result, it is possible to do simultaneous UV-visible and IR measurements on the same matrix sample. However, KBr is slightly hygroscopic, and thus the outermost windows of the matrix system decompose slowly over time, reducing their transparency, and thus the quality of the spectrum. So, wherever possible, quartz windows have been used for UV experiments, to achieve the best data.

Similarly, when IR experiments were performed, the spectrometer used employed CsI optics, which have an infrared transparency from 4000 cm^{-1} to 200 cm^{-1}. In most infrared experiments, CsI windows were employed, although some experiments involve a KBr window as the window attached to the cold substrate. The IR source power in the 400 to 200 cm^{-1} region is very weak, so, these slight

differences are not very significant. The major advantage of CsI over KBr is the softness of the CsI material compared to the brittleness of KBr. Thus, when tightening windows where CsI is present, there is much less likelihood of generating a crack that will undermine the cooling or vacuum properties of the system. Nevertheless, CsI is much more hygroscopic than is KBr, and thus CsI windows degrade more quickly, and become cloudy. This degradation causes mostly scattering of visible light, and leaves the mid IR range mostly unaffected, excepting extreme cases, and so the resiliency of CsI compared from KBr in matrix infrared experiments is an extreme benefit.

Since a dedicated IR spectrometer to the matrix system in which UV-visible experiments were performed was not always available, it was frequently necessary to perform separate experiments on duplicate matrix apparatus, each with their own dedicated spectrometer. In such a way, replicate experiments are compared from separate “nearly identical” systems. While it is reasonable to assume that the two systems provide the same results, it is important to note that the measurements acquired in this way are not made on identical matrix samples. As a result, it is not always possible to rule out variations in the chemistry on different matrix systems, that arise due to leaks, variations in temperature, or apparatus design.

Finally, a section describing the irradiation of samples is described below. Irradiation involves shining broadband or wavelength filtered light directly on the prepared matrix sample. The irradiation is performed through a window perpendicular to the spectroscopic measurements, and thus, this window needs

only allow light from the lamp to be introduced into the sample. As a result, this window is typically UV quartz, to eliminate the possibility of degradation over time.

3.2.2 Ultraviolet visible (UV-visible) spectroscopic analysis

Most of the experiments performed in which the detection method was ultraviolet visible spectroscopy were performed on a duplicate matrix isolation experimental assembly. This second system had the capability of reaching temperatures of 13K, and employed quartz or KBr windows. Specific cases where the nature of the window is important are indicated in the text, as appropriate. In general, all spectra acquired using UV-visible spectroscopy have been acquired using a Cary 1 UV-visible slit-based double-beam spectrometer, in absorption mode. Spectra were acquired in double beam mode, referenced to air. All spectra were collected under baseline correction mode, using an initial baseline spectrum of the cold spectroscopic window, prior to deposition of any gas to form the matrix. Typical acquisition parameters involve single beam widths of 0.5 mm, averaging time of 0.2 s, and a data collection interval of 0.4 nm. These parameters result in spectral acquisition speed of approximately 120-150 nm per minute, and thus a typical spectroscopic acquisition requires about 6-10 minutes, under these conditions.

The particular spectrometer employs two radiation sources, and rotating wavelength filters, in order to scan all wavelengths during spectral acquisitions. The visible source is a tungsten lamp, and the ultraviolet source is a deuterium lamp. Lamp changeover occurs in the region of 350 nm, where the power of the

visible source is becoming very weak, and the power of the overlapping deuterium source begins to become stronger. Some spectra show evidence for the lamp changeover near 350 nm, and where these artifacts are observed, a note is given in the figure caption.

Unlike the infrared experiments described below, UV-visible spectroscopic experiments suffer significantly from scattering of light, however, the spectrometer can observe products in the matrix under much shorter deposition times. Thus, typical UV-visible sample matrices are grown for a period of approximately 30 minutes of deposition. In all cases, spectra are acquired in a range of 800 to 200 nm, although frequently the visible region has few absorption bands for metallic systems. Absorptions in this region tend to indicate the presence of metal dimers or small clusters, or other metal-dependent products.

3.2.3 Infrared spectroscopic analysis

Most of the experiments employing infrared spectroscopy were performed on a separate matrix isolation system, nearly identical to the apparatus used for the UV-visible experiments. The only main difference between the two experimental systems is the deposition temperature, which was much higher (17K) for some experiments where infrared spectroscopy was used. In all cases, infrared spectra were collected in absorption mode, over the range 4000 cm^{-1} to 200 cm^{-1} at 1 cm^{-1} resolution, using a Bomem Michelson MB 102 Fourier transform infrared spectrometer and Bomem/Grams32 software. The digitized spectra were saved to disk by the software program as data points, and various

baseline corrections, peak integrations, or other file manipulations such as spectral subtractions were sometimes used to analyze data.[4]

Where used, measurement of absorption peak areas has been performed by using the Bomem/Grams32 software integration option. In cases where qualitative comparisons are made, replicate measurements following experimental changes to the system have been made by ensuring the left hand and right hand integration points are identical. Generally, differences smaller than a threshold of 0.001 units are not considered significant.

By far, the spectral subtraction technique wherein the subtraction of two "adjacent" spectra of the same matrix to yield a "difference spectrum" associated with an experimental change (such as irradiation or annealing) is one of the most common methods used for the interpretation of data. Since the two spectra are recorded from the same matrix sample, the difference of the absorption spectra for the "after change" minus "before change" cases gives a difference spectrum reflecting growth or losses of absorption features in the matrix due to the applied change. When used, figure captions highlight the use of difference spectra. Because of the high reproducibility of spectral acquisitions in the matrix sample, difference spectra can often be very sensitive, and can sometimes be used to see small changes as small as 0.001 absorbance units.

---

[4] Whenever baseline corrections, peak markings, or other modifications to the initial spectra were performed, a copy of the data was made to ensure that the original spectrum was preserved.

A special case of difference spectrum arises when comparing the absorption spectrum of a matrix formed without the presence of metal, with the corresponding matrix formed codeposited with metal. In this case, the difference spectrum is of two separate matrices, which are formed under identical conditions, but are not the same matrix. Instead, the matrices are representative duplicates of each other, with the non-metal matrix representing a control, or reference.

The primary use of infrared spectra in this work is for the exact identification, or partial characterization, of structural aspects of reaction intermediates and products formed when transition metal centres react with small molecules. As a result, group frequency approaches are used, and careful consideration and comparison of infrared spectra with those acquired from similar reaction systems is of extreme benefit. Additionally, the use of isotopes can help substantially when identifying absorption modes in the IR that are associated with specific nuclei.

3.2.4 Cleaning protocols for optical clarity in spectra

After a matrix experiment is completed, the compressor is turned off, and the temperature of the cold tip begins to rise. As a result, a matrix formed on the spectroscopic window correspondingly warms, eventually evaporating. During this evaporation process, species in the matrix are free to move, and in the case of metal atoms, aggregation and clustering occurs. While the majority of isolated species sublime from the matrix, and are pumped away to vacuum, metallic species in the matrix can sinter causing aggregated metal particles to

accumulate on the surface of the spectroscopic window. These aggregated particles can cause significant scatter of the light emanating from the spectrometer source. This effect is particularly significant at longer wavelengths, and can significantly degrade the quality of results in higher energy IR and in UV-visible experiments. Thus, between successive matrix experiments, it is necessary to open the matrix system and clean the spectroscopic window, to ensure high quality spectroscopic results for all experiments.

Cleaning protocols for spectroscopic windows in specific matrix isolation experiments have been described by Dunkin.[1] In the experiments described in this work, the simplest method for cleaning the windows is to wipe the surface of the spectroscopic window on both sides with a small amount of liquid methanol or ethanol absorbed in a lint-free tissue. The vapour pressure of these materials ensures that they vaporize easily under vacuum, and do not reside within the matrix system and arise as impurities in further matrix experiments. In cases of extreme matrix surface contamination, liquid water can be used in place of either of the alcohols, as this method dissolves a layer of the CsI surface, and scrapes off any surface metal aggregates very efficiently. In either case, matrix spectra acquired following cleaning of the window are of much higher quality than those when the system has not be cleaned.

3.3 Temperature control: thermal annealing of matrices

Each matrix system is equipped with a temperature sensor that can measure the temperature near the matrix tip. For the experiments performed on the infrared system, the temperature sensor measures the temperature close to

the matrix tip, near the region where the system is coldest. Typical temperatures on this system have ranged from 15 to 17K, as the system ages.

The temperature controller which displays the system temperature also functions as a resistive heater, capable of supplying heat directly to the matrix tip. When engaged, the heater supplies energy to the tip, outstripping the cooling capacity of the expander head, and raising the temperature at the matrix tip to a fixed set point. Thus, any given matrix can be raised in temperature to a fixed value, thereby increasing the available thermal energy to all species isolated in the matrix. After the system has been increased in temperature for a few moments, the heater can be switched off, allowing the compressor to remove the excess thermal energy and returning the system to the minimum temperature, re-establishing the structure of the matrix. This increase of temperature, followed by re-cooling is known as thermal annealing of the matrix.

Although the increase in temperature as a result of thermal annealing of the matrix is generally insufficient to allow reactive collisions furthering reactions, the increase in temperature can be enough to allow small variations of conformation or aggregation within the matrix. Thus, conformational changes of isolated molecules, or exchanges between kinetically and thermodynamically favoured trapping sites within the rare gas crystal can occur. Typically, these changes result in very slight shifts in matrix spectra. However, in some cases, similar molecules can be trapped in different sites within a matrix cage. Unlike the gas-phase, where these similar molecules would all give rise to the same absorption spectrum, the different interactions with the various matrix trapping

environments can cause shifts in the absorption of the molecules in the spectrum. Annealing the matrix can cause unstable trapping sites to convert into thermodynamically stable sites, which in turn can cause losses of some product bands, with a corresponding sharpening of the stable major product band. Thus, in cases where a number of features are observed in a given spectrum around the same absorption position, thermal annealing is often used as a technique to eliminate matrix *'sites',* thereby clarifying fundamental absorption positions of matrix-isolated species.

3.4 Gas flow-rate: Rate of matrix gas deposition

Another variable in matrix experiments is the rate of introduction of the matrix sample onto the surface of the cold tip. The rate of gas-sample introduction is controlled with a mass flow controller (MKS 1100 series), as described above. The range of flow rate of gas used in these experiments varies from 0.5 sccm (**s**tandard **c**ubic **c**entimeters per **m**inute) to 5.0 sccm. These values correspond to approximate values of 1.0 to 10.0 mmoles of total gas per hour. In general, no major effects are observed in recorded spectra under any flow conditions, other than an increase in the amount of absorbing species under higher flow. The trend in integrated area of an absorption band for a given species is consistent with a linear increase in flow rate, as would be expected. However, it is worth recognizing that the initial transfer of thermal energy to the tip increases with higher flow rate of gas, since the higher flow rates correspond to higher densities of gas encountering the cold tip per unit time. C

Correspondingly, the time it takes for a matrix to condense would be

expected to increase with increased flow rate. As a result, it might be expected to observe different chemistry at different flow rates, corresponding to greater extents of reaction time, or greater diffusion in matrices formed at higher flow rates. In cases where these effects are significant, a note will be made in the text to account for this phenomenon.

3.5 Irradiation of preformed matrices

Once isolated in the matrix, most species are trapped such that they cannot undergo further chemical transformations directly, due to the limitations of available thermal energy. However, photochemical excitation can promote reactivity by directly imparting energy into the system, without direct thermal excitation. Thus, chemical reactivity of species can be observed following excitation with various wavelengths of light. In the gas-phase, these excitations and subsequent reactions could be quite exothermic, resulting in significant decomposition or several subsequent reaction steps. However, the stabilizing nature of the matrix environment can dissipate the excess internal energy efficiently, especially in the condensed phase, and thus photochemical induced intermediates can be relatively easily observed.

The easiest method to observe absorptions of species in the matrix is to record the UV-visible spectrum of isolated products. However, molecular products generally have broad, featureless absorptions in their UV-visible spectra, which are difficult to characterize when these species are present in low concentrations. These features can often be very similar to the absorptions of the reagent species, as well, and thus direct characterization using UV-visible

spectroscopy is quite difficult. In practice, only metal atoms, and small metal clusters show appreciable and easily identifiable UV-visible absorption spectra. Therefore, UV-visible spectroscopy is not always easily used for understanding photochemical excitations.

The controlled introduction of light into the system can be performed using a broadband irradiation source, and series of bandpass cutoff filters, which restrict the transmission of light to specific wavelengths. In these experiments, controlled irradiations have been performed by using a Kratos LH-150W Hg arc lamp, and various bandpass filters as specifically indicated, where used, in the text of the results sections. Generally, this method can be used to understand the photochemical behaviour of species isolated in the matrix. The systematic use of bandpass filters which restrict the transmitted light from low energy to high energy allows for an exploration of photochemically induced reactions. Recording spectra following each irradiation of the matrix allows for the observation of bands associated with products generated through photochemical excitation. When no products have been observed, the next wavelength range can be introduced, and following irradiation, the spectrum recorded.

It is worth noting that, in these cases where bandpass filters are used to photochemically generate products, it is possible for the generated product to have an absorption falling in the wavelength region transmitted by the bandpass filter. Thus, it may not be possible to observe the product directly, if the excitation of the product leads to reversion of that product to reactants, or to decomposition of the product via some alternative reaction channel. If exact

excitations can be known, it is thus preferential to use a monochromator that selectively excites the reagents, allowing for the build up in the matrix of any photochemically generated products. However, as mentioned previously, it is difficult to know the exact absorptions of the products, and thus, the use of photochemical techniques in matrix systems can be difficult, although valuable.

3.6 Furnace Assembly used for deposition of metal atoms

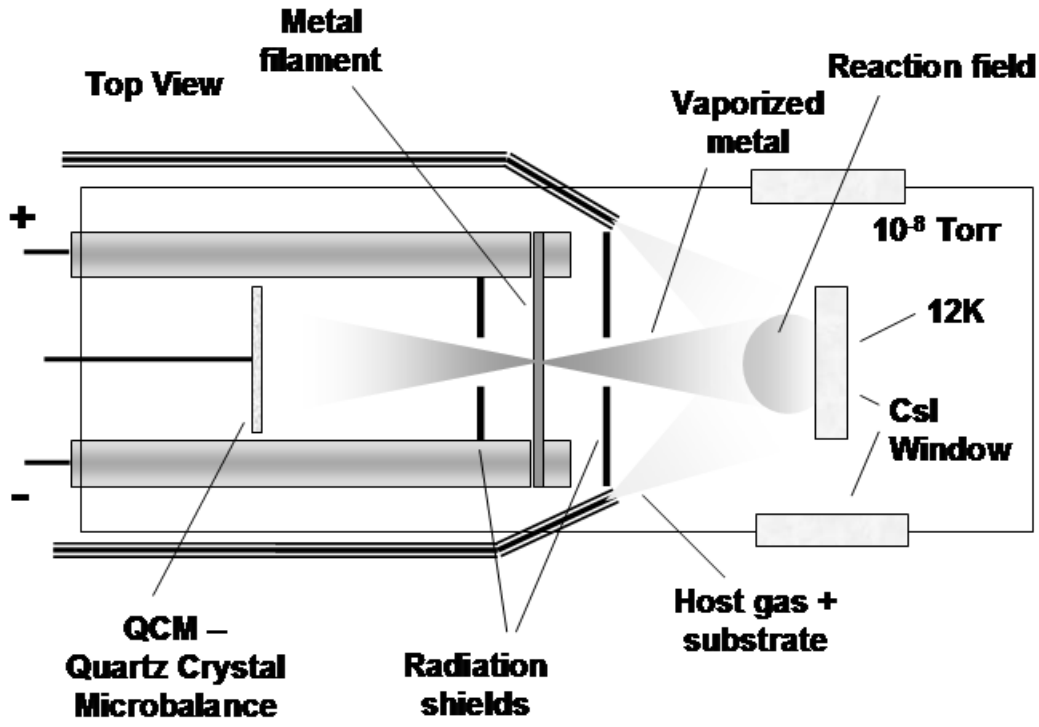

Figure 5: Schematic of the interior of the metal furnace assembly used for generation of gas-phase metal atoms in the matrix isolation apparatus. The electrodes and metal filament are cooled with water during metal deposition.

In Figure 5, a basic schematic of the furnace assembly used for the vaporization of metal atoms from a variety of metal sources (listed below) is given. The basic design uses current from a variable AC power supply, which runs through water-cooled copper electrodes that serve both as the holder and coolant of the metal source. A variety of metal sources, described below, can be used in this design, as it is sometimes necessary to use different vaporization methods for different metals. In all cases, as the current is increased, the temperature near the centre of the metal source increases, as this is the point furthest from cooling by the electrodes. When this region reaches the vaporization temperature of the metal, metal atoms begin to directly vaporize. Vaporizing metal comes from the source of vaporization in all directions, and the metal can be collected in the flow of gas reaching the cold window, and simultaneously on the quartz crystal microbalance, described below. The distance between the metal source and the matrix system, and the metal source and quartz crystal microbalance is equal. Thus, the amount of metal collecting on the matrix surface can be approximately represented by the amount of metal reaching the quartz crystal microbalance. As metal condenses with the matrix sample gas and entrained reagents, spontaneous reactions can occur, and stabilized reaction intermediates, reaction products, and remaining reagents become trapped in the matrix following condensation.

Once vaporization has begun, increasing the current will cause additional vaporization of metal, which can be used as a means of increasing the flux of metal atoms into the matrix system. This method can be used to increase metal

dependent reaction products, but, some care must be taken since there are two major consequential factors to increased metal flux. The first consequence is an increase in the temperature of the metal filament, and the second consequence is the formation of metal-metal aggregates (dimers, clusters) in the matrix.

3.6.1 Blackbody emission from the metal source

The majority of transition metal systems under investigation in this work are the metals of the first transition series, with some metal centres originating from the second transition row. For all of these metals, the vaporization temperatures range from 900 K to greater than 3000 K. The higher temperature species emit a significant intensity of visible radiation, in some cases appearing as white light emission sources, with significant intensity throughout the visible range. The position of the metal source directly in front of the depositing matrix ensures that, during metal deposition, the matrix is bathed in this visible emission throughout the experiment. As a result, metal atoms, reagent gases or reaction products isolated in the matrix can be photoexicted by the spontaneous emission from the filament, unavoidably leading to reaction products formed in the matrix that are a result of the excited state chemistry. When considering reactivity of metal centres, it is always necessary to include the possibility of excited state atomic metal, and possible photochemistry of isolated species. Subsequent experimentation employing a different metal atom source then represents an alternative complementary experimental method, for further exploring the impact of photochemical excitation in proposed reaction steps. Where mechanistic steps involving light emanating from the glowing filament during metal deposition

are invoked in the following chapters, a note will be made to highlight these points.

3.6.2 The quartz crystal microbalance (QCM): quantifying metal flux

Each metal furnace assembly is equipped with a quartz crystal microbalance, in which a crystal with an initial oscillation frequency of about 5 MHz is used as a means of quantifying the metal being vaporized from the filament. A detailed explanation of the technical aspects and utility of the quartz crystal microbalance in this application is given by Moskovits and Ozin in *Cryochemistry*.[2] In general, as metal is deposited on the surface of the electrode on the oscillating quartz crystal, the mass of the crystal begins to increase. The oscillation of the quartz crystal is mass dependent, and, for a given crystal, the measured frequency of the oscillation will decrease by one cycle for approximately every 20 ng of material deposited on the electrode surface. Thus, by knowing the identity of the material being deposited, measurement of the number of cycles that decrease over a fixed unit of time gives a quantitative measurement of the mass of material deposited during that time. In the case of transition metal atoms, the masses of the first transition row are quite similar, and thus typical experiments involve deposition rates corresponding to the decrease of 1 to 10 cycles of metal per minute of matrix deposition. For second row metals, where used, the mass of a given metal atom is approximately twice the mass of its corresponding first row metal, and thus, ranges corresponding to decreases of 2 to 20 cycles were used to give the same relative amount of metal, in a given experiment.

None of the metals used in this study suffered any problems in combination with the quartz crystal microbalance technique. However, the quantification of metal is sensitive to the position of the quartz crystal in its holder, and when improperly aligned, readings can become unstable. Thus, not every experiment can be quantified directly, in terms of exact metal load in the matrix. As well, the lifetime of a quartz crystal is variable with each crystal. Typically, a given quartz crystal will survive a change between 6 and 10 thousand total cycles, before the crystal will no longer function for quantifying metal deposition.

An additional consequence of aging crystals is the absorption of light by the metal deposited on the surface. As the metal is deposited on the surface of the electrode, the shiny silver electrodes become covered in black metallic soot. This black surface absorbs the radiation emitted from the filament during deposition, and causes a temperature increase on the crystal. This temperature increase can interfere with the measurement made by the quartz crystal, leading to inaccurate measurements of the metal being deposited into the matrix. Thus, even in well controlled experiments, it is not always possible to directly know the amount of metal deposited into a matrix. Where possible, matrix UV-visible experiments have been used to determine the composition of metallic species in the matrix, as is demonstrated in the initial results of Chapter 4. As one means of reducing the absorptions and extending the liftetime of quartz crystals, radiation shields can be used which limit the exposure of the electrode surface of the quartz crystal to metal, and to radiation leading to temperature increases.

3.6.3 Radiation shields: Factors affecting metal quantification

In front of the quartz crystal, and at the coupling of the furnace to the cold-tip in the main vacuum system, there is a small aluminum shield with a small hole permitting vaporized metal to pass. These shields, referred to as the radiation shields, restrict the amount of light which is allowed to reach either the surface of the quartz crystal microbalance, or the surface of the matrix cold tip. In both cases, the elimination of this light reduces the contribution of the radiation from the filament to the increase in temperature of the cold tip, or temperature effects on the quartz crystal microbalance that interfere with metal quantification. In most cases, these aluminum shields are identical replicates in both positions. However, in some cases, to extend the lifetime or working range of the quartz crystal, the hole in the radiation shield leading to the quartz crystal is smaller than the hole leading to the matrix tip. Leaving the matrix tip as a larger hole allows for a greater yield of metal to interact in the matrix on condensation, allowing greater yield of products to be observed by spectroscopic analysis.

The only direct impact of this change in radiation shields occurs when quantifying the metal entering the matrix. Since these two radiation shields are equidistant from the metal source, by assuming that the metal source is a uniform distributor of metal in all directions, it is thus possible to make a simple first order correction for the amount of metal deposited in both cases. Under these assumptions, the ratio of the mass of metal reaching the matrix (M_{matrix}) to the size of the hole leading to the matrix ($HoleArea_{matrix}$) and the corresponding

ratio of the mass of metal reaching the quartz crystal ($M_{q.c.}$) to the hole size leading to the quartz crystal ($HoleArea_{q.c.}$) are equivalent, and thus:

$$\frac{M_{matrix}}{HoleArea_{matrix}} = \frac{M_{quartz.crystal}}{HoleArea_{q.c.}}$$

$$\rightarrow M_{matrix} = \frac{M_{q.c.} * \pi r_{matrix}^{2}}{\pi r_{q.c}^{2}}$$

$$\rightarrow M_{matrix} = \frac{M_{q.c.} * r_{matrix}^{2}}{r_{q.c}^{2}}$$

Therefore, it is possible to measure the amount of metal at the quartz crystal microbalance, and knowing the radii of the holes leading to the matrix tip and the quartz crystal, it is possible to estimate the mass of metal deposited throughout the matrix.

3.7 Metal source preparation and protocols

All metals studied in this work were vaporized from a thin strip of the pure metal, held firmly between the two electrodes listed in Figure 5, above. Metal filaments were prepared by cutting a thin strip directly from a foil of pure metal. Typical foil thickness was approximately 0.1 mm. Filament lengths and widths varied depending on the type of metal used, but ultimately the size was determined by the distance between the electrodes (~5 cm).

When working with the metal samples, gloves were used to prevent the introduction of oils onto the surface of the metal strip. In particular, with the transition elements from the left hand side of the table (the early transition metals), resistively heating the metals in the presence of the oils results in the carbidization of the metal, leading to a metal filament which corrodes quickly in the centre upon heating.

When heating and cooling the filament, care was taken to ensure that the rate of increase or decrease of current was performed very slowly, to allow the filament to slowly warm or cool, as appropriate. Rapid heating or cooling of the filament causes the filament to become quite brittle, ultimately snapping, and requiring replacement. Additionally, as filaments are used for successive experiments, the centre portion of the filament becomes much more thin. The resistance of the thinning filament increases, and, with prolonged use, the current required to vaporize metal generally increases. During experiments, it is necessary to continuously monitor the current and the metal deposition rate using the quartz crystal microbalance, to ensure that metal is being consistently vaporized from the filament during a metal deposition. For most experiments, metal vaporization rates on the quartz crystal microbalance were on the order of 3 to 5 cycles per minute, which generally resulted in a majority of monatomic metal condensed in the matrix. Experiments in which the metal deposition parameters were tested are given in the beginning of Chapter 4.

3.8 Gas sample preparation

Gas-samples are prepared on a separate vacuum line, pumped in the same manner as described for the matrix systems above. The only major difference between the gas-handling line, and a typical matrix system, is the smaller size of the vacuum line, and the absence of a compressor and cold-tip for experimentation.

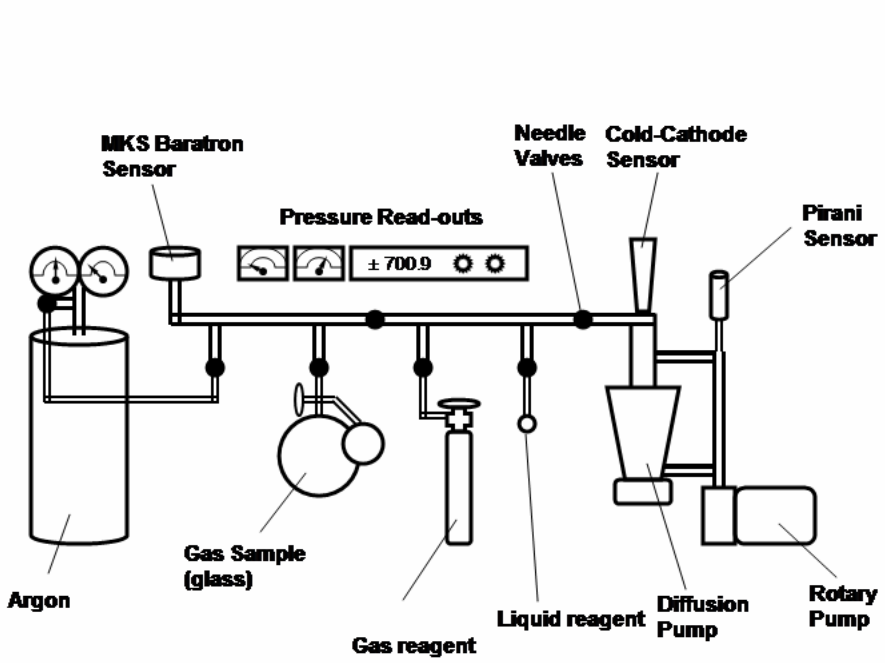

Figure 6: Schematic representation of the gas-handling line used for preparation of matrix gas-mixtures.

Gases are introduced into a sample bulb directly from stock sources, by connecting gas-cylinders or liquid samples (as described below) through various ports on the gas-handling line. A schematic of the gas-handling line is given as Figure 6.

Briefly, reagent gases are delivered from the stock bottle directly into the evacuated gas-bulb to a fixed pressure monitored via absolute pressure measurements using an MKS Baratron gauge. Thus, achieving a specific reagent to rare gas mixture is achieved by treating reagents as ideal substances, and introducing reagents on the basis of their pressures, according to Dalton's law of partial pressures. Thus, for the preparation of a 770 Torr total pressure sample bulb at a proportion of 1 to 10 ethene to argon would require first the introduction of 70 Torr of ethene, which is then diluted to a total pressure of 770

Torr with Ar. Since originally 70 Torr of the gas was ethene, the remaining P_T – P_{ethene} = 770 Torr – 70 Torr = 700 Torr is the partial pressure of Ar, added. Since the total volume of each gas is the same, in this vessel, and each is present under the same conditions of T, the relative mole ratio of each species arises as a simplification of the ideal gas law, summarized in the following equations:

$$\frac{n(ethene)}{n(Ar)} = \frac{P_{ethene}V/RT}{P_{Ar}V/RT} = \frac{P_{ethene}}{P_{Ar}} = \frac{70Torr}{700Torr} = \frac{1}{10} \qquad \text{(Eq. 1)}$$

For lowered concentrations of reagents, it is sometimes difficult to prepare the sample directly, since the pressure of the reagent may need to be much lower than 1 Torr. As a result, a secondary gas-bulb which is composed of two separate, but linked components, with the first component having 1/10 the volume of the second component can be used. In this design, a reagent gas can be initially introduced into the smaller component, at 10 times the pressure required in the larger component, and sealed in the smaller component with an isolation valve. Evacuation of the gas system, retaining the reagent gas in the sealed portion can be performed, after which, the required amount of rare gas can be introduced in the larger bulb. Once both components are filled with the required amounts of gas, the master valve is sealed isolating the gas-sample bulb system from atmosphere. Once sealed from the atmosphere, the valves isolating the smaller and larger components of the gas-bulb from each other can be opened, allowing the gases to mix.

As an example, if one were to prepare a mixture of ethene to argon at a ratio of 1 to 1000, one would seal 7 Torr of gas in the smaller component, 1/10 of

the volume of the larger component (i.e. V_{small} = 0.1 V_{large}). After evacuating the remainder of the system, the larger component, of volume V_{large}, would be filled to 700 Torr. Since both components are subject to the same conditions of T, it follows that (assuming ideal conditions):

$$\frac{n(ethene)_{small}}{n(Ar)_{large}} = \frac{P_{ethene}V_{small}/RT}{P_{Ar}V_{large}/RT} = \frac{P_{ethene}\left(0.1V_{large}\right)}{P_{Ar}V_{large}} = \frac{0.1(7Torr)}{700Torr} = \frac{1}{1000} \quad \text{(Eq. 2)}$$

Typically, these gases are allowed to mix overnight, to ensure sufficient time for adequate mixing of the materials to form a uniform gas mixture. This mixing time is not required in the simpler case, where both reagents are introduced into the same gas-bulb.

3.8.1 Gas phase reagents: preparation and usage

In most cases, gas-phase reagents can be used directly, without any further purification, from stock sources stored in gas-cylinders. Table 1 lists all reagents used in the experiments described hereafter, the associated reagent purity, material phase, and supplier information.

Table 1: Table of reagents, purity, and chemical suppliers used in matrix isolation experiments presented in this work.

Reagent	**Formula$_{(phase)}$**	**Purity**	**Supplier**
Argon	$Ar_{(g)}$	99.995%, UHP	Praxair, Matheson
Krypton	$Kr_{(g)}$	99.995%, UHP	Matheson
Xenon	$Xe_{(g)}$	99.995%, Research	Praxair
Ethene	$C_2H_{4\ (g)}$	99% (C.P, chemical purity) and 99.99% high purity	Matheson, Aldrich
d_4-ethene	$C_2D_{4\ (g)}$	99% atom D	C/D/N Isotopes
1,1-d_2-ethene	$CH_2{=}CD_{2\ (g)}$	99% atom D	C/D/N Isotopes
Ethane	$C_2H_{6\ (g)}$	99%, C.P.	Matheson
d_6-ethane	$C_2D_{6\ (g)}$	99% atom D	C/D/N Isotopes
Water	$H_2O_{\ (l)}$	Purified by freeze, pump Thaw cycles on vac line	No supplier
Heavy water	$D_2O_{\ (l)}$	99% atom D	Aldrich
d_1-water	$HOD_{\ (g)}$	Prepared by exchange of D_2O/H_2O in matrix line	No supplier
Vanadium foil	$V_{\ (s)}$	99.99%	Alfa Aesar

3.8.2 Liquid phase reagents: preparation and usage

Unlike gas-samples which are typically stored in lecture bottles or other gas-handling equipment, liquid samples are typically exposed directly to atmosphere, and have the capacity to dissolve atmospheric impurities such as water, nitrogen, and oxygen. These impurities can have a dramatic influence in the chemistry under study, and thus, must be minimized as much as possible.

Liquid samples are connected to the gas-handling line by introduction of a small amount of the material in a round bottom flask, connected to the vacuum system with an isolation valve. Cooling the liquid sample with liquid nitrogen freezes the liquid and dissolved impurities, while any impurities that cannot freeze under liquid nitrogen temperatures remain in the headspace of the flask. Opening the frozen system to vacuum evacuates these impurities that are initially present. Once the impurities have been removed, the isolation valve is closed and the frozen sample is allowed to return to room temperature. Dissolved impurities restore equilibrium between the liquid and their vapour composition in the headspace of the flask corresponding to Raoult's law.[1] Recooling the liquid with liquid nitrogen and evacuating the headspace as before removes another fraction of impurity gases, and the repetition of this process eventually purifies the liquid sample. This process of freezing the sample, pumping, thawing and repeating is referred to as a freeze-pump-thaw degas cycle, and is used whenever liquid samples are necessary.

The only other consequence of liquid samples arises in gas-sample preparation. Unlike pure gases, liquid samples can only be introduced into the gas-sample up to their vapour pressure. Thus, it is not always possible when using liquid samples to prepare mixtures in all proportions, since the vapour pressure of a liquid may not always be 760 Torr, under the given conditions of gas-sample preparation. As most samples in this work are prepared directly from gas-phase reagents, this is only a problem when water isotopomers are used. However, typical water introductions involve no more than 5-10 Torr of water, which is well below the vapour pressure of water that can be achieved.

3.8.3 Drying protocols for elimination of water

In some experiments, the presence of water in the experimental gas-sample is implicated as a reactive matrix impurity. Thus, experiments were performed in which the amount of water was increased, and also where attempts were made to decrease the amount of water in the system. The introduction of water is straightforward, and involves nothing more than preparing a gas-sample using liquid water, the vapour from which can be introduced as a reagent. However, samples where water is removed require more extensive preparation.

The easiest method to eliminate water in the gas sample involves flowing reagents through a long copper coil cooled with a slush-bath of temperature-lowered alcohol, during preparation of the gas-sample. Although an easier method would be the direct use of liquid nitrogen, this method is impractical, as it has the disadvantage of freezing out water and most of the hydrocarbon reagents used in typical experiments. As a result, the alcohol slush bath is used

to hold the temperature below the freezing point of water, but above the freezing point of desired reagents. By this process, water can be removed directly from the prepared gas sample relatively efficiently, however, under no conditions can water be removed from gas-samples entirely. The persistence of water vapours within the vacuum system is constant, and thus, considering the impact of water on chemistry in the matrix system is always necessary. In cases where water is considered to be a significant contaminant, deuterated water (or an isotopically substituted hydrocarbon) is used to directly observe the experimental impact. This method can be very successful, however, the exchangeability of the O-D bonds of D_2O inside the glass gas bulbs, and metal matrix systems, can cause significant challenges. As a result, significant protocols are necessary for using deuterated samples in which exchangeable protons are present.

3.8.4 Deuteration protocols to eliminate H/D exchange in water

When using materials that have exchangeable protons, the experimental system must be conditioned with material that will coat the inside surfaces with the specific isotopic species that is under study. Thus, when fully deuterated water is used, the inside surfaces of all aspects of the gas-handling line, the sample gas-bulb, and the experimental system used for the study are exposed to vapour from a pure D_2O source. In order to maximize this effect, repeated exposures are necessary, before successful experiments can be achieved.

Even following exposure of the interior surfaces of matrix systems with D_2O, the persistence of H/D exchange is observed. Thus, in cases where D_2O is used, the presence of HOD is always observed, however, this species can

sometimes be used to obtain additional isotopic results, simultaneous with D_2O results. Since water is pervasive in matrix systems, it is a well studied species and when the use of isotopic water and the subsequent characterization of products involving water and water isotopomers is important, these factors will be dealt with in further detail.

3.9 Theoretical Methods and Software Tools

Many of the experimental results generated in the following chapters correspond to the generation of new molecules, the spectroscopic absorptions and characterization of which have been previously unreported. While the reported species share similar characteristics to those molecules observed in related studies, significant changes in the spectroscopic absorptions and molecular properties can arise, due to complicated changes in the electronic structure of the molecules. Thus, computational simulations of molecular spectroscopy become an important tool for identification, in experimental systems. The following sections describe some of the basic tools that can be used for predicting, and simulating the spectra of suspected molecules arising from our experimental system, as a means for making partial or conclusive identifications

3.9.1 Gaussian 98 calculations

The Gaussian software package from Gaussian Inc. represents a staple in the suite of tools in current chemical analysis. The basic software package contains tools which can perform many different types of *ab initio* based calculations, leading to atomic and molecular properties of chemical systems. In

general, these *ab initio* methods are based in the solution of the Schrodinger equation, for which complicated mathematical transformations and approximations are invoked in order to obtain the molecular wavefunctions that represent approximate solutions for systems involving many electrons. A general overview of theoretical based methods employed in these calculations is provided in "*Exploring Chemistry with Electronic Structure Methods: A guide to using Gaussian"* by Foresman and Frisch.[3]

3.9.2 General computational methods

The major calculation type used in this work employs density functional theory (DFT), specifically the B3LYP functional, which is based on the work of Becke, and Lee, Yang and Parr.[3] This functional has been used widely in a number of different examples in the literature, and generally, the prediction of vibrational frequencies and energies by this functional is well suited for identification of unknown species in experimental systems. The vibrational wavenumber positions of organic molecules, and even for complexes of molecules, can be predicted reliably with this method.

Where used, all calculations presented have involved optimization of the system, in attempt to find the lowest energy nuclear geometry for the system being investigated. Once this geometry has been located, the software calculates the associated vibrational frequencies of the molecule. When a structure corresponding to an energy minimum on the nuclear potential energy surface has been located the associated frequencies will all be real values, and no imaginary components. Single imaginary frequencies in the predicted

vibrational spectrum correspond to transition states linking two minima on a potential energy surface. For a spectrum involving more than one negative vibrational frequency, a so called “saddle point” is obtained. Our investigations have only been concerned in vibrational output corresponding to minima on the potential energy surface, and thus, further information regarding transition states and saddle points has been omitted. Additional information regarding either of these topics can be obtained in detailed computational references.[4]

3.9.3 Basis sets

In general, the choice of basis set is a critical choice when performing quantum mechanical calculations. By using basis sets that are too limited, or too expansive, calculations can lead to significant errors. As a result, benchmarking tests are generally performed for calculation types and basis sets, to ascertain their particular capability for solving specific problems. In cases where suitable benchmarks do not exist, the simplest method to determine the reliability of a method/basis set is to use that method to calculate a known molecule. Comparison of the results for the known system, with those predicted, provides a means of determining the reliability of the calculation. In cases where computations are used in this work, benchmarks of this variety are also given, as a reliability criterion.

It is worth noting that, the infrared spectra predicted by the Gaussian program suffer from a systematic error in the absolute position of the predicted wavenumber value, as a consequence of the assumption that the vibrational frequencies arise from a harmonic potential. Therefore, to directly compare with

experimental values, a scaling factor to correct for the overestimation of these predicted values is applied to the wavenumber positions, as a first-order correction. The use of scaling factors in this way is a common practice, and as such these scaling factors, for various basis sets, have been summarized by performing large-scale benchmarking tests.[5] In these benchmarking tests, well-characterized molecules are predicted by the software tools, and compared with the experimental spectra. The ratio of experimental wavenumber to theoretical wavenumber value is then used as the scaling factor for the associated method and basis set being used. In later sections of this work, the infrared spectrum of an unobserved isotopomer of ethane has been calculated using this same process (see Chapter 5). In this specific case, C_2H_6 and C_2D_6 are well-known experimentally, and thus these molecules have been used as benchmarks to generate scaling factors to correct the predicted ethane isotopomer spectrum. These scaling-factor corrected spectra can then be used for qualitative comparison with the experimental results using the SWIZARD program for spectral simulation. Note: Though scaling factors can be used to vary the absolute position of predicted wavenumber values, the relative intensities, and number of infrared active bands are not changed under scaling-factor correction. Thus, when predicted values are used as a criterion for unknown molecule identification, matching the number of experimentally observed modes and the experimental relative intensities with those predicted by the computational software is a reliable criterion for assigning an identification using computational support.

3.9.4 SWIZARD software for spectral simulation

For direct comparison of computed vibrational spectra with experimental results, it is quite beneficial to compare the calculated results directly with the experimental spectra. The Gaussian output lists only vibrational wavenumber positions, however, it is convenient to compare these directly with the spectra from the spectrometer. The SWIZARD program is one method by which Gaussian output files can be used as input to generate representative simulations from spectral files. This program takes the reference positions listed in the output, and applies a simple broadening function with a given constant line-broadening, to generate realistic looking spectra. In cases where this software has been used, additional information is given in the chapters with details corresponding to the specific results.

3.10 References for Chapter

[1] See for example: Dunkin, I.R.; *Matrix Isolation Techniques*, Oxford University Press, New York, **1998**.

[2] See, for example: Moskovits, M.; Ozin, G.A.; *Cryochemistry*, Wiley, New York, **1976**.

[3] See, for example: Foresman, J.B. and Frisch, A.; *Exploring Chemistry with Electronic Structure Methods: A Guide to Using Gaussian.*, Pittsburg, **1993**.

[4] See for example: Lewars, E.G.; *Computational Chemistry: Introduction to the Theory and Applications of Molecular and Quantum Mechamics*. Kluwer, Boston, **2003**.

[5] Merrick, J.P.; Moran, D.; Radom, L.; *J. Phys. Chem. A.*, **2007**, ASAP Alert, doi: 10.1021/jp073974n

Chapter 4

Generation and reactivity of vanadium metal centres in matrices containing low concentrations of ethene: UV-visible and infrared spectroscopic analysis.

4.0 Introduction

In order to study the reactivity of transition metal centres within the matrix isolation environment, the first step involves the verification that such transition metal centres can be easily generated in the experimental apparatus. The preliminary results involve the use of vanadium metal, and in the following sections, the generation and observation by UV-visible spectroscopy of vanadium metal centres in argon will be presented.

The absorption spectrum of vanadium in the gas-phase is characterized in Moore's tables,[1] and additionally vanadium metal centres have previously been isolated in argon, and analyzed by UV-visible spectroscopy,[2,3] with detailed comparisons to the gas-phase absorption spectra. Therefore, these works serve as an excellent reference guide for ascertaining the reliability of this particular experimental apparatus for generating such metal centres.

Following the successful generation of these species under our experimental conditions, the extension to complementary UV-visible experiments involving argon matrices containing dilute amounts of ethene (C_2H_4) was performed, in order to observe the extent of reactivity, if any, of vanadium with

ethene. Since results in later chapters involve variation in matrix cold-window temperature, the matrix deposition gas-flow rate, and the rate of metal flux into the matrix, some experiments investigating the impact of changes in these parameters were also explored, and are presented in this section. Additionally, complementary IR studies to the UV experiments presented in this chapter have been performed on a different matrix isolation apparatus. Thus, a comparison of different factors on each system is considered, to determine the experimental impact, if any, of performing experiments in the separate systems.

Finally, for cases where evidence of reactivity is directly observed in the UV-visible experiments, some infrared experiments have been performed to determine, if possible, structural aspects of the reaction products of V metal centres with ethene. Many of these results arise following irradiation of the matrix with wavelengths corresponding to known V atom excitations. A complementary study of V/ethene reactivity has recently been performed by Cho and Andrews using laser ablation,[4] and the results presented in this work complement their work quite well. The majority of their products are observed following irradiation of matrix samples with wavelengths corresponding to V atom excitations. The specific major products are products of V insertion into the C-H bonds of ethene, and both the quartet-H-V-C_2H_3 and doublet-$H_2V(C_2H_2)$ species have been identified in their work. No other major products of C-H bond insertion have been observed. This section serves as a verification of the spectra obtained in their apparatus, with the opportunity to make some corrections to their pioneered spectra.

4.1 Experimental considerations

In some experiments, a separate matrix isolation expander head was used, capable of reaching temperatures as low as 13K. This expansion head was only used in the case of matrix-isolation UV-visible experiments. For the matrix-isolation infrared experiments, the lowest temperature achieved by the cold tip varied between 15 and 17 K, as the instrument aged throughout the project. Some experiments using the 15-17K head were performed in the UV-visible apparatus, to determine any differences in reactivity that arise due to the increased temperatures.

For typical UV-visible experiments, matrix deposition times were approximately 20 minutes, at flow rates from 0.5 to 5.0 sccm, as indicated in the text. A variety of matrix gas-samples have been used, including pure argon, and various concentrations of ethene in argon (from 1:600 to 1:10 ethene to Ar). Otherwise, no additional experimental considerations beyond those presented in the technical section, Chapter 3, were used.

In later sections of this chapter, comparisons of new features observed in our work, under experimental conditions nearly identical to those used by Cho and Andrews are reported.[3] It is thus worth noting that, in the two different experimental systems, the data acquisition intervals in the infrared spectra are not equivalent, and there is a difference in the resolution of the individual spectrometers used. As a result, an estimated associated uncertainty of as much as 2 cm^{-1} can arise in the compared experimental spectra. Therefore, values quoted in this work that are within 2 cm^{-1} of those values quoted in the

Cho and Andrews results may well arise from the same originating species. Consequently comparative absorptions which have qualitatively the same behaviour under experimental changes in both experimental systems, but are within 2 cm^{-1} of each other will be assigned as the corresponding species.

4.2 Ultraviolet visible results: Codeposition of V with pure Ar

A representative UV-visible absorption spectrum in the region of 200 to 650 nm, for the codeposition of V with pure Ar, at 13 K is presented in Figure 7. The flow of gas used in these experiments is 0.5 sccm, with a metal deposition rate of 3-5 cycles per minute. In the spectrum, major new features appear at 313 nm and 471 nm, with a variety of other weaker features, all of which correspond to the spectrum of V atoms isolated in Ar, as characterized initially by Devore.[2]

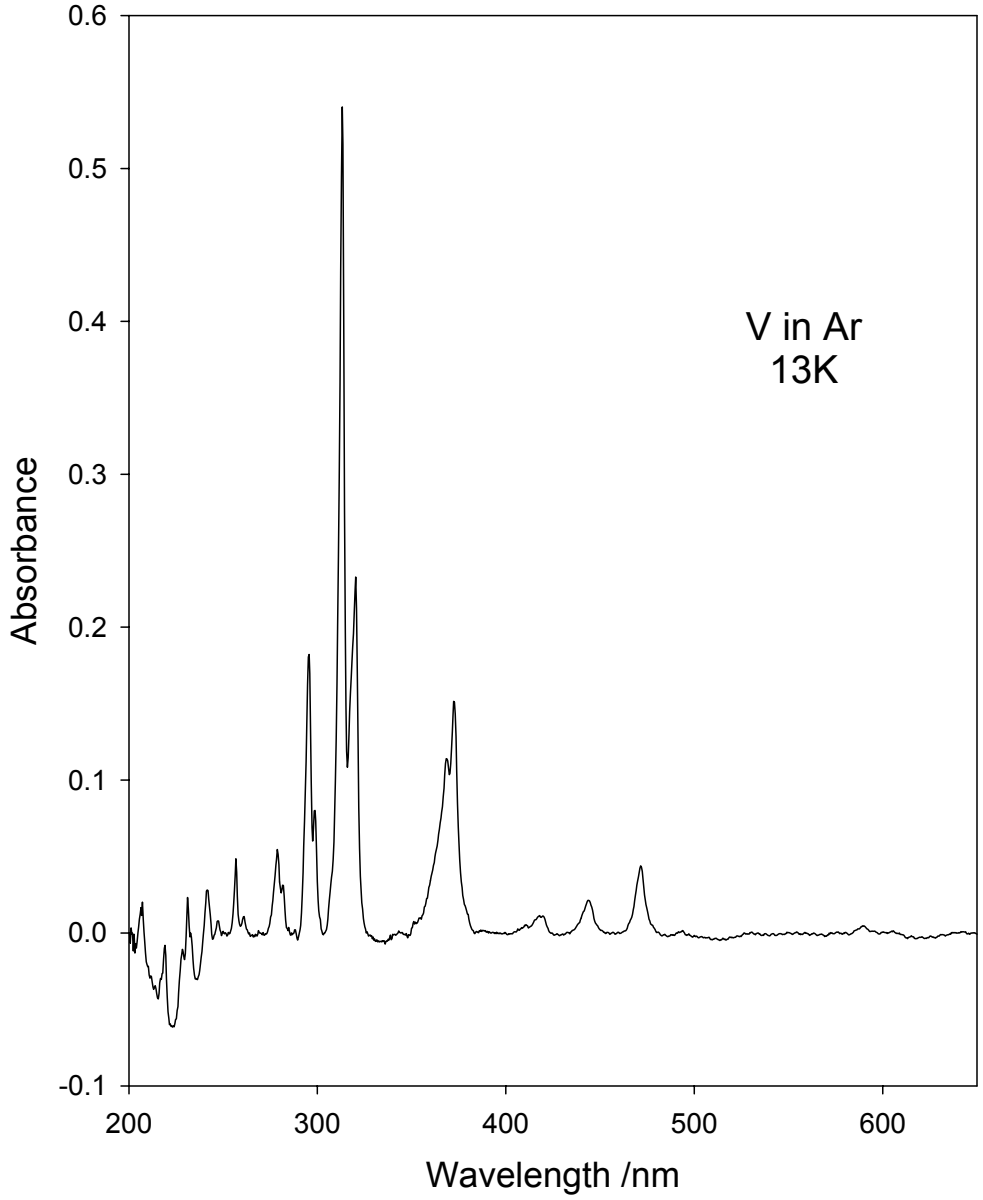

Figure 7: UV-visible absorption spectrum of pure argon condensed with vaporized V metal, at 13K.

As would be expected, the intensity of the V atom features is directly dependent on the amount of metal that is deposited into the matrix. In considering future infrared spectroscopic experiments, obtaining the most intense absorption spectral results will require sufficient yield of metal atoms to maximize the yield of metallic-based products. Thus, some consideration of the impact of increasing the metal flux into the matrix upon condensation is beneficial.

4.3 Codeposition of V in pure Ar: Increasing deposition temperature

In Figure 8, a comparison of the UV-visible spectrum of a pure argon matrix formed by co-condensation of the matrix gas with either a low flux (<3 cycles per minute) of vaporized V metal, or a correspondingly higher flux (> 10 cycles per minute) of metal vapor is presented. These matrices have been deposited on the matrix expander head reaching only 17K. As can be seen from the figure, new features are present in the spectrum for the matrix formed under high-flux of metal, that are absent from the spectrum obtained under lowered metal flux. Each of the new features corresponds to the spectrum of V_2, isolated in Ar, as characterized by Klotzbucher *et al*.[3]

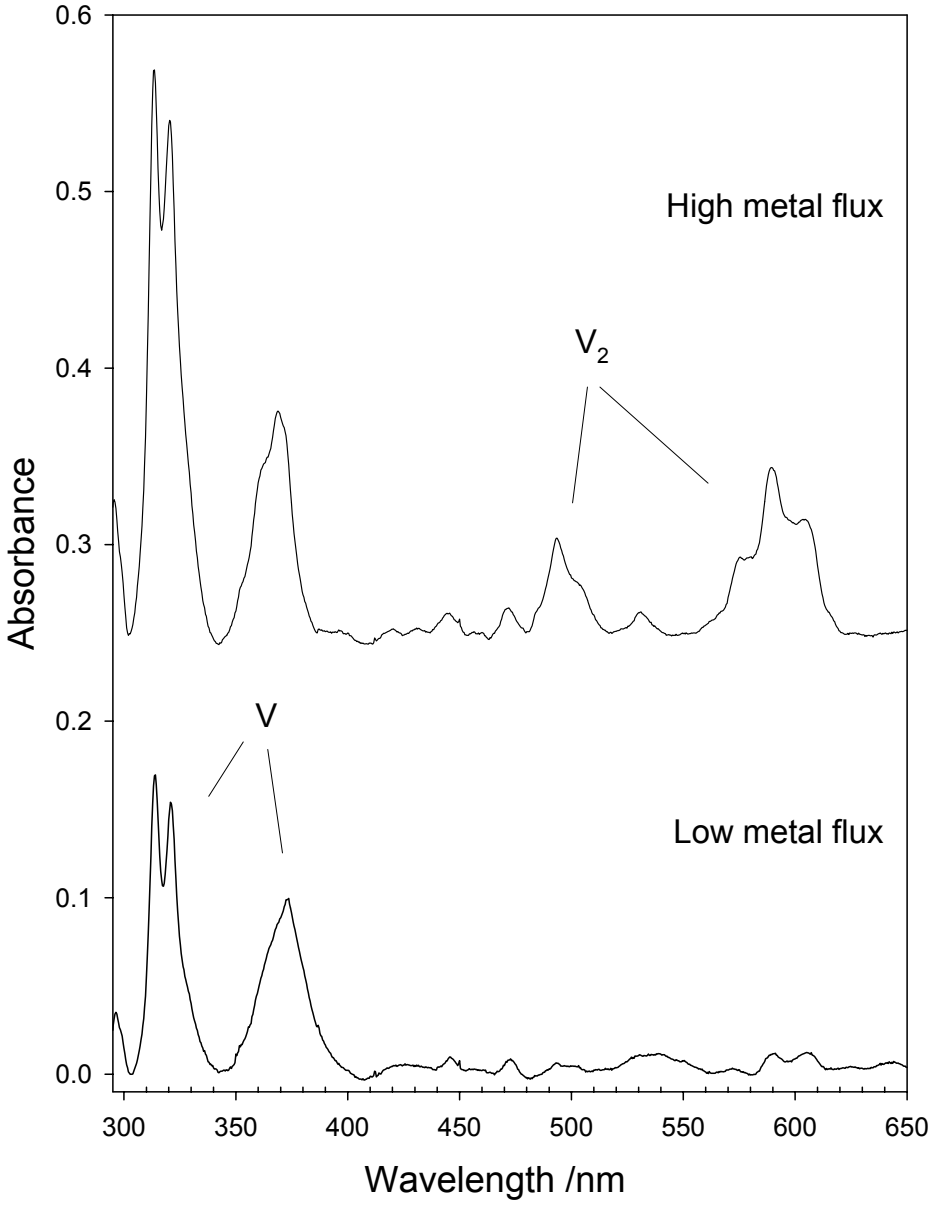

Figure 8: Comparison of the UV-visible absorption spectrum of argon matrices co-deposited with a) slow vaporization of V (< 3 cycles per minute), and b) rapid vaporization of V (> 10 cycles per minute). Spectra have been offset by an additive constant for clarity.

The appearance of V_2 species in these spectra with enhanced metal flux could result either from the increase in metal, or the change in temperature of the matrix cold tip, during matrix deposition. The absence of metal dimer in Figure 7, for which the matrix deposition occurs at 13K with a metal flux similar to the higher metal flux in Figure 8, suggests that the matrix-tip temperature is the major contributing factor. Since most of the infrared experiments presented below have been performed using the 17K expander head, additional experiments investigating metal atom deposition and aggregation on this expander head were also performed.

4.4 Codeposition of V with pure Ar: Effects of gas-flow rate

The only other experimental parameter which must be explored, beyond concentration of the hydrocarbon diluted in the matrix gas sample, is the flow rate of matrix gas during matrix deposition. UV-visible absorption spectra have been recorded for a series of sequential matrix depositions in which the flux of metal was maintained at a near constant value of 3 cycles per minute, while the gas-flow rate during matrix deposition was varied from 1.0 to 5.0 sccm. Since these matrices were deposited sequentially on the same matrix surface, differences in sequential spectra provide information on the arising changes. Figure 9 and Figure 10 present net changes in the integrated area of absorption features arising from the metal monomer and metal dimer with various gas-flow rates. These values have been internally normalized to their maximum value to be directly compared, as the only unobscured features directly measurable have significantly different absorption intensities.

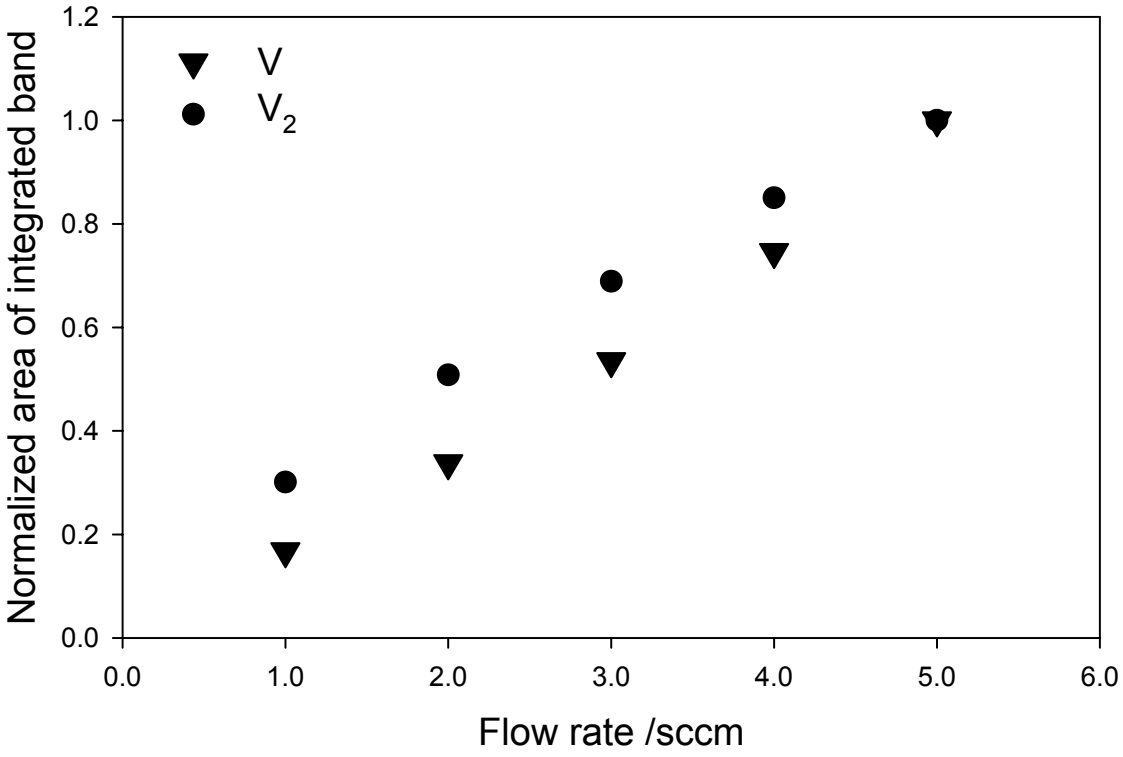

Figure 9: Comparison of the yield of atomic and dimeric V species isolated in Ar at 17 K, for constant metal flux and varied matrix gas-flow rates during deposition. Successively increasing flow-rate data is accumulated on top of the previously formed matrix, and thus integrated areas are cumulative areas. For clarity, integrated absorption areas for each species have been internally normalized for direct comparison.

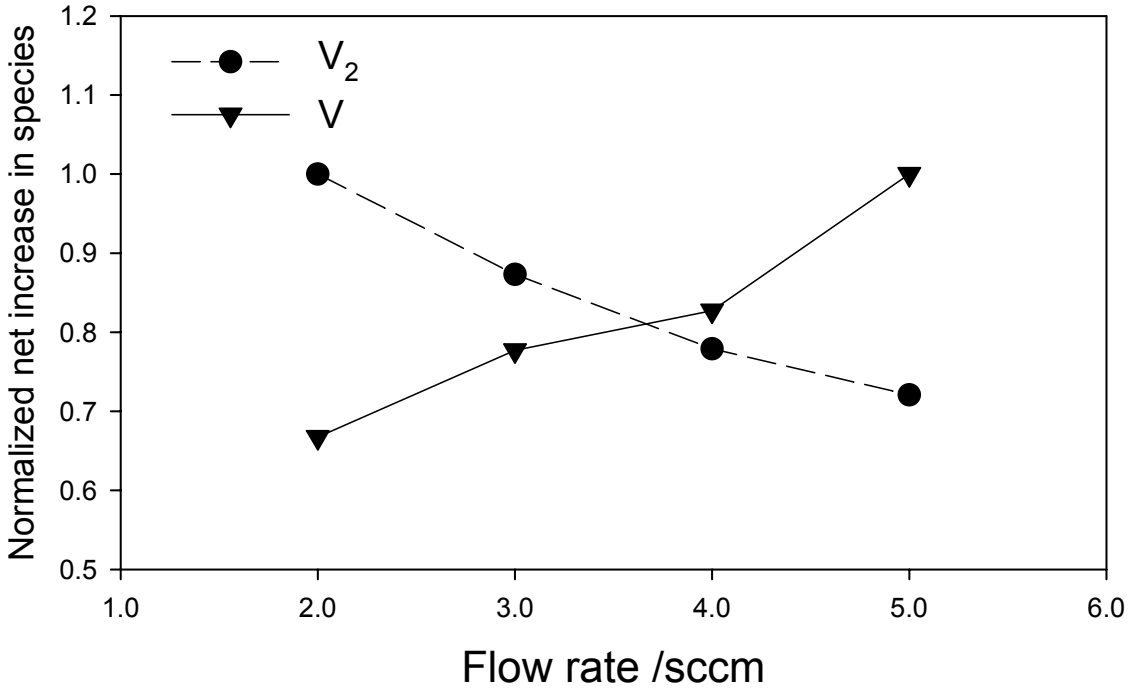

Figure 10: Comparison of the net increase in absorption of atomic and dimeric V with flow rate. The net increase is calculated by integration of the cumulative area and subtracting the previous cumulative area. All data have been internally normalized for clarity.

Figure 9 presents the normalized total yield of V atom and V_2, as the flow rate is increased. Recalling that the given matrices are formed sequentially, that the trend in Figure 9 is increasing linearly suggests that both V and V_2 are produced at an effectively constant proportion for a given metal flux, as the flow rate is increased.

To further clarify this point, Figure 10 presents the net increase in the integrated area of features attributed to the metal atom and metal dimer, as a function of the matrix gas-flow rate. These values have been obtained by measuring the total area under a given absorption band, and then subtracting the measured area from the previous experiment. Again, these values have been normalized relative to the strongest net change in each case to be presented on the same scale. For the atom, the results seem to suggest a slight increase in the relative yield with increasing flow, while, for the dimer a decrease in formation is observed. Thus, although gas-flow rate does not seem to have a dramatic influence on the V/V_2 relative yields, there is some advantage to using higher flow rates to isolate V monomers.

4.5 Irradiation of the matrix by the filament during deposition

Since the vaporization of metal by resistively heating a thin filament causes the emission of visible light toward the matrix during deposition, some consideration must be given to the possibility of photoexcitation of species during the initial formation of the matrix. During a typical deposition, the vanadium filament glows yellow-orange, with significant visible light emanating from the point of vaporization. The expected radiation profile can be modeled by

assuming the filament is a blackbody at temperature $T_{boiling}$ of the metal, and thus, the wavelength dependent intensity profile of the filament is given by the Planck distribution:

$$\rho = \frac{8\pi hc}{\lambda^5}\left(\frac{1}{e^{hc/\lambda kT} - 1}\right) \qquad \text{(Eq. 4.1)}$$

where the intensity of light emitted from the blackbody, ρ, is a function of the wavelength, λ, and the temperature, T, of the emission source.[e]

For the vaporization of V from a pure metal source, the normal boiling point is $T_{boiling}$ = 3680 K. In Figure 11, the spectrum of V atoms isolated in Ar is presented, and a dotted line representing the intensity normalized blackbody emission from the filament at this temperature has been superimposed. As can be inferred from the figure, a significant intensity overlapping with resonant V atom excitations is emitted from the glowing filament, during deposition. Additionally, when V_2 absorptions are considered (see Figure 8), the absorptions fall in a range where the intensity from the filament is even greater. Thus, direct resonant excitation of atomic and dimeric V in the matrix is a possibility which must be considered when interpreting results.

[e] The remaining constants in the equation are the physical constants: π, c, h, k, which have been defined in SI units as an appendix, for convenience.

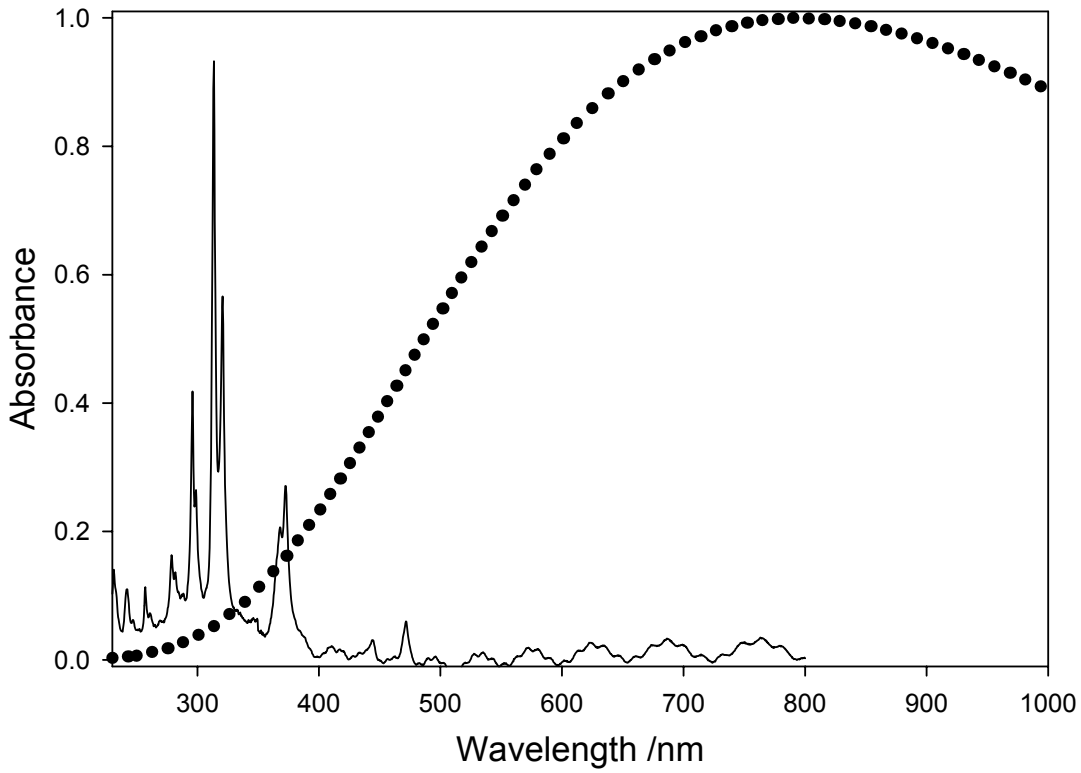

Figure 11: Comparison of the UV-visible absorption spectrum of V atoms isolated in Ar with the wavelength emission distribution of a blackbody at T = 3680 K (normal T_b for V metal). The dotted line represents the emission distribution modeled using the Planck distribution.

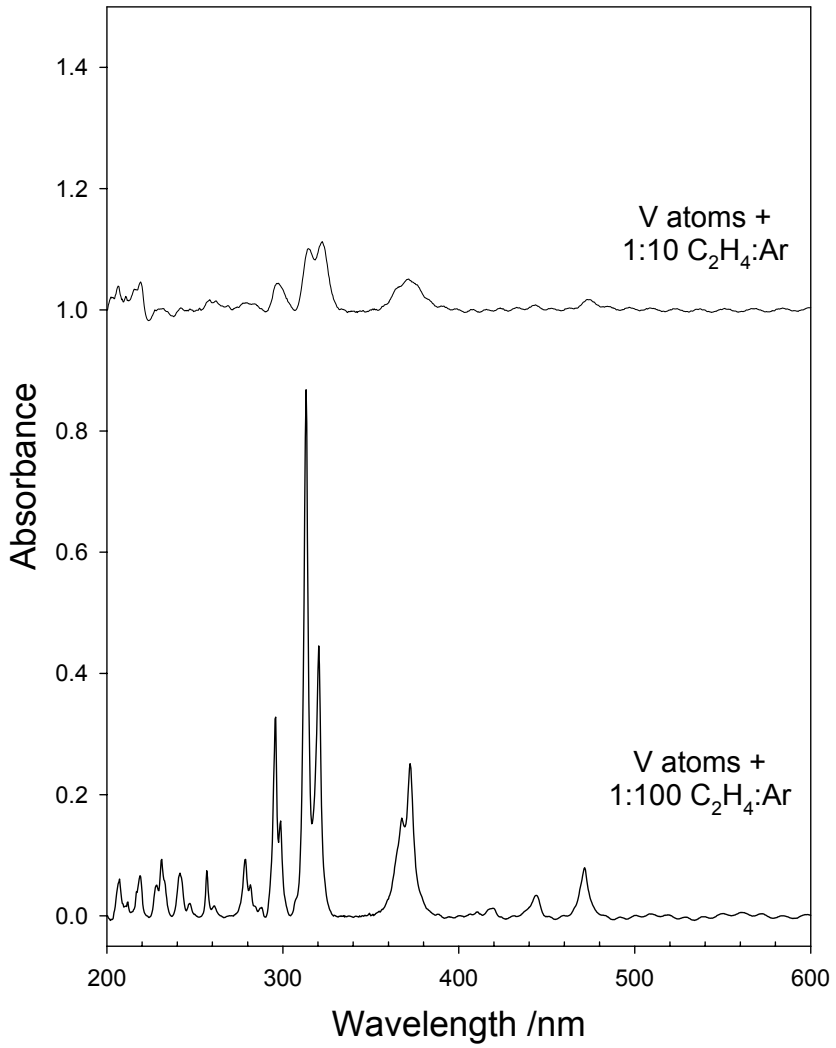

Figure 12: Comparison of the UV-visible absorption spectrum of V co-condensed with Ar containing increasing concentration of ethene. Absorptions due to V broaden and diminish with increase ethene concentration. Spectra have been offset by an additive constant for clarity.

4.6 Absorption of metallic species in presence of hydrocarbons

As the matrix gas sample is changed from pure argon, to argon containing increasing fractions of ethene (C_2H_4), it is necessary to consider the impact, if any, on the absorption spectrum of V metallic species isolated in the ethene-containing matrices. Figure 12 presents the UV-visible absorption spectrum of matrices containing 1:100 ethene and 1:10 ethene:Ar co-condensed with vapour from a V filament. For the higher concentration of ethene in Ar, the absorption spectrum arising from isolated V atoms is decreased, and is also significantly broadened. Secondly, in both spectra, there is a complete absence of features associated with metallic dimer upon deposition.

The reaction of V atoms with small hydrocarbons in the gas-phase has previously been explored in the work of Ritter and coworkers.[5] Their results demonstrate that none of the ground-state first-row transition metals react significantly with ethene. Thus, the direct observation of decreased metal atom absorptions with increasing ethene concentration is perplexing. However, the fact that the V atom can undergo resonant excitation by emission from the filament suggests that irradiation of matrices with light corresponding to V atom excitations may provide additional insights.

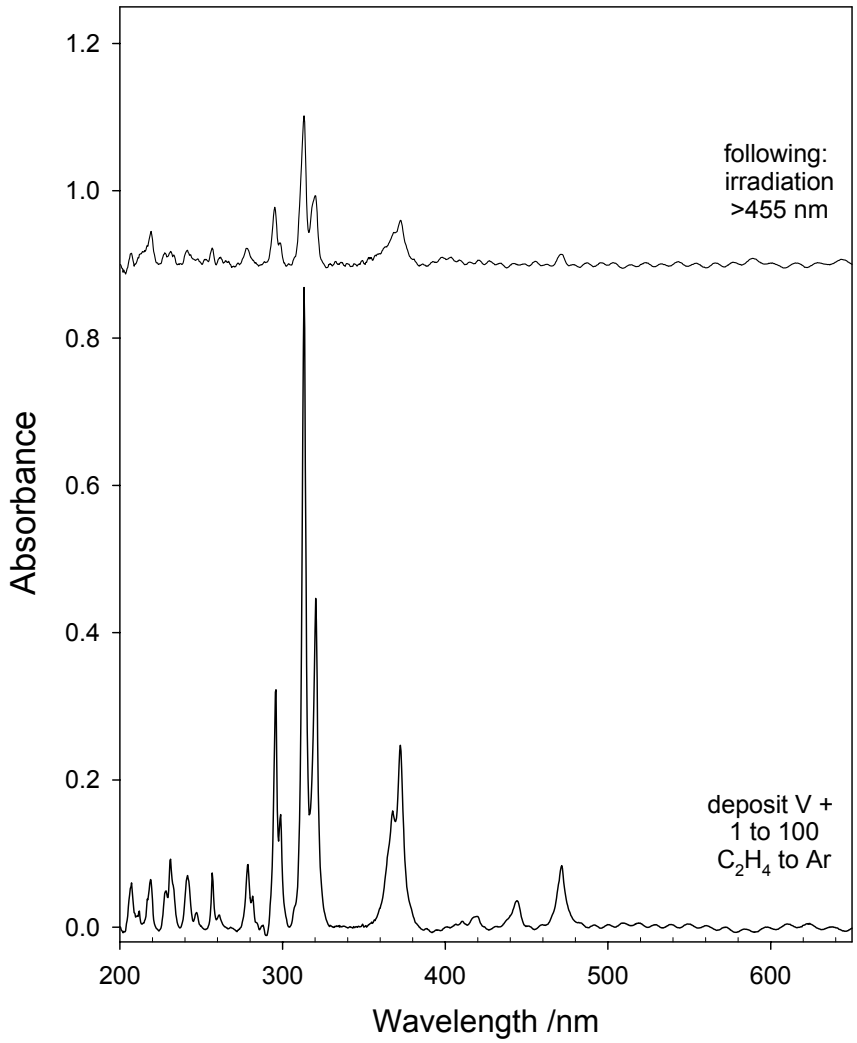

Figure 13: UV-visible absorption spectrum of atomic V isolated in 1:100 C_2H_4:Ar immediately following matrix deposition (bottom spectrum), and following 3 minutes irradiation >455 nm light (top spectrum). Spectra have been offset by an additive constant for clarity.

Figure 13 presents the UV-visible absorption spectra of V atoms isolated in a matrix formed with a 1:100 ethene:Ar gas-sample prior to, and following, irradiation >455 nm light. As can be seen from the spectra, the initially present isolated V atoms are significantly consumed following irradiation of the matrix with >455 nm light for only 3 minutes. No additional significant product absorptions are evident in the UV-visible spectra following the irradiation. However, the significant loss of isolated V atoms following irradiation suggest that a complementary study where infrared analysis of the matrix is performed could lead to evidence of products resulting from V atom photochemistry.

4.7 UV-visible discussion: V and V_2 formation

Analysis of the UV-visible spectra obtained from argon matrices formed during vanadium vaporization clearly demonstrates the isolation of atomic V, and in some cases, of V dimer. Since the dimer is not formed under all conditions, an analysis of the conditions which promote dimer formation is thus necessary.

4.8 Effect of temperature and matrix composition on V/V_2 formation

First, it is interesting to note that, unlike the spectrum for V in Ar presented in Figure 7 which was collected at 13K, both of the spectra for V in Ar presented in Figure 8 have been collected on a matrix expander head for which the operating temperature is 17 K. Thus, it would appear that, while no dimer is formed at the lower temperature in Figure 7 (despite relatively similar metal fluxes to those used under the 'high flux' results presented as the topmost spectrum of Figure 8), a considerable production of dimer is evident under higher metal flux at higher temperatures. Thus, formation of V_2 may arise from the

increased temperature of the matrix tip, and may also be due to the increase in metallic flux during deposition.

The increase in temperature of the matrix tip leading to increased metal aggregation suggests that the infrared experiments, all of which were performed on the higher temperature matrix tip, will always yield a fraction of metallic dimer. As a result, when considering results in the infrared experiments, it may be necessary to consider explanations involving reactivity of dimeric metal species.

Interestingly, when krypton or xenon are used as the matrix host, the presence of metal dimer on codeposition of the matrix gas-sample with vaporized metal decreases with the increasing molecular mass of the matrix gas used. Although at first this trend of decreased dimer formation seems to correspond to the increased freezing temperature of the rare gases, thereby suggesting a more efficiently immobilized metal atom on matrix condensation, the trend in atomic polarizability of the noble gas is well-regarded as the dominant contributing factor inhibiting metal aggregation.[3] For the rare-gas atoms (Rg), the trend in polarizability of the noble gases is Xe > Kr > Ar, with an approximately two-fold decrease in atomic polarizability between each successive species. As a result, the formation of V-Rg van der Waals complexes on matrix deposition leads to a decrease in the mobility of the metal atom, since there is considerable mass-increase of the V-Rg species. Thus, the formation of V-Rg complexes inhibits V dimer formation. In the case where Xe is used as the matrix, no evidence for dimer formation is observed under nominal working conditions, where a correspondingly large yield of V_2 would be observed in Ar. Interestingly, the

polarizability, α, of ethene is nearly identical to that of Xe, having a ratio: α(ethene)/α(Xe) = 1.051.[6] Thus, if the decrease in dimer formation tracks with the supposition that stronger van der Waals complexes are formed with increasing polarizability of a collision partner, introducing ethene into the gas-mixture should result in decreased metallic dimer as V-C_2H_4 van der Waals complexes form. Indeed, when ethene is added to the matrix sample, as seen in Figure 13 above, there is a complete absence of metal dimer in the recorded UV-visible spectrum following deposition of the matrix, even for the lowest ethene concentration (Figure 13, bottom spectrum, 1:100 C_2H_4:Ar). Thus, this observation may support the idea that V-ethene van der Waals complexes are formed on matrix condensation, thereby decreasing the mobility of the metal in the matrix, and eliminating a channel leading to V_2 formation. Kafafi and coworkers have previously reacted Fe atoms with C_2H_4,[7] and note evidence in their infrared spectra for Fe/C_2H_4 complexes, which have been proposed as complexes arising from metal ethene hydrogen bonding or complexation. As the valence electronic structure of both V and Fe are similar (outer $4s^2$ configurations), the observation of similar complexation for these two metals would not be unexpected.

An alternative explanation for the inhibition of dimer formation when ethene is present could result from the reactivity of metallic dimer with ethene, either spontaneously or through photochemical excitation. If V_2 were reactive when ethene were present, the UV-visible absorption spectrum would provide evidence for the inhibition of metallic dimer. Thus, it is not possible, based on

these results alone, to explain the absence of metal dimer, when ethene is present. Further analysis would be required in order to elucidate which of these two proposed dimer inhibition mechanisms is active. As a means of identifying this, one could introduce 1% Xe in Ar during codeposition with V at 17K, and track the formation of V_2 as the Xe availability is increased. The Xe, while unreactive, should have a similar propensity to forming V-Xe van der Waals complexes as does ethene. Thus, the UV-visible spectrum of V in argon containing Xe should show inhibition of V_2 in the same manner as observed in the spectra of V isolated in a matrix composed of 1:100 C_2H_4 : Ar.

4.9 Effect of matrix gas flow-rate on V/V_2 formation

When pure Ar is used as the matrix material, and the flow rate of the matrix gas is increased while the metal flux is held constant, the relative formation of V and V_2 products in the matrix maintains essentially constant. (Figure 9). Since these results were acquired for a series of matrix-depositions in which the matrices are formed on top of each other, differences in the area of absorption features provide information about net changes for each experimental change. Figure 10 represents these changes graphically, and it can be seen that as the flow rate is increased two different trends are observed for V and V_2. From Figure 10, as the flow rate is increased, an increase in metal atom is observed, while a corresponding decrease in dimer is observed. That monomer is favoured at the expense of dimer formation is an expected result, given that the formation of each dimer must occur at the expense of two monomer units. Thus, although one might expect that matrix formation at higher flow rates should

result in significant diffusion during the freezing of the matrix, it would appear that metal is actually more efficiently isolated in matrices formed using higher gas-flow rates.

Since the flux of metal is held constant in these experiments, the observations arising from analysis of Figure 9 and Figure 10 can be rationalized by a decrease in the density of metal atoms in the matrix on formation. Since the amount of gas reaching the surface in tandem with the vaporized metal would be increased with increasing flow rate, this would directly result in a relative dilution of the metal vapour, resulting in fewer metal-metal interactions necessary for dimer formation. Although these trends suggest that under higher flow rates V is formed preferentially to V_2, it is worth noting that the relative decrease of V_2 formation with increasing flow is slow. Although monomer is preferred at higher flow rates, a significant amount of V_2 is formed even at the highest flow. Since higher flow rates introduce higher yield of gas to the matrix tip, most experiments have been performed under the lower flow rate conditions, to minimize the total amount of gas used in any experiment, and to maximize spectral clarity.

4.10 Irradiation of matrices during metal deposition

During matrix formation, whenever metal is co-deposited into the matrix, a significant irradiation of the matrix surface with visible light occurs. Figure 11 gives the absorption spectrum of atomic V, with the estimated Planck blackbody emission distribution for a blackbody at $T = T_{boiling}$ for V. A significant fraction of the light emitted from the filament overlaps with V absorptions, demonstrating that V atoms in the matrix can be electronically excited by the glowing filament.

When considering the V_2 species, the absorptions are at higher wavelength, where even more appreciable emission intensity exists. Correspondingly excited V_2 species could react in the matrix, if formed. However, given the expected inhibition of V_2 species, as described above for cases when ethene is present, it seems more reasonable to consider the chemistry in terms of excited V atoms, rather than considering dimer chemistry.

Additionally, as the hydrocarbon concentration in matrices increases, the absorptions due to isolated metal atoms become broadened, and increasingly indistinct. Such observations have been observed previously by Ozin and coworkers.[8] The extent of broadening of the fundamental absorptions of V atoms supports the idea of metal-hydrocarbon van der Waals complexes formed with the polarizable hydrocarbon (compared to Ar). These weak van der Waals interactions represent perturbations of the V atom, and therefore perturbations on the fundamental absorption positions of the atom, relative to the gas phase. Hence, the metal atom absorptions would be expected to be broadened due to complexation, as is observed in the UV-visible spectra of Figure 12. The direct impact of these V-ethene van der Waals complexes is to increase the width of absorptions possible for a V atom, thereby increasing the probability of excitation by the weak emission source of the metal filament. For increasing hydrocarbon concentration in the matrix, whenever a photoexcitation is a required initiating step, an increase in the amount of product resulting from excitation should be observed. At much higher hydrocarbon concentrations, additional van der Waals complexation of the V atom would be expected, and the probability of excitation

would increase, correspondingly. Thus, it appears clear from these results that, whenever metal and hydrocarbon are simultaneously present, there is significant light available from the filament to induce chemistry, if ground-state reactivity should not be expected.

To investigate any V/ethene chemistry which can be induced by photochemical irradiation, matrices formed containing V and ethene in Ar were exposed to irradiation from a broadband source. In particular, when V is deposited in argon matrices containing ethene at 1:100 ethene:Ar, the spectrum of the initially formed matrix provides evidence for the isolation of metal atoms (see Figure 13). Subsequent irradiation of the matrix with light >455 nm, corresponding to some of the weakest V atom excitations, leads to major loss of isolated V atoms, after only 3 minutes of irradiation. Irradiation of pure Ar matrices containing V with >455 nm light causes no significant loss of isolated V. Thus, given that the most available reagent in the 1:100 C_2H_4:Ar matrices is C_2H_4, for which anticipated V-C_2H_4 van der Waals complexes are formed, it would be expected that the observed loss of V following irradiation is due to reactivity of excited state V atoms with C_2H_4. Thus, under these experimental conditions, a corresponding infrared analysis should show evidence for C_2H_4 loss following irradiation, with concomitant growth of products due to V + C_2H_4 reaction channels.

4.11 Infrared experiments

To further understand the UV-visible results presented above, complementary matrix experiments were performed using infrared spectroscopy as the method of detection. In particular, evidence in support of the reactivity of, or inhibition of, V_2 in matrices has been investigated. Given the observed depletion of metal atoms following irradiation of matrices with light corresponding to V excitations, photochemically induced products are expected.

4.12 Reaction of V with C_2H_4 in Ar, 1:200 C_2H_4:Ar

In Figure 14 portions of the infrared spectrum in the V-H stretching mode region for matrices formed following the reaction of V and C_2H_4:Ar (1:200) are given. By comparing the infrared spectra of matrices formed with the same gas-mixture, in which the only difference is the addition of metal, it is immediately clear that all absorptions due to matrix-isolated water[9] and matrix-isolated ethene[10] are diminished in the spectrum of the matrix in which metal is present. However, despite the significant losses of C_2H_4 and H_2O features, on deposition with metal, the only new product features which are present are weak. These new features occur at absorption positions of 2891 cm^{-1}, 1552 cm^{-1}, 1465 cm^{-1}, 1375 cm^{-1}, and 1304 cm^{-1}. The features at 2891 cm^{-1}, 1465 cm^{-1}, and 1375 cm^{-1}, are associated with ethane, C_2H_6, isolated in Ar.[11] The feature at 1304 cm^{-1} corresponds to matrix-isolated methane, CH_4.[11] The feature at 1552 cm^{-1}, however, has never been identified previously.

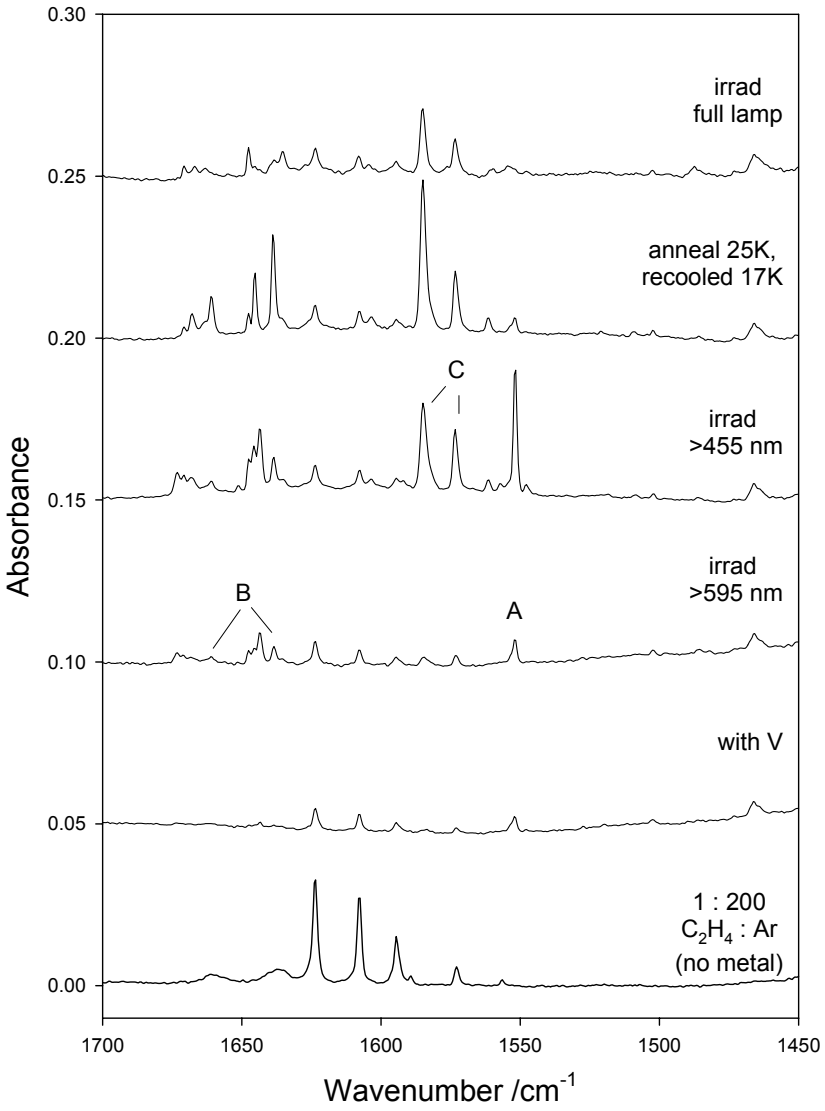

Figure 14: Portions of the infrared absorption spectrum in the V-H stretching following the reaction of V with 1:200 C_2H_4:Ar, after various experimental changes. The features labeled A correspond to an unknown product species, while B and C are the doublet-$H_2V(C_2H_2)$ and quartet-H-V-C_2H_3 species. Species A may be a configurational isomer of species C. Spectra have been offset by an additive constant for clarity.

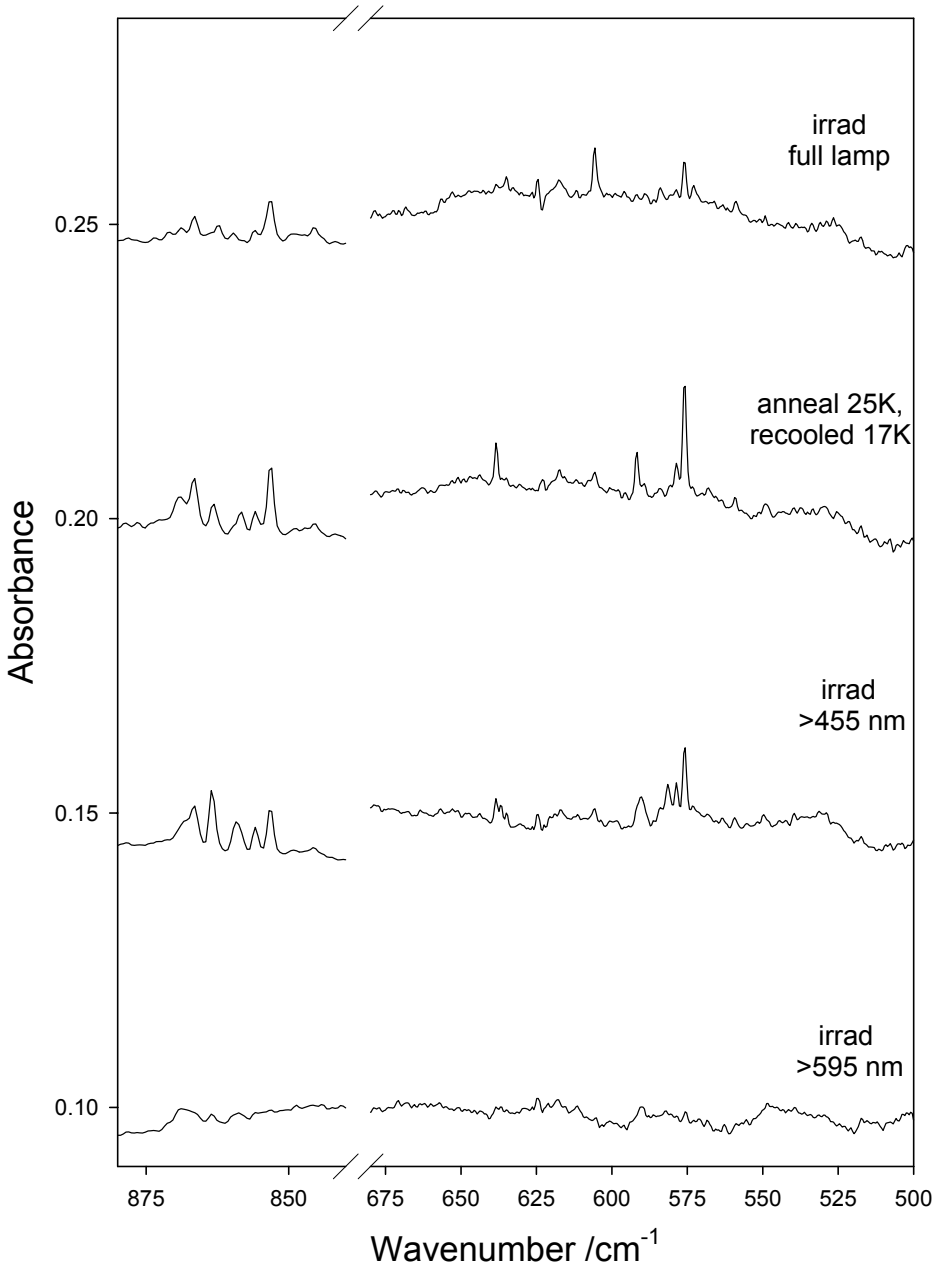

Figure 15: Portions of the infrared absorption spectrum in the V-C stretching mode region for V deposited with 1:200 C_2H_4:Ar, following various experimental changes. Only those spectra with new absorptions in this region have been displayed. These spectra are otherwise the same as the spectra in Figure 14. Spectra have been offset by an additive constant for clarity.

Table 2: Wavenumber positions for the various products observed in the infrared spectra following reaction of V + 1:200 C_2H_4:Ar. Entries marked with "i" represent increases following the experimental change listed at the top of the column. Entries marked with "d" represent decreases following the experimental change. Wavenumber values are in cm^{-1} units.

Wavenumber	deposit with V	>595 nm	>455 nm	anneal 25K	full lamp	product identity	Group code
2891	i					C_2H_6	
1673.3		i	i		d	site	
1667.8			i	i	d	$^2H_2V(C_2H_2)$ conformation	**B2**
1660.9		i	d	i	d	$^2H_2V(C_2H_2)$	**B**
1647.8		i	i		d	site	
1645.8		i	i	i	d	$^2H_2V(C_2H_2)$ conformation	**B2**
1643.5		i	i	i	d	site	
1638.4		i	d		d	$^2H_2V(C_2H_2)$	**B**
1584.5		i	i	i	d	^4H-V-C_2H_3 conformation	**C2**
1573.2			i		d	^4H-V-C_2H_3	**C**
1561.5			i		d	^4H-V-C_2H_3 conformation	**C2**
1557.6			i		d	^4H-V-C_2H_3 conformation	**A**
1552	i	i	i	d		^4H-V-C_2H_3 conformation	**A**
1547.4			i		d	^4H-V-C_2H_3 conformation	**A**
1465	i					C_2H_6	
1383.6			i	i	d	^4H-V-C_2H_3	**C**
1375	i					C_2H_6	
1304	i					CH_4	
1069		i	i	d		^4H-V-C_2H_3 conformation	**A**
866.7			i		d	site	
863.6			i		d	site	
859.2			i		d	site	
855.8			i		d	site	
852.9			i	i	d	^4H-V-C_2H_3	**C**
591.9				i	d	^4H-V-C_2H_3 conformation	**C2**
581.6			i		d	^4H-V-C_2H_3	**C**
578.6			i		d	site	
575.7			i	i	d	^4H-V-C_2H_3 conformation	**C2**

Irradiation of the matrix with light >595 nm (see Figure 14 and Figure 15) causes the weak growth of the feature at 1552.1 cm^{-1}, and also the growth of features at 1673.3 cm^{-1}, 1660.9 cm^{-1}, 1647.8 cm^{-1}, 1645.8 cm^{-1}, 1643.5 cm^{-1}, 1638.4, 1584.5 cm^{-1} and 1069 cm^{-1}. A summary table of the absorption positions, tentative identifications, and the corresponding effects following experimental changes are summarized in Table 2. The following sections contain further characterization of features, assigned to specific molecules. For ease of comparison, a summary of the isotopic comparisons is given in the Appendices section at the very end of this document, as Table 5.

Further irradiation of the matrix with light >455 nm, corresponding to the first major observed V atomic transitions, causes much more pronounced growth of features at 1673.3 cm^{-1}, 1667.8 cm^{-1}, 1647.8 cm^{-1}, 1645.8 cm^{-1}, 1643.5 cm^{-1}, 1584.5 cm^{-1}, 1573.2 cm^{-1}, 1561.5 cm^{-1}, 1557.6 cm^{-1}, 1552.1 cm^{-1}, 1547.4 cm^{-1}, 1383.6 cm^{-1}, 1069.4 cm^{-1}, and additionally new features at 866.7 cm^{-1}, 863.6 cm^{-1}, 859.2 cm^{-1}, 855.8 cm^{-1}, 852.9 cm^{-1}, 581.6 cm^{-1}, 578.6 cm^{-1}, and 575.7 cm^{-1}. The features at 1660.8 cm^{-1} and 1638.8 cm^{-1} are decreased following irradiation >455 nm for five minutes. Continued irradiation >455 nm shows no significant changes in the spectrum. Many changes occur in the infrared spectrum recorded following an annealing of the matrix to 25 K for 5 minutes, followed by the recooling of the matrix to 17K. Particularly, the major features present in the spectrum at 1552.1 cm^{-1} (1557 cm^{-1} and 1547 cm^{-1}) and 1069 cm^{-1} (labeled A in Figure 14 and Figure 15) disappear completely following annealing, and cannot be regenerated under any further experimental changes. That these features

track together under all experimental changes suggests they belong to a single molecule, and thus, these features are assigned together as group A. Corresponding to the loss of the group A absorptions, several other absorptions intensify significantly, at wavenumber positions: 1667.8 cm^{-1}, 1660.8 cm^{-1}, 1645.1 cm^{-1}, 1638.8 cm^{-1}, 1585.5 cm^{-1}, 1383.3 cm^{-1}, 853.3 cm^{-1}, 591.9 cm^{-1}, and 575.7 cm^{-1}.

Fortunately, many of these features have been previously identified by Cho and Andrews in their recent study,[4] and the major absorptions are due to doublet-$H_2V(C_2H_2)$ (1661 cm^{-1}, 1638 cm^{-1}, labeled species B in Figure 14 and Figure 15, and to quartet-H-V-$CH{=}CH_2$ (or quartet-H-V-C_2H_3) species (1573 cm^{-1}, 1383 cm^{-1}, 853.3 cm^{-1}, and 583 cm^{-1}, labeled species C in Figure 14 and Figure 15). The remaining features at 1667.8 cm^{-1}, 1645.1 cm^{-1}, 1585 cm^{-1}, 591.9 cm^{-1}, and 575.7 cm^{-1} are not clearly identified in the work of Cho and Andrews, however, these features separate into two distinct groups: Group B2: 1667.8 cm^{-1}, 1645.1 cm^{-1} and Group C2: 1585 cm^{-1}, 591.9 cm^{-1}, and 575.7 cm^{-1}. The features in group B2 behave qualitatively as the features attributed to $H_2V(C_2H_2)$, and thus, these features seem to correspond to a molecule with a similar structure. Similarly, the features of Group C2 behave exactly as the quartet-H-V-C_2H_3 absorptions above, under all conditions, and the major absorptions are very close to absorption positions due to quaret-H-V-C_2H_3. Thus, these species are tentatively assigned to conformational isomers of doublet-$H_2V(C_2H_2)$ (B2) and quartet-H-V-C_2H_3 (C2), respectively. The remaining features, all of which lie very close to these assigned features, are assumed to be absorptions of similar

molecules trapped in matrix sites. No further attention will be paid to these site absorptions in discussions.

Further irradiation of the matrix with the full output of the lamp results in the decrease in all features previously listed. Continued irradiation can eliminate all features, completely. In some matrices, new features near 590 cm^{-1} are the only features remaining, following annihilation of reaction products. This region corresponds to V-C motions, for which the absorption is likely due to some small metal-carbon species. However, further evidence of this species has not been well observed in our experiments, and no additional attention to these modes is paid in this work.

4.13 Reaction of V with isotopes of ethene: C_2D_4

To further identify the reaction product species, the deposition of V atoms with isotopomers of ethene in Ar has also been performed. Figure 16 and Figure 17 present portions of the infrared spectrum in the V-D and V-C stretching mode region for V atoms co-deposited with 1:200 C_2D_4:Ar, following various experimental changes. A table of these absorption values, their behaviour following experimental changes, and the associated product identities is given as Table 3. As with the C_2H_4:Ar experiments, all features associated with H_2O and C_2D_4 isolated in Ar are diminished when metal is present. In the infrared spectrum of the matrix immediately following deposition with metal, weak new features are present at 2979.0 cm^{-1}, 2947.0 cm^{-1}, 2238.4 cm^{-1}, 2235.8 cm^{-1}, 2233.2 cm^{-1}, 2226.0 cm^{-1}, 2216.4 cm^{-1}, 2085.4 cm^{-1}, and 1119.8 cm^{-1}. These features correspond to a number of reaction products, some of which have been

previously identified. In particular, the features at 2235.8 cm^{-1}, 2233.2 cm^{-1} and 2085 cm^{-1} occur at the exact wavenumber position for the major absorption of C_2D_6 isolated in Ar, and these absorptions are assigned accordingly to C_2D_6. Further investigation of the formation of this product, the formation of which is generally favoured under higher concentrations of ethene, is given in Chapter 6.

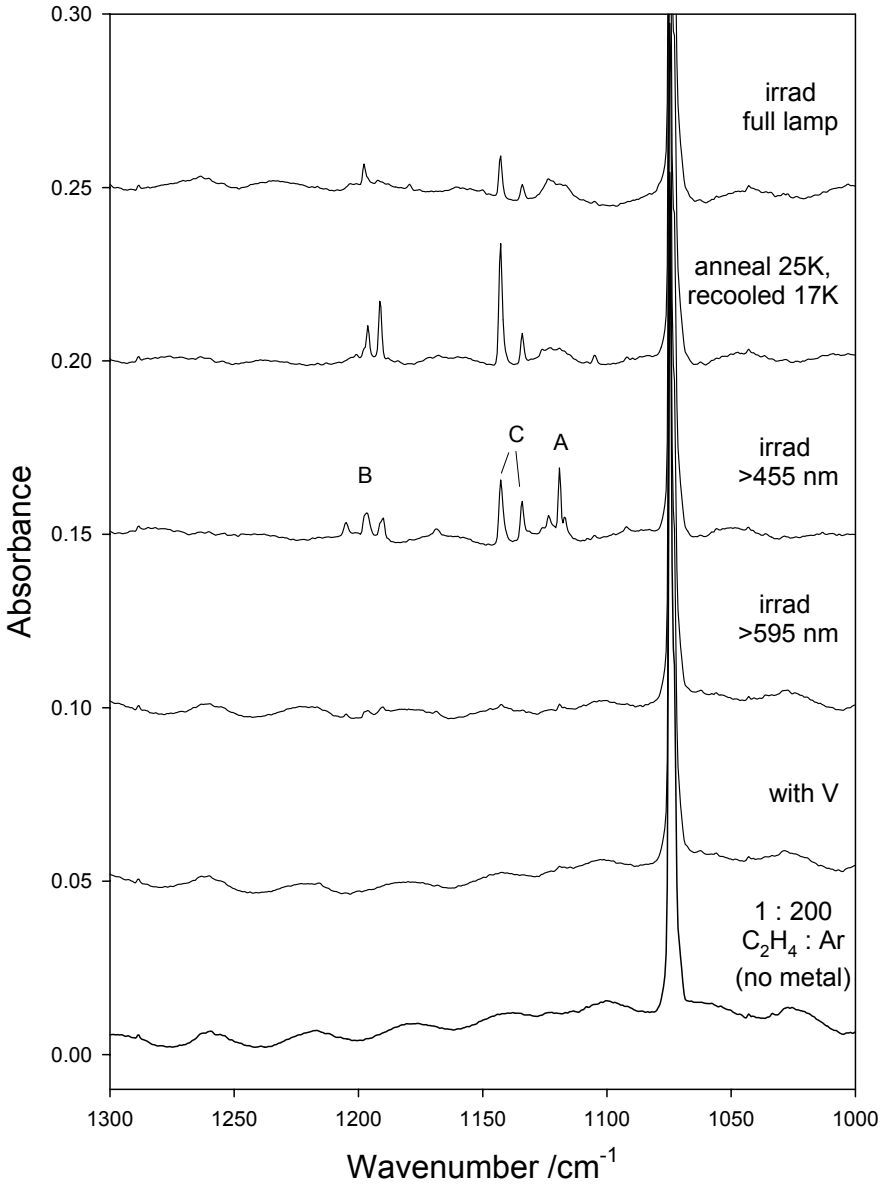

Figure 16: Portions of the infrared absorption spectrum in the V-D stretching following the reaction of V with 1:200 C_2D_4:Ar, after various experimental changes. The features labeled A correspond to an unknown product species, while B and C are the doublet-$D_2V(C_2D_2)$ and quartet-D-V-C_2D_3 species. Species A may be a configurational isomer of species C. Spectra have been offset by an additive constant for clarity.

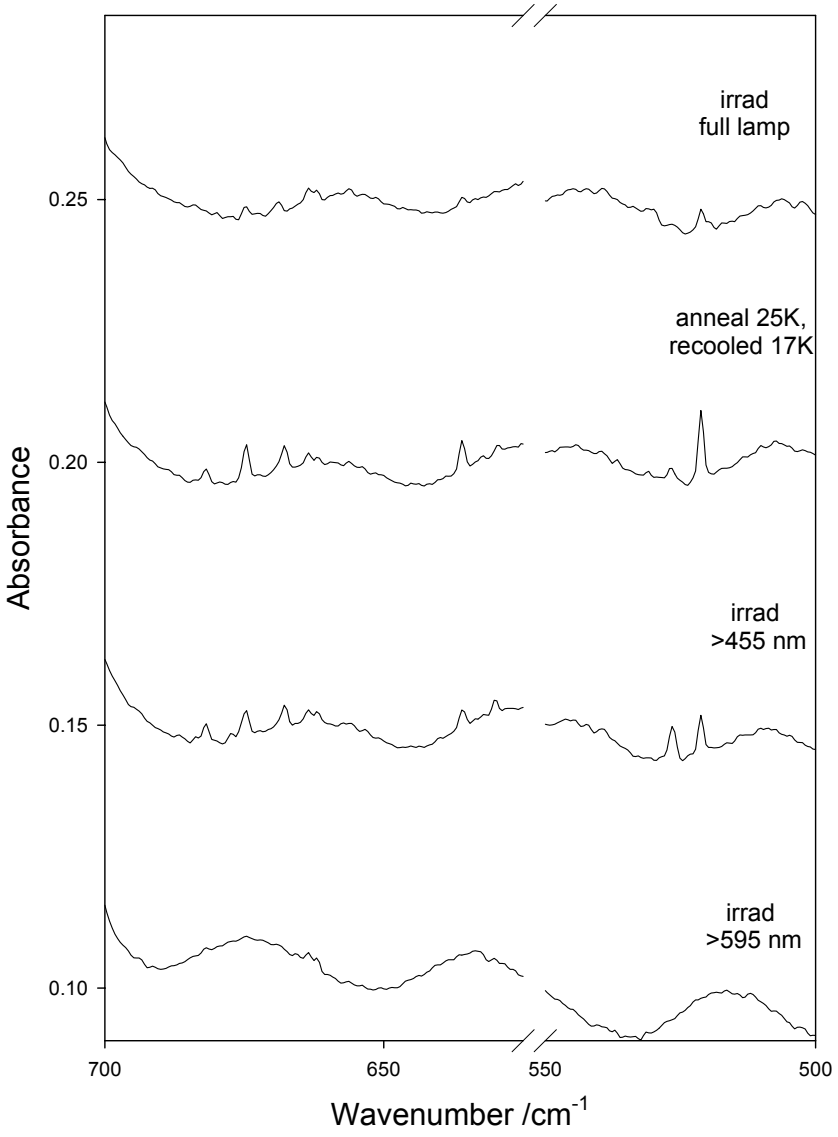

Figure 17: Portions of the infrared absorption spectrum in the V-C stretching mode region for V deposited with 1:200 C_2D_4:Ar, following various experimental changes. Only those spectra with new absorptions in this region have been displayed. These spectra are otherwise the same as the spectra in Figure 16. Spectra have been offset by an additive constant for clarity.

Table 3: Wavenumber positions for the various products observed in the infrared spectra following reaction of V + 1:200 C_2D_4:Ar. Entries marked with "i" represent increases following the experimental change listed at the top of the column. Entries marked with "d" represent decreases following the experimental change. Wavenumber values are in cm^{-1} units.

Wavenumber	deposit with V	>595 nm	>455 nm	anneal 25K	full lamp	product identity	Group code
2979	i					CHD_2CHD_2	
2947	i					CHD_2CHD_2	
2238.4	i					C_2D_6	
2235.8	i					C_2D_6	
2233.2	i					C_2D_6	
2226	i					CHD_2CHD_2	
2216.4	i					C_2D_6	
2085.4	i					C_2D_6	
1205.1		i	i	d	d	$^2D_2V(C_2D_2)$ conformation	**B2**
1197.8		i	i	i	d	$^2D_2V(C_2D_2)$	**B**
1191.4		i	i	i	d	$^2D_2V(C_2D_2)$	**B**
1142.6		i	i	i	d	^4D-V-C_2D_3 conformation	**C2**
1133.6		i	i	i	d	^4D-V-C_2D_3	**C**
1123			i	d		site	**A'**
1119.8	i	i	i	d		^4D-V-C_2D_3 conformation	**A**
1117			i	d		site	**A'**
1092.2			i			^4D-V-C_2D_3	**C**
681.7			i	i	d	^4D-V-C_2D_3 conformation	**C2**
674.5			i	i	d	^4D-V-C_2D_3	**C**
635.6			i	i	d	^4D-V-C_2D_3	**C**
526.2			i	d	d	site	
521.1			i	i	d	site	

The remainder of the features, 2979.0 cm^{-1}, 2947 cm^{-1}, and 2226 cm^{-1} correspond to C-H and C-D stretching features, for which the only source of H in these experiments is water, and the only C-D source is C_2D_4. These features behave similarly to the C_2D_6 formed, and are assigned as an ethane isotopomer generated by the reaction of V + H_2O + C_2D_4. A further investigation of this chemistry is given as Chapter 5. Finally, the feature at 1119 cm^{-1} has the same behaviour on deposition as the group A features when 1:200 C_2H_4:Ar is used, and thus, this feature is associated with the isotopomer of the same unknown molecule.

Following irradiation of the matrix with light >595 nm, several new features are observed in the 1250-1100 cm^{-1} range of the infrared spectrum. These features are at absorption positions of: 1205.1 cm^{-1}, 1197.8 cm^{-1}, 1191.4 cm^{-1}, 1142.6 cm^{-1}, 1133.6 cm^{-1}, and 1119 cm^{-1}. Annealing of the matrix causes the loss of the features at 1205 cm^{-1}, and loss at 1119 cm^{-1}. Correspondingly, the features at 1197.8 cm^{-1}, 1191.4 cm^{-1}, 1142.6 cm^{-1}, and 1133.6 cm^{-1} become sharper, as in the case of matrices formed containing C_2H_4.

As before, irradiation with >455 nm light causes much greater growth in the regions of 1250-1100 cm^{-1}. Growth of features occurs at 1205.1 cm^{-1}, 1197.8 cm^{-1}, 1191.4 cm^{-1}, 1142.6 cm^{-1}, 1133.6 cm^{-1}, and 1119 cm^{-1}, with other weaker features at 1123 cm^{-1}, 1117 cm^{-1}, 1092.2 cm^{-1}, 681.7 cm^{-1}, 674.5 cm^{-1}, 635.6 cm^{-1}, 526.2 cm^{-1}, and 521.1 cm^{-1}. Following annealing of the matrix to 25 K and recooling to 17 K results in the loss of features at 1205 cm^{-1}, 1123 cm^{-1}, 1119 cm^{-1}, 1117 cm^{-1}, and 527.1 cm^{-1} while the features at 1197.8 cm^{-1}, 1191.4 cm^{-1},

1142.6 cm^{-1}, 1133.6 cm^{-1}, 681.7 cm^{-1}, 674.5 cm^{-1}, 635.6 cm^{-1} and 521.5 cm^{-1} sharpen and intensify.

Again, many of these features have been previously identified by Cho and Andrews. In particular, the features at 1197.8 cm^{-1}, and 1191.4 cm^{-1}, exhibit the same behaviour as the group B features observed when C_2H_4 is used, and these absorptions correspond to the doublet-$D_2V(C_2D_2)$ molecule. The feature at 1205 cm^{-1} has not been previously identified, but exhibits the same characteristics as the doublet-$H_2V(C_2H_2)$ molecule listed above and is assigned to the group B2, as before.

Similarly, the absorptions, corresponding to group C, at 1133.6 cm^{-1}, 1092.2 cm^{-1}, 674.5 cm^{-1}, and 635.6 cm^{-1} have been assigned by Cho and Andrews to quartet-D-V-C_2D_3. The remaining features at 1142.6 cm^{-1}, and 681.7 cm^{-1} exhibit identical behaviour and similar wavenumber positions to the group C features under all experimental changes, and are assigned to the conformational isomer of the quartet D-V-C_2D_3 species as group C2 (similar to above). The features at 1119 cm^{-1} (1123 cm^{-1} and 1117 cm^{-1} are either sites or rovibrational lines) have the same behaviour as the features belonging to group A above, when C_2H_4 is used, and these are assigned to a single unidentified molecule.

As before, prolonged irradiation with the full output of the lamp causes the complete destruction of all the new features listed above, with the exception of the hydrogenated products present on initial deposition. No additional features are significant in these spectra.

4.14 Reaction of V with ethene isotopomers: V + 1:200 $^{13}C_2H_4$:Ar

Finally, when V atoms are codeposited with Ar containing $^{13}C_2H_4$, all features associated with $^{13}C_2H_4$ and water are diminished, and several new features are present in the infrared spectrum, analogous to the experiments similarly performed with the other isotopomers of ethene. Specifically, new features are present, when V is added, at: 2946 cm^{-1}, 2918 cm^{-1}, 2885 cm^{-1}, 1551.6 cm^{-1}, 1461.9 cm^{-1}, and 1365.6 cm^{-1}. Of these features, the features at 2946 cm^{-1}, 2918 cm^{-1}, 2885 cm^{-1}, 1461.9 cm^{-1}, and 1365.6 cm^{-1} correspond to $^{13}C_2H_6$, and factors leading to formation of this hydrogenated product are described in later chapters (see Chapters 5 and 6). Thus, the only remaining unidentified feature in these spectra is the 1551.6 cm^{-1} absorption. A table of these absorption values, their behaviour following experimental changes, and the associated product identities is given as Table 4.

Portions of the infrared spectra in the V-H and V-C stretching mode region for matrices formed containing V and ^{13}C-enriched C_2H_4, following various experimental changes, are presented as Figure 18 and Figure 19. As with the other isotopomers of ethene, when the initially deposited matrix is irradiated with light >595 nm, new absorptions occur at: 1672.6 cm^{-1}, 1660.1 cm^{-1}, 1647.6 cm^{-1}, 1645.7 cm^{-1}, 1643.3 cm^{-1}, 1638.6 cm^{-1}, 1551.6 cm^{-1}, and 1040 cm^{-1}. In the infrared spectrum recorded following annealing of the matrix to 25 K, the features at 1672.6 cm^{-1}, 1647.6 cm^{-1}, 1643.3 cm^{-1}, 1551.6 cm^{-1}, and 1040 cm^{-1} disappear, with significant growth of the features at 1660.1 cm^{-1}, 1638.6 cm^{-1}, and also new features at 1589.7 cm^{-1} and 1582.2 cm^{-1}. These last features grow similarly to

the 1585 cm^{-1} feature that is observed with $^{12}C_2H_4$ is used, and the average position of these bands would be 1585 cm^{-1}, suggesting this splitting may arise as a result of Fermi resonance with this ethene isotopomer.

Following irradiation of the matrix with >455 nm light, a tremendous increase in absorption bands in the infrared spectrum is observed. Although there is a decrease in the features at 1660.1 cm^{-1} and 1638.8 cm^{-1}, large growth occurs for features at 1672.6 cm^{-1}, 1647.6 cm^{-1}, 1645.7 cm^{-1}, 1643.3 cm^{-1}, 1589.7 cm^{-1} and 1582.2 cm^{-1}, 1573.0 cm^{-1}, 1556.9 cm^{-1}, 1551.6 cm^{-1}, 1547.8 cm^{-1}, 1345.8 cm^{-1}, 1040.9 cm^{-1}, 854.8 cm^{-1}, 847.6 cm^{-1}, 844.2 cm^{-1}, 569.9 cm^{-1}, 566.5 cm^{-1}, and 563.8 cm^{-1}. In the infrared spectrum recorded following annealing of the matrix to 25 K, the features at 1672.6 cm^{-1}, 1647.6 cm^{-1}, 1643.3 cm^{-1}, 1556.9 cm^{-1}, 1551.6 cm^{-1}, 1547.8 cm^{-1}, 1040 cm^{-1}, 854.8 cm^{-1}, 569.9 cm^{-1}, and 566.5 cm^{-1} all decrease, with the growth of 1660.1 cm^{-1} and 1638.8 cm^{-1}, 1589.7 cm^{-1} and 1582.2 cm^{-1}, 1346 cm^{-1}, 844.2 cm^{-1} and 563.8 cm^{-1}. Prolonged irradiation of the matrix with the full output of the lamp causes the complete destruction of all of these species.

As with the previous isotopomers, the mass of features can be distilled into groups of previously assigned molecules. In particular, the features at 1660.1 cm^{-1} and 1638.8 cm^{-1} correspond to group B behaviour, and are assigned as the doublet $H_2V(^{13}C_2H_2)$ molecule. As was previously the case, features at 1672.6 cm^{-1}, 1647.6 cm^{-1} exhibit similar behaviour to group B, and are assigned as group B2. The feature at 1573.0 cm^{-1} is assigned as group C to the quartet H-V-$^{13}C_2H_3$ molecule. The other group C features in the $^{13}C_2H_4$ spectrum appear

only weakly, in agreement with the weak intensity of the 1573 cm^{-1} feature. The remaining features at 1589.7 cm^{-1} and 1582.2 cm^{-1}, 1345.8 cm^{-1}, 854.8 cm^{-1}, 847.6 cm^{-1}, 844.2 cm^{-1}, 569.9 cm^{-1}, 566.5 cm^{-1}, and 563.8 cm^{-1} have the same characteristics, but slightly differing wavenumber values, as the quartet H-V-C_2H_3 molecule and are assigned, once again, as group C2. The remaining features at 1556.9 cm^{-1}, 1551.6 cm^{-1}, 1547.8 cm^{-1}, 1040.9 cm^{-1} are assigned as group A, and represent two new unknown molecules.

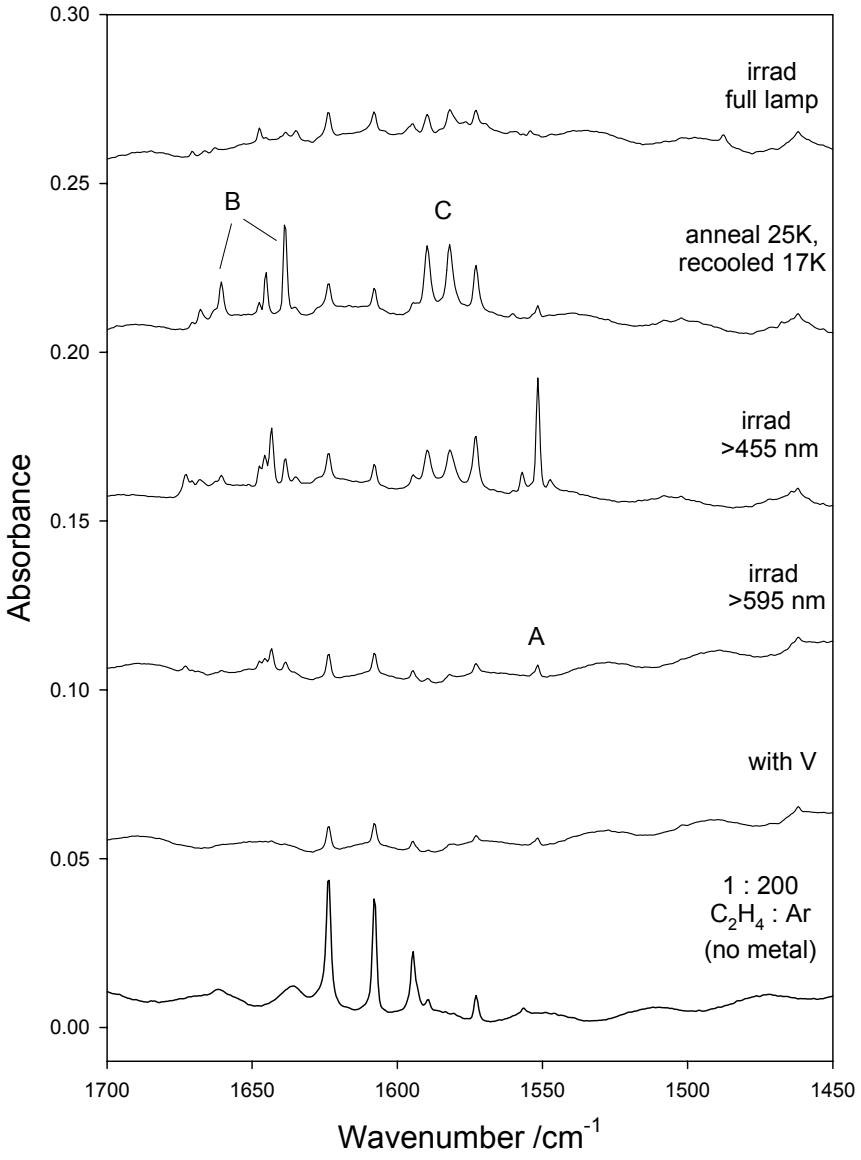

Figure 18: Portions of the infrared spectrum in the V-H stretching region for V atom reactions with 1:200 $^{13}C_2H_4$: Ar. The features labeled A correspond to an unknown product species, while B and C are the doublet-$H_2V(^{13}C_2H_2)$ and quartet-H-V-$^{13}C_2H_3$ species. Species A may be a configurational isomer of species C. Spectra have been offset by an additive constant for clarity.

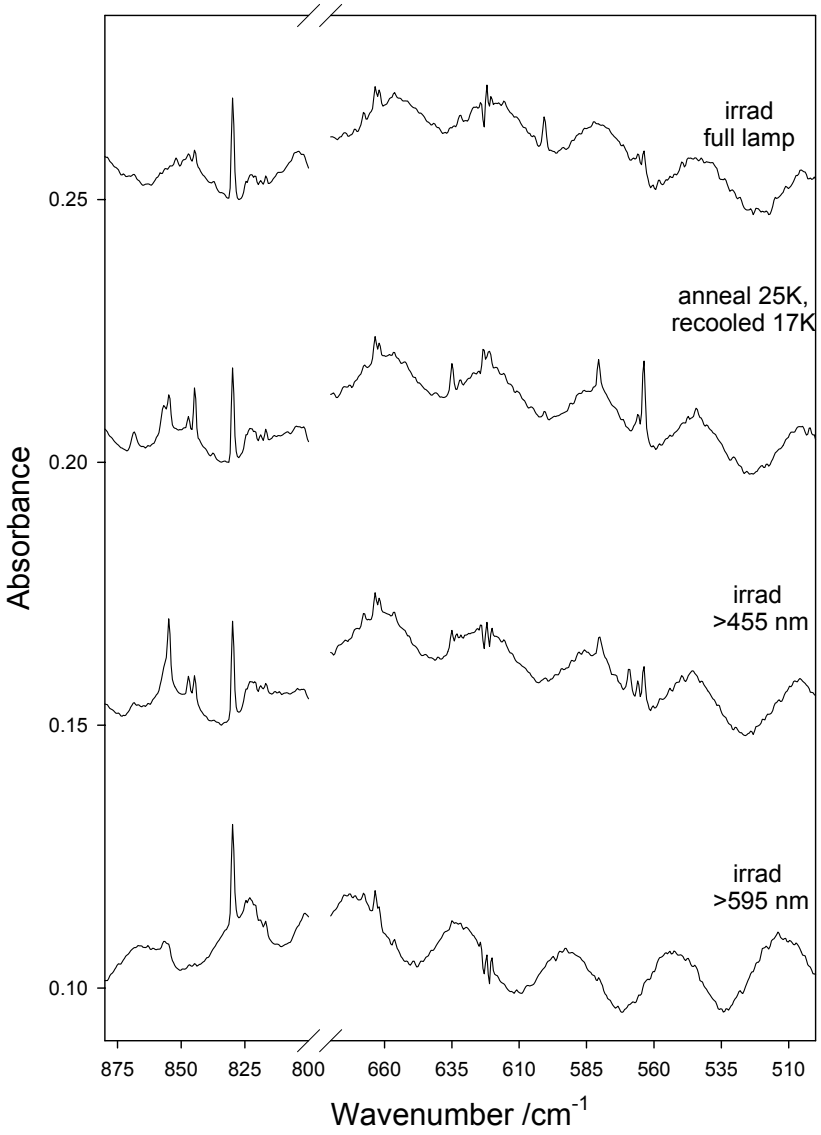

Figure 19: Portions of the infrared absorption spectrum in the V-C stretching mode region for V deposited with 1:200 $^{13}C_2H_4$:Ar, following various experimental changes. Only those spectra with new absorptions in this region have been displayed. These spectra are otherwise the same as the spectra in Figure 18. Spectra have been offset by an additive constant for clarity.

Table 4: Wavenumber positions for the various products observed in the infrared spectra following reaction of V + 1:200 $^{13}C_2H_4$:Ar. Entries marked with "i" represent increases following the experimental change listed at the top of the column. Entries marked with "d" represent decreases following the experimental change. Wavenumber values are in cm^{-1} units.

Wavenumber	deposit with V	>595 nm	>455 nm	anneal 25K	full lamp	product identity	Group code
2946	i					$^{13}C_2H_6$	
2918	i					$^{13}C_2H_6$	
2885	i					$^{13}C_2H_6$	
1672.6		i	i	d		$^{2}H_2V(C_2H_2)$ conformation	**B2**
1660.1		i	d	i	d	$^{2}H_2V(C_2H_2)$	**B**
1647.6		i	i	d		$^{2}H_2V(C_2H_2)$ conformation	**B2**
1643.3		i	i	d		site	
1638		i	d	i	d	$^{2}H_2V(C_2H_2)$	**B**
1589.7			i	i	d	^{4}H-V-C_2H_3 conformation	**C2**
1582.2			i	i	d	^{4}H-V-C_2H_3 conformation	**C2**
1556.9			i	d			**A'**
1551.6	i	i	i	d		^{4}H-V-C_2H_3 conformation	**A**
1547.8			i	d			**A'**
1461.9	i					$^{13}C_2H_6$	
1365.6	i					$^{13}C_2H_6$	
1345.8			i	i	d	^{4}H-V-C_2H_3 conformation	**C2**
1040.9		i	i			^{4}H-V-C_2H_3 conformation	**A**
854.8				d		^{4}H-V-C_2H_3 conformation	**C2**
847.6						^{4}H-V-C_2H_3 conformation	**C2**
844.2				i	d	^{4}H-V-C_2H_3 conformation	**C2**
569.9				d		^{4}H-V-C_2H_3 conformation	**C2**
566.5				d		^{4}H-V-C_2H_3 conformation	**C2**
563.8				i	d	^{4}H-V-C_2H_3 conformation	**C2**

4.15 Discussion of Infrared results

Following deposition of matrices formed containing metal atoms, a number of new product absorptions are always observed. In particular, products consistent with hydrogenation of the ethene molecule are observed, such as C_2H_6 (and isotopomers), and also products consistent with C=C bond cleavage, such as CH_4. The formation of these products requires extensive analysis, and each is explored further in later chapters. However, in order to understand the chemistry in those chapters, the products resulting from irradiation of these matrices may be required. Thus, the analysis of these new products, following deposition and irradiation of formed matrices is given here.

Similar experiments to ours have been completed previously by Cho and Andrews, where the only differences in experimental parameters are the matrix temperature (8K in their work) and the method of metal generation (laser ablation in their studies). As would be expected, we observe similar products in our spectra to the products observed in their experiments. However, some interesting variations occur in our matrices, including new features that are unobserved in their work.

One of the primary differences in our spectra arises from features due to quartet-H-V-C_2H_3, for which Cho and Andrews do observe multiplets of features, although, their spectra consistently show a major feature when C_2H_4 is used, at 1573 cm^{-1} (Group C above). For their product, this absorption is the major V-H stretching feature of a primary V/C-H bond insertion, while features at 1585 cm^{-1}

have similar behaviour, but are minor isolated species compared with the species giving rise to the 1573 cm^{-1} absorption. In our work, the 1573 cm^{-1} absorption is minor, while absorptions due to the 1585 cm^{-1} species (group C2) are generally maximized. The remarkably similar behaviour of these species in the two experimental systems suggests these are two isomers, and very likely simple conformational isomers, involving rotations of the V-H or V-C_2H_3 portions of the H-V-C_2H_3 molecule. Thus, it is expected that, under the conditions used in the apparatus giving rise to these results, we observe a complementary secondary isomer, that is not favoured in the Cho and Andrews apparatus. One possible explanation for this difference in formation is the different temperature of the two experimental systems, which may result in the differing yield of kinetic versus thermodynamic product environments during matrix condensation.

For all of the isotopes, the very slight shifts observed near fundamentals assigned to H-V-C_2H_3 by Cho and Andrews support this supposition, and thus, the majority of the newly observed modes (group C2 for each isotope) can be assigned straightforwardly to a simple configurational isomer of H-V-C_2H_3, for which the exact geometry is not known. Further computational investigations may provide additional information leading to plausible structures.

The most interesting new features observed in our matrices formed containing vanadium atoms and 1:200 C_2H_4:Ar, correspond to group A in all isotopic cases, and are observed in the infrared spectra immediately following deposition of the matrix. The group A features, grow selectively following irradiation with light >595 nm, very slowly. It is interesting to note from the UV-

visible discussion above, that both the V atom and the V_2 species have absorptions in the range of 590 nm, although the very weak absorption for the atom is not observed directly in our UV-visible spectra. That transition is, however, listed in Moore's tables,[1] as a very weak transition. The dimer absorption, by comparison, is significantly stronger, as can be seen from Figure 9. However, when vapour from the V filament is co-deposited with argon containing ethene, a complete **absence** of the features due to metallic dimer are observed, as described above. Thus, in the corresponding infrared experiments (performed with the same matrix tip), the growth of the group A features following irradiation with >595 nm light is not likely to result from V_2 chemistry, but instead to V/C_2H_4 chemistry.

Continued irradiations with >595 nm can cause continued growth, slowly, of the features corresponding to group A. Given that the intensity of light that is generated from the broadband irradiation of the lamp, the flux of photons available for absorption by V_2 would be sufficiently large after a single burst of light form the lamp. Since the species giving rise to these group A absorptions does not grow rapidly following irradiation with light corresponding to the intense V_2 absorption, but instead slowly, in agreement with a very weak V atomic transition, it seems reasonable to conclude that the observed group A features are indeed a result of atomic V reacting with C_2H_4. Furthermore, these features increase much more dramatically when stronger V atom excitations are excited using >455 nm light – and thus, it seems conclusive that all of these features are a result of V/C_2H_4 photochemistry.

When the C_2D_4 isotope is used, the group A feature arising from C_2H_4 at 1552 cm^{-1} shifts to 1119 cm^{-1}. The ratio of the absorption wavenumber when V reacts with C_2H_4 to the same absorption wavenumber when V + C_2D_4 is observed is: 1552 cm^{-1} / 1119 cm^{-1} = 1.39. This ratio of modes is consistent with a V-H stretching vibrational mode, and thus, it would appear that the feature at 1552 cm^{-1} is a result of V-H motion. When CH_2=CD_2 is used to perform the experiments, features at 1552 cm^{-1} and 1119 cm^{-1} appear in the infrared absorption spectrum, following irradiation of the matrix with >595 nm light. Thus, it seems clear that these features are associated with a photoinduced V reaction with ethene. That these features are present in the metal-containing spectra immediately following deposition of the matrix is clear evidence that some V/C_2H_4 C-H bond insertion chemistry is photoinduced by irradiation from the filament during deposition.

When the same experiments are performed with $^{13}C_2H_4$, the group A features appear again in the spectrum. That this feature at 1552 cm^{-1} when C_2H_4 is used does not shift with ^{13}C substitution implies that the motion giving rise to the absorption feature involves absolutely no C motion. This observation is completely consistent with a V-H stretching motion, and thus, it seems reasonable to assign the 1552 cm^{-1} feature as a result of a V-H stretch.

Although no analogue in the group A features for C_2H_4 at 1069 cm^{-1} is observed when C_2D_4 is used in these experiments, when $^{13}C_2H_4$ is used, a new feature does appear at 1040 cm^{-1}. The ratio of these features is 1069 cm^{-1} / 1040 cm^{-1} = 1.03. Since these are metal dependent, and shift significantly with

^{13}C substitution, this suggests that the absorption is due to significant M-C motion. The expected $^{12}C/^{13}C$ ratio for pure stretching absorptions would be: $(13/12)^{1/2} = 1.04$, and thus, the ratio observed experimentally seems to strongly support the assignment of this absorption as principally V-C motion. The exact type of V-C motion is unknown.

When the infrared spectrum is acquired following thermal annealing of the matrix to temperatures of 25 K or beyond and then recooling of the matrix back to 17 K, the group A features are always significantly decreased. That these features decrease so readily under very low thermal conditions suggests that the products are quite unstable, and can rapidly interconvert even within the matrix environment to more stable species. There appears to be an increase in features associated with both the major products of Cho and Andrews (doublet-$H_2V(C_2H_2)$ and quartet-H-V-C_2H_3), with the loss of the group A features, following annealing. The loss of group A features, with corresponding increase in the $H_2V(C_2H_2)$ and H-V-C_2H_3 features suggests that these group A absorptions arise from an isomer of $H_2V(C_2H_2)$ or HVC_2H_3. Since the growth of features associated with HVC_2H_3 is more significant, when the group A features disappear, it seems straightforward to propose the identity of the group A features as a very unstable rotational conformer of the HVC_2H_3 molecule. This conformation must readily convert, irreversibly, to the more stable product upon annealing.

In the computational work of Cho and Andrews, at least two minima corresponding to different rotations of the V-H bond with respect to the V-C_2H_3

unit have been found, for which the isomer observed at 1573 cm^{-1} in their spectra is proposed as the lowest energy structure. Thus, the observation of an increase in absorption at 1573 cm^{-1}, with the corresponding loss of the group A absorption features is consistent with the theory proposed above. Indeed, the group A features are observed following irradiation of similar matrices formed by Cho and Andrews, where the only differences in their experiments are matrix-condensation temperature, and the method of metal atom generation (laser ablation). However, no attempt to assign the 1552 cm^{-1} mode specifically is made within their work, nor has it even been identified in their product listing.

Further support of the group A and group C species as isomers of the H-V-C_2H_3 species can be obtained by analysis of the V-C stretching region. There are additional features in our spectra at 591.9 cm^{-1}, and 575.7 cm^{-1} that are observed in the work of Cho and Andrews, but not dealt with explicitly in their discussion. In our experiments, these two features have the same behaviour as the features associated with quartet-H-V-C_2H_3 absorptions. Thus, it would appear that these two features are associated with at least one of the isomers of H-V-C_2H_3. The spectra of Cho and Andrews give an absorption of H-V-C_2H_3 at 583.3 cm^{-1}, which is also observed very weakly in our spectra. Interestingly, this absorption assigned to V-C stretching falls at the averaged position of the 591 cm^{-1} and 575 cm^{-1} set of absorptions, which suggests that these two absorptions arise from some symmetric and anti-symmetric coupling of molecular motion.

Considering this theory, it is possible to propose two possible isomers of H-V-C_2H_3, one in which the π-bond of the vinyl group is internally coordinated to

the metal via agostic interactions, and a second structure in which the π bond of the vinyl group is quite distant from the metal centre. Since the features at 1585 cm^{-1} and 1573 cm^{-1} are believed to result from two different conformational isomers of the H-V-C_2H_3 species, it seems reasonable to expect that both of these two isomers could be isolated in the matrix. For the structure in which the π-bond of the V-C_2H_3 unit is donated to the metal, a pseudo-cyclic structure would be formed, having two similar V-C bonds. Thus, both symmetric and asymmetric C-V-C coupling would be expected in the infrared absorption spectrum. Thus, the fact that features at 591 and 575 cm^{-1} are observed, and that these species have the same behaviour upon experimental changes as the other quartet-H-V-C_2H_3 absorptions suggests that these two isomers could be responsible for the set of quartet-H-V-C_2H_3 modes. In our spectra, the 1585 cm^{-1} mode and the 591 and 575 cm^{-1} are all maximized simultaneously, and this would suggest that these modes belong to the same isomer. Thus, it is likely that these group C2 absorptions correspond to the H-V-C_2H_3 isomer having the π bond of the vinyl group donated into the metal centre. Therefore, the modes at 1573 cm^{-1} and 583 cm^{-1} (which are always simultaneously weak in our spectra) must correspond to the other H-V-C_2H_3 species, where the π-bond of the vinyl group is not coordinated to the metal species.

By similar arguments, all of our experiments give rise to absorptions due to the doublet $H_2V(C_2H_2)$ molecule, referred to as group B. Under certain experimental changes, a second set of absorptions having characteristically similar behaviour, occur at slightly higher wavenumber values. These new

absorptions, listed as group B2, seem likely to arise from an isomer of $H_2V(C_2H_2)$ by similar arguments to those made for the two conformational isomers of H-V-C_2H_3, above. No additional information is present that can provide information on the change in structure of the two isomers, from our experimental spectra. Thus, no additional considerations of these species can be made. One reasonable theorization is the bending of the H_2V portion of the molecule, following irradiation of the sample, as a result of perturbation from the matrix, or other matrix isolated species. Annealing of the matrix would result in the minimization of the perturbation, eliminating the group B2 series of absorptions, as is observed in the experimental spectra.

There remain some other simple discrepancies in the work of Cho and Andrews, when comparing their results with our spectra. In general, the intensity of our spectra is larger than the intensity in the corresponding experiments performed in their system. Since the conditions used in both experimental systems are otherwise similar, the generation of their reaction products in our system represents an opportunity to verify their assigned spectral details, which they have assigned for the first time.

For the reaction of V with C_2H_4, a new feature is observed at 2569.0 cm^{-1}, attributed to a significantly anharmonic C-H stretching mode of HV-C_2H_3, which shifts to 1989.8 cm^{-1} when C_2D_4 is used, and to 2561.9 cm^{-1} when $^{13}C_2H_4$ is used. As we have never observed any of these features in spectra where significantly increased yields of the HV-C_2H_3 isomer are observed, these additional features must belong to another molecule or set of molecules. As the

Cho and Andrews work uses laser ablation, it is possible that these additional spectral features arise from artifacts of the laser ablation technique, which would be absent in our complementary experiments employing thermal vaporization of metal atoms.

Additionally, a feature observed in V with C_2H_4 spectra at 1383.2 cm^{-1} gives a shift in the Andrews spectra to 1092 cm^{-1}, when C_2D_4 is used, but no similar absorption is observed for $^{13}C_2H_4$. We do observe a feature at 1345 cm^{-1}, when $^{13}C_2H_4$ is used, and this feature has the appropriate behaviour necessary to assign this absorption as the $^{13}C_2H_4$ counterpart of the H-V-$^{13}C_2H_3$ molecule.

It is interesting to note that, irradiation with light >455 nm in our experiments (>420 nm in Cho and Andrews) causes the growth of quartet-H-V-C_2H_3 species, and also of doublet-$H_2V(C_2H_2)$ species directly. Annealing of the resultant matrix causes the sharpening of features associated with the doublet $H_2V(C_2H_2)$ molecules. The simultaneous appearance of these two products following irradiation requires some consideration. For direct photoinduced formation of doublet-$H_2V(C_2H_2)$ from quartet-H-V-C_2H_3, it would be expected that $H_2V(C_2H_2)$ is formed by the second insertion of the V centre into the closest C-H bond of the CH_2 portion of the vinyl species. Experiments involving CH_2=CD_2 show selective formation of HDV(DCCH),[4,12] demonstrating that the two hydrogen atoms in the H_2 portion of $H_2V(C_2H_2)$ originate from the two different carbon atoms of the C_2H_4 molecule. However, the thermodynamic calculations of Cho and Andrews show this process to be significantly endothermic. As a result, photoexcitation of the quartet H-V-C_2H_3 species **must** be required to

induce the second C-H bond insertion. A resultant spin change is necessary to produce the observed doublet-$H_2V(C_2H_2)$ molecule, which should not be possible by direct photoexcitation. The formation of quartet-$H_2V(C_2H_2)$ would be possible, however, this species is quite high in energy, compared from $V(C_2H_2) + H_2$. Elimination of molecular hydrogen from the quartet-$H_2V(C_2H_2)$ species would then result in $V(C_2H_2)$ and H_2 in the matrix. This process would then be entirely allowed on the basis of spin conservation. However, the observed reaction product is doublet $H_2V(C_2H_2)$, which is even lower in energy than the quartet $V(C_2H_2) + H_2$ products. Thus, this reaction should occur spontaneously, and may have only a small reaction barrier to the formation of the products. Assuming significant overlap in the doublet and quartet potential energy surfaces of these similar geometry molecules, the earlier formed quartet-$V(C_2H_2)$ species, trapped near molecular hydrogen, could then produce the doublet-$H_2V(C_2H_2)$ species by an intersystem crossing to the lower spin product surface without a need to photoexcite the molecule. That the spectroscopic features associated with the $H_2V(C_2H_2)$ product can sharpen upon thermal annealing may well support this theory. Additionally, since H_2 is quite mobile in the matrix and all features associated with $V(C_2H_2)$ and H_2 are weak[f] in the infrared spectrum these species would be invisible, until the V-H stretching modes of the doublet-$H_2V(C_2H_2)$ product became visible. The availability of H_2/D_2, as evidenced by the formation of VH_2/VD_2 following irradiation in Cho and Andrews work supports this theory, as well. Thus, these results suggest that molecular hydrogen can be

[f] This statement is supported both by the calculations of Cho and Andrews, and by reasons of selection rules for infrared spectroscopy.

photoeliminated from the quartet-H-V-C_2H_3 species, and that the formation of doublet-$H_2V(C_2H_2)$ is possibly due to a thermal reaction of quartet-$V(C_2H_2)$ with molecular hydrogen.

Finally, when looking more closely at the spectrum presented by Cho and Andrews for the $H_2V(C_2H_2)$ molecule, a feature at 1527 cm^{-1}, which is unobserved in C_2D_4 work, but shifts to 1487 cm^{-1} when $^{13}C_2H_4$ is used, is never observed in any of our spectra. Thus, we believe that these product features are not due to the $H_2V(C_2H_2)$ molecule, and that instead these features must arise from some competitive chemistry, which is unavailable in our experiments generated via thermal vaporization of metal atoms.

4.16 Summary and conclusions

Analysis of the UV-visible spectra of argon matrices formed containing the products of vaporization of vanadium from a thin metal strip give evidence consistent with the isolation of V atoms and V dimer. Increasing the temperature of the matrix cold tip favours the formation of metallic dimer, while, increasing the flow rate of the gas during matrix deposition slightly favours monomer isolation. As the concentration of ethene present in the matrix gas sample is increased, absorptions in the UV-visible spectrum due to dimer disappear, likely as a result of metal-ethene van der Waals complexes. This latter point is supported by the broadening of V atomic absorptions at higher ethene concentration in the matrix. Irradiation of matrices containing V atoms and ethene with light corresponding to the highest energy V atom excitations (>455 nm) results in the destruction of all features associated with V atom absorptions in the spectrum.

When metal atoms are deposited under matrix isolation conditions with ethene in argon, at a concentration of 1:200, major new products are evident through analysis of the infrared spectra. These products are identified as ethane, methane, two possible isomers of doublet-$H_2V(C_2H_2)$, and three conformational isomers of quartet-H-VC_2H_3. These latter three species are formed only following irradiation of the matrix with various wavelengths of light corresponding to V-atomic transitions, and can subsequently be destroyed with prolonged irradiation with shorter wavelengths.

4.17 References for Chapter 4

[1] Moore, C.E.; Circ. U.S. Natl. Bur. Stand., 467, 1, **1947**.

[2] Devore, T.C.; *J. Chem. Phys.*, **1975**, 62, 520.

[3] Ford, T.A.; Huber, H.; Klotzbucher, W.; Kundig, E.P.; Moskovits, M.; Ozin, G.A.; *J. Chem. Phys.*, **1977**, 66, 524.

[4] Cho, H.G.; Andrews, L.; *J. Phys. Chem. A*, **2007**, 111, 5201.

[5] Ritter, D.; Carroll, J.J.; Weisshaar, J.C.; *J. Phys. Chem.,* **1992**, 96, 10636.

[6] See, for example: Weast, R.C; Lide, D. R. (eds); CRC Handbook of Chemistry and Physics, 70th ed., CRC Press, Boca Raton, **1989**.

[7] Kafafi, Z.H.; Hauge, R.H.; Margrave, J.L.; *J. Am. Chem. Soc.*, **1985**, 107, 7550.

[8] Klotzbucher, W.E.; Mitchell, S.A.; Ozin, G.A.; *Inorg. Chem.*, **1977,** 16, 3063.

[9] Ayers, G.P.; Pullin, A.D.E.; *Spectrochim. Acta*, **1976**, 32A*,* 1629.

[10] Cowieson, D.R.; Barnes, A.J.; Orville-Thomas, W.J.; *J. Raman Spec.*, **1981**, 10, 224.

[11] Thompson, M.G.K.; Parnis, J.M.; *J. Phys. Chem. A*, **2005**, 109, 9465.

[12] Lee, Y.K.; Manceron, L.; Papai, I.; *J. Phys. Chem. A*, **1997**, 101, 9650.

Chapter 5

Reactivity of ethene with metal hydrides generated from M + H_2O

5.0 Introduction[g]

In the initial investigations of early transition metal atoms reacting with ethene, an observed hydrogenation process implicated a reaction of more than one ethene molecule.[1] At lower ethene concentrations, as was explored in Chapter 4, C-H bond insertion involving photoexcited V atoms occurs with visible light. These results are consistent with the kinetics results of Ritter and coworkers,[2] when studying gas-phase V atom and ethene chemistry. The results showed clear evidence for C-H bond insertion products such as the vinyl vanadium hydride, H_2C=HC-V-H, and a coordinated acetylene dihydride, (η^2-C_2H_2)VH_2, [3] formed following irradiation of the matrices with wavelengths corresponding to excitations of matrix isolated V atoms.[4] While the majority of results of Chapter 4 were in excellent agreement with the results of Cho and Andrews, the results presented in that chapter also suggested evidence consistent with the further reactivity of those transient species with additional ethene. A more detailed investigation of metal atoms reacting with multiple

[g] A similar but modified version of this chapter been submitted to: *Inorganic Chemistry*. It is currently under review.

ethene molecules is presented in detail as the next chapter of this work. Such results, observed under conditions where the concentration of ethene was very high, were expected to decrease dramatically as the concentration of ethene was diminished.

Subsequent to this work, the surprising persistence of ethane formation has been observed, even under conditions where only a single ethene might be expected to react. This has led to consideration of the availability of other sources of metal hydrides, which provide the key M-H bonds necessary for ethene hydrogenation products to be observed. In the case of low ethene concentration, the only other source of H atoms in the experiments is water, an unavoidable impurity, which was previously believed to be uninvolved in the formation of ethane at high ethene concentrations. In light of these new results of ethane formation under lowered ethene concentration, an investigation of alkene hydrogenation involving the metal hydride bonds formed by metal atom reactions with either ethene or with water has been performed. To differentiate the chemistry of the two potential metal hydride sources, selective experiments involving only C_2D_4 and H_2O have been used as a means of mapping the source of H/D involved in the overall hydrogenation. This method has proven successful in identifying products implicating both insertion of metal atoms in the C-H (C-D) bond of ethene, and the O-H bond of water, as discussed in detail below. In all cases, the insertion of ethene into M-H bonds of the intermediates formed following C-H or O-H bond insertion is believed to be a key step leading to the resultant hydrogenated ethene products.

5.1 Experimental details

Unless otherwise specified, matrix deposition times were 1 hour in these experiments, at flow rates indicated in the text. In the case of computational results, simulated spectra have been generated for various isotopomers of ethane with Gaussian 98 software[5] using the B3LYP[6,7] functional and the 6-311G(df,p) basis set using the SWIZARD program.[8] The half-bandwidths of simulated spectra, $\Delta_{1/2}$, were taken to be equal to ~3 cm^{-1} to be comparable with our experimental matrix-isolated spectra. For a direct comparison with experiment, wavenumber positions for simulated spectral data have been scaled by an appropriate factor as indicated in the text in the results sections, below. Otherwise, all other technical details of the matrix experiments were performed as described in Chapter 3.

5.2 Experimental Results

Co-deposition of V atoms in Ar matrices containing C_2H_4 and H_2O under relatively low concentrations of each species (1:2:1000, H_2O:C_2H_4:Ar), resulted in the observation of C_2H_6 as the major product in the infrared spectrum. A set of similar reactions in which the only variable parameter was the flow rate of the gas mixing with the vaporized metal showed a trend of increasing ethane formation following matrix deposition, as the flow rate of the gas was increased. Figure 20 demonstrates the variation in the measured peak area for three of the major absorption bands of ethane generated by the reaction of V atoms and C_2H_4 in Ar, as a function of the gas-flow rate during matrix deposition. At higher flow rates, the formation of ethane was maximized, indicating that such conditions are

optimal for exploring the formation of ethane in this apparatus. In all further results, the gas-flow rate used for matrix preparation was 5.00 sccm (standard cm^3).

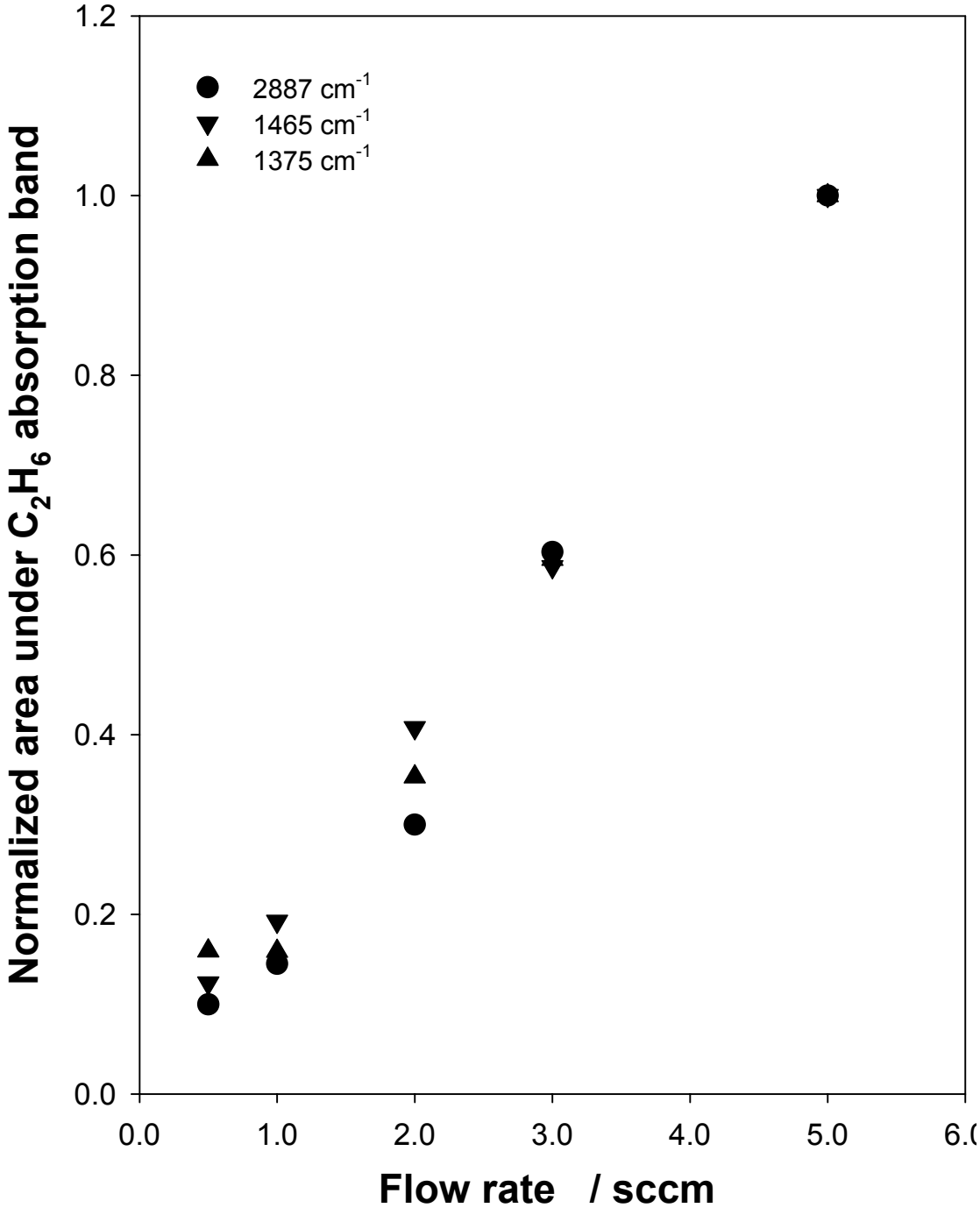

Figure 20: Comparison of ethane yield with gas-flow rate for V + C_2H_4 reaction under matrix isolation conditions.

When V atoms are co-deposited with Ar containing only dilute H_2O, all infrared spectral features associated with matrix isolated H_2O are substantially decreased. Concurrently, weak features at 1710 cm^{-1}, 1680 cm^{-1} and 1029 cm^{-1} are observed in the spectrum, immediately after deposition. These features correspond to OVH_2 isolated in an argon matrix.[9] Furthermore, under conditions where the ethene in the matrix is dilute (<1:500 C_2H_4:Ar), these weak features associated with OVH_2 can be increased by annealing the matrix from 17 to 25K. Surprisingly, no evidence for a feature at 1567 cm^{-1} is observed, corresponding to the HO-V-H species,[9] nor is the feature at 1583 cm^{-1} originally assigned to HO-V-H by Kauffman *et al*.[10] In cases where the concentration of ethene is most dilute (< 1:2000 C_2H_4 to Ar), irradiation of matrices containing V atoms with light of wavelengths >455 nm caused the growth of a feature at 1508 cm^{-1} corresponding to VH_2.[11] Similar matrices prepared containing 1:2000 C_2D_4:Ar showed continued formation of VH_2 following irradiation, while no evidence for VD_2 was observed. As the only source of H present in these experiments is H_2O, this suggests that a relatively rapid reaction with V and H_2O under deposition conditions occurs, ultimately eliminating molecular hydrogen.

In contrast, as the concentration of C_2D_4 in argon is slowly increased, spectral features corresponding to OVH_2 were diminished. As well, as the concentration is increased through to 1:200 C_2D_4:Ar, irradiation of the matrix with wavelengths >455 nm no longer showed evidence for VH_2 formation. Instead, a set of new features was present on deposition at 2947.5, 2238.7, 2235.7, 2232.8, 2226.3, 2216.8, 2158.2, 2134.5, and 2084.9 cm^{-1}, with corresponding increases

in intensity as the concentration of C_2D_4 was raised. Representative spectra demonstrating the increase in these features with V atoms reacting with increasing concentration of C_2D_4 can be seen in Figure 21.

Of these new features, there are two clear sets based on correlation in variation of integrated peak areas, as the experimental conditions were changed. One set "A", at 2238.7, 2235.7, 2232.8, 2216.8, 2134.5 and 2084.5 cm^{-1} behaved similarly in all experiments in which they were present, and occurred at wavenumber positions corresponding to the most intense features in the Ar matrix-isolated spectrum of C_2D_6.[1] Thus, the features corresponding to set A are identified as C_2D_6 isolated in Ar. The remaining features, set "B", at 2947.5, 2232.8 (overlapped with C_2D_6), 2226.3, and 2158 cm^{-1}, showed a similar behaviour in all experiments, and have the same characteristics of a completely saturated hydrocarbon containing at least one C-H bond but primarily C-D bonds. No other major modes were present in the spectra in which set A and B appeared. As can be seen in Figure 21, the set of features labeled "B" began to appear first in the most dilute spectra containing C_2D_4. As C_2D_4 concentration was increased, the B set of features slowly grow, with a more marked increase in features associated with set A demonstrating that these two species are generated by competitive mechanisms.

Given that the major features observed in set B are observed with concomitant loss of H_2O and C_2D_4, and that the set contained one major C-H stretching mode absorption and several C-D stretching mode absorptions similar to those associated with C_2D_6, we have assigned the features to a saturated

hydrocarbon product of V + H_2O + C_2D_4. The simplest saturated hydrocarbon product involving H_2O and C_2D_4, which contains only C-H and C-D bonds, is expected to be an ethane isotopomer of the stoichiometry $C_2D_4H_2$. Given this stoichiometry, two major isomers are possible: CD_2H-CD_2H (which has two rotatonal conformations) and CDH_2-CD_3. The gas-phase spectrum of CD_2H-CD_2H is known by the work of Van Riet,[12] although the CH_2D-CD_3 spectrum is not studied in that work. All of the modes observed in set B are common to the gas-phase CD_2H-CD_2H spectrum, although no intensity data for these isomers is provided, and thus the absence of key modes of significant intensity cannot be immediately considered. As a result, we have undertaken B3LYP/6-311G(df,p) calculations of the vibrational spectrum of the two ethane isotopomers as a means of further confirming the identity of the features corresponding to set B as CD_2H-CD_2H.

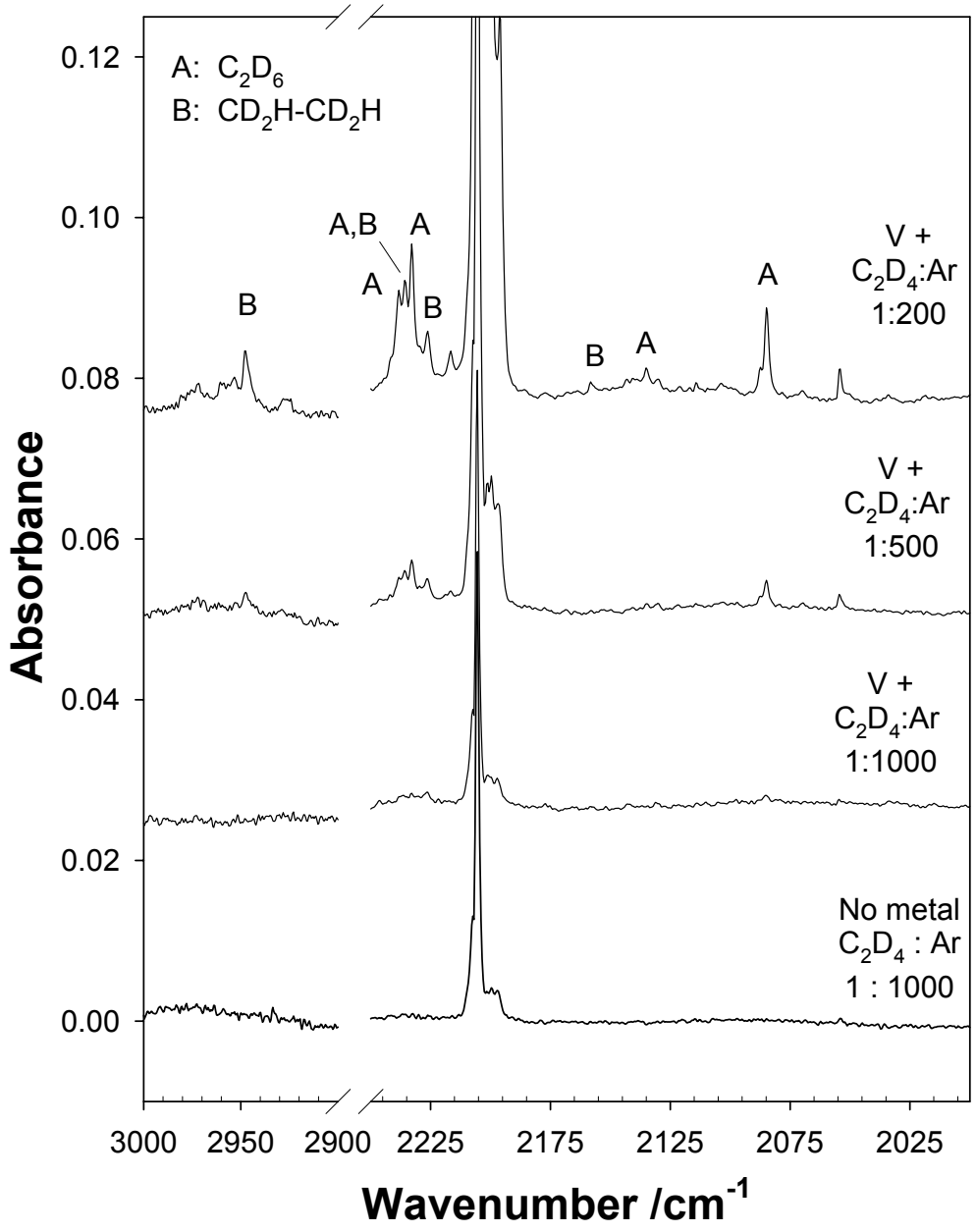

Figure 21: Portions of the infrared spectra in the C-H and C-D stretching region for V atoms reacting with H_2O and C_2D_4 isolated in Ar at C_2D_4 concentrations ranging from 0.01% to 0.5% C_2D_4. The bottom reference spectrum containing no metal is of the lowest C_2D_4:Ar concentration. Major product bands have been labeled for clarity, while any unmarked features correspond to C_2D_4 in Ar.

5.3 Computational Results

In order to directly compare calculated vibrational spectra with the corresponding experimental infrared spectra, the calculated vibrational frequencies for ethane isotopomers generated with Gaussian 98[5] have been simulated as spectra using the SWIZARD program.[8] In all cases, a scaling factor of the calculated data is necessary for a direct comparison with experiment.

Originally, a single scaling factor was intended for scaling hydrocarbon stretching features, based on the ratio of the experimentally observed C-H stretch of C_2H_6 to the computationally predicted value. However, when that factor calculated based on C_2H_6 is applied to the calculated values of C_2D_6, the C-H scaling factor does not accurately shift the data to the observed experimental spectrum of C_2D_6. Scott and Radom[13] report differences in associated scaling factors, including mild differences for high and low vibrational frequency modes, and thus it seems entirely appropriate to use specific scaling factors that are properly representative of the associated experimental system. Recognizing that such subtle differences can occur, it seemed prudent to use separate scaling factors based on C_2H_6 and C_2D_6 for comparison of our mixed-isotopic ethane calculations. Thus, separate scaling factors for each of the C-H and C-D stretching regions have been applied, based on C_2H_6 and C_2D_6 experimental results. Given that both C_2H_6 and C_2D_6 have been observed in spectra of our own matrices, we have used the observed spectra and calculated our scaling factors based on the C-H or C-D stretching mode predicted to have greatest intensity for C_2H_6, and C_2D_6 respectively using B3LYP/6-311G(df,p).

The scaling factor is then calculated as the ratio of the experimental wavenumber position in an Ar matrix for C_2H_6 or C_2D_6 to the corresponding calculated value. These scaling factors are, for C_2H_6: 2980 cm^{-1} / 3098 cm^{-1} = 0.962 and for C_2D_6: 2233 cm^{-1} / 2295 cm^{-1} = 0.973. Thus, for simulated spectra in the C-H stretching region, all of the calculated wavenumber values have been multiplied by 0.962 for comparison with experiment (given as Figure 22), and for a comparison of experimental and simulated spectra in the C-D stretching region, all of the calculated wavenumber values have been scaled by a factor of 0.973 for comparison (given in Figure 23). In both cases, these calculated scaling factors are in excellent agreement with similar scaling factors recently calculated in benchmarking tests of organic molecules by Merrick *et al*.[14]

Although the simplest addition product of H_2 to C_2D_4 is CD_2H-CD_2H, the isomeric possibility CDH_2-CD_3 has also been considered as a means of investigating the possibility of H/D scrambling or possible C_2D_4 rearrangements on the metal atom during reaction. The simulated spectra of the *anti* rotamer of CD_2H-CD_2H and the spectrum of CDH_2-CD_3 are also presented in Figure 22 and Figure 23, for comparison. Although the *gauche* rotamer of CD_2H-CD_2H has a unique predicted spectrum, there are but two major differences from the spectrum of the *anti* rotamer of CD_2H-CD_2H. First, a small predicted blueshift of the C-H stretching wavenumber positions, and secondly there is predicted intensity in both of the symmetric and asymmetric C-H stretch, with approximately 13 cm^{-1} splitting. Thus the simulated spectrum of the *gauche* rotamer of CD_2H-CD_2H has been omitted from Figure 22 and Figure 23 for

clarity. For ease of comparison, and as C_2D_6 is an identified reaction product in these spectra, the spectrum of C_2D_6 serves as a reference point for further identification of the secondary product(s) using the shifts in predicted wavenumber positions of modes associated with C_2D_6.

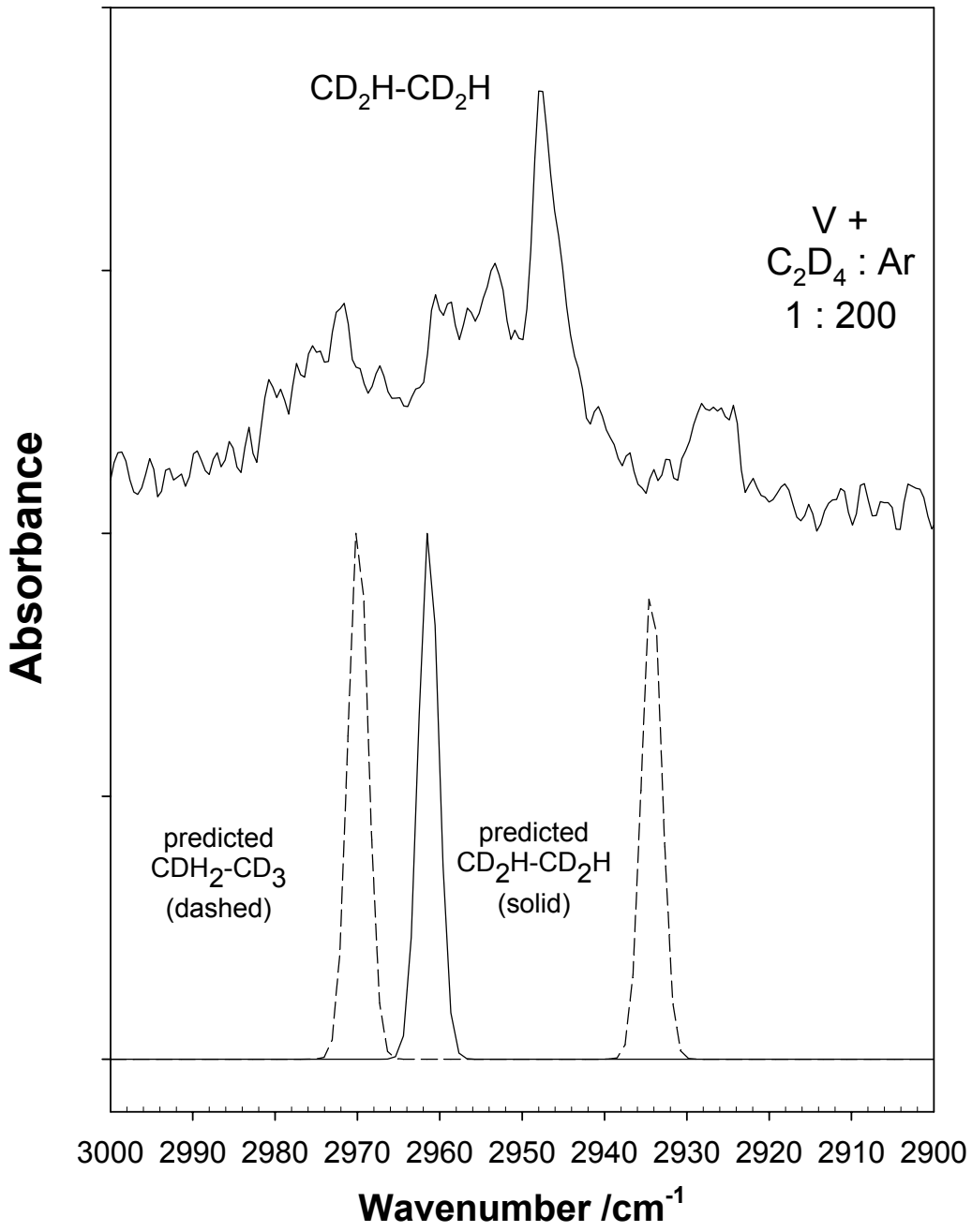

Figure 22: Portions of the simulated spectrum in the C-H stretching region for the two suspected isotopomers of ethane generated using the B3LYP/6-311G(df,p) method with Gaussian 98 and SWIZARD software. For comparison, a portion of the C-H stretching region of the infrared spectrum of an Ar matrix formed containing V atoms codeposited with 1:200 C_2D_4 :Ar is also presented.

In Figure 22, a comparison of the C-H stretching region of the experimental infrared spectrum of a matrix containing V atoms in 1:200 C_2D_4:Ar with the simulated spectra of CD_2H-CD_2H and CDH_2-CD_3 is given. The experimental spectrum showed one major feature corresponding to a C-H stretching vibration in this region. On first comparison, the simulated spectrum of CD_2H-CD_2H had exactly one C-H stretching vibration in this region. In contrast, the spectrum of CDH_2-CD_3 should be expected to show both a symmetric and asymmetric set of C-H stretches due to coupling of the two adjacent H atoms in this isomer. The calculated difference in the symmetric and asymmetric C-H stretching wavenumber positions, $\Delta\nu$, for the CDH_2-CD_3 isomer is approximately 35 cm^{-1}. No splitting of the major absorption in the C-H region of the experimental spectrum corresponding to this $\Delta\nu$ value is observed, although the weak, broad features present on either side of the main C-H absorption in Figure 22 may be evidence for small amounts of this isomer.

As a comparison, similar matrices were prepared involving Nb atoms under similar conditions for which the same spectra in this region are considerably more intense, and the broad weak features in Figure 22 which might be expected to correspond to CDH_2-CD_3 do not intensify. Instead, the triplet of features surrounding the 2947 cm^{-1} feature grows, with approximately 6-7 cm^{-1} splitting on either side of the major band. Interestingly, the *gauche* CD_2H-CD_2H rotamer predicts a coupled set of C-H stretching vibrations with approximately 13 cm^{-1} splitting between the symmetric and asymmetric vibrations, and a relative intensity profile similar to that observed around the 2947

cm^{-1} feature. Thus, the observed triplet of features in the C-H stretching region seems to be in excellent agreement with a mixture of the rotamers of CD_2H-CD_2H, rather than any signals originating from a CDH_2-CD_3 isomer.

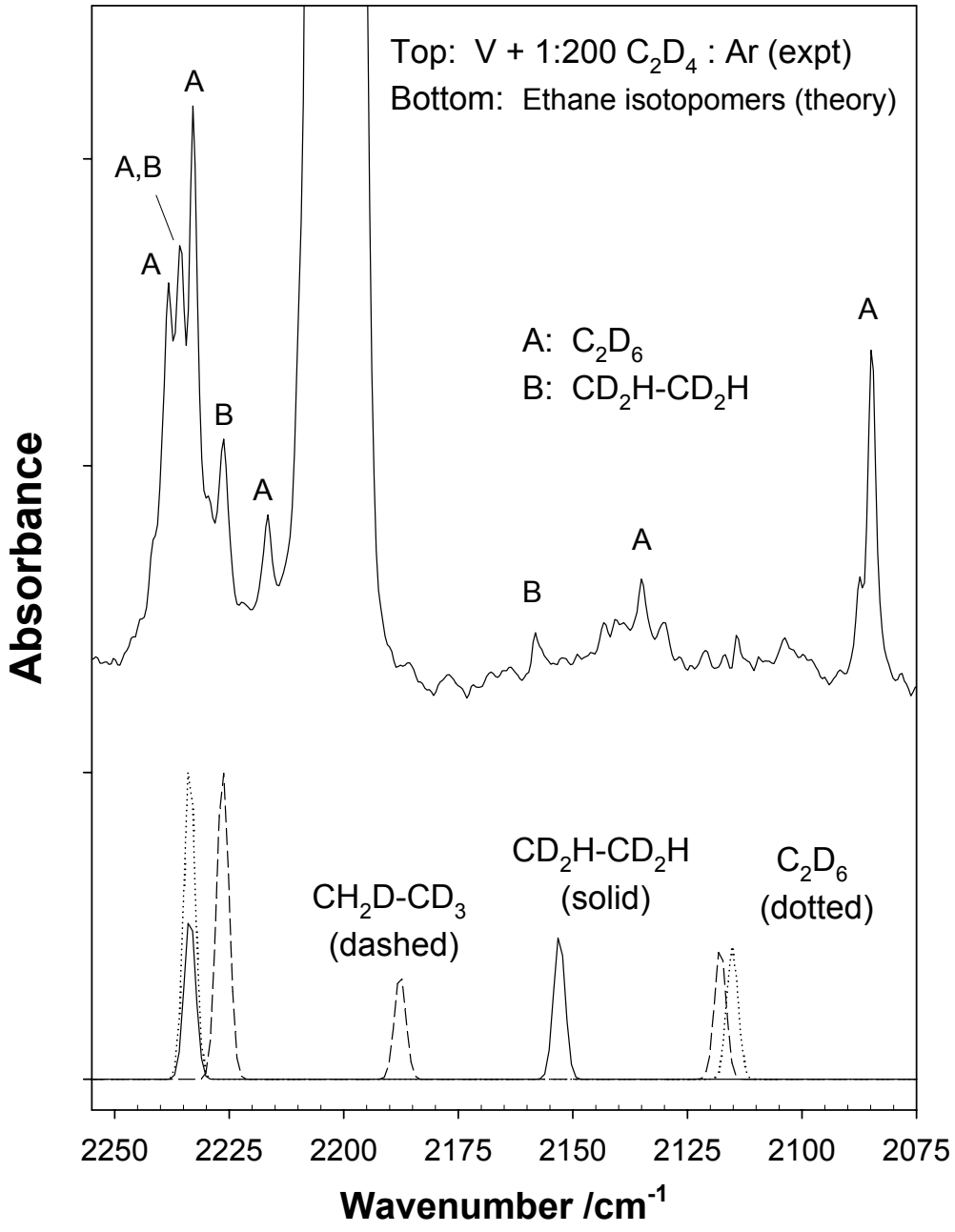

Figure 23: Portions of the simulated spectrum (bottom) in the C-D stretching region for the two suspected isotopomers of ethane generated using the B3LYP/6-311G(df,p) method with Gaussian 98 and SWIZARD software. For comparison, a portion of the C-D stretching region of the infrared spectrum of an Ar matrix formed containing V atoms and 1:200 C_2D_4 :Ar is also presented.

A similar comparison of the C-D stretching mode region of the experimental infrared spectrum of V + C_2D_4 in Ar with the predicted C_2D_6, CD_2H-CD_2H and CDH_2-CD_3 spectra is provided in Figure 23. In Figure 23, the features marked A in the experimental spectrum correspond to matrix-isolated C_2D_6 in Ar. The calculated spectrum of CDH_2-CD_3 is predicted to have a red-shifted mode compared from the predicted mode of greatest intensity in this region for C_2D_6. An absorption does exist in this region of the spectrum (at 2216 cm^{-1}), although it is unlikely that this mode is attributed to CDH_2-CD_3 given that the intensity of the mode in this region should be similar to any absorptions that would be observed in the C-H stretching region, as predicted by the calculations. Since only weak evidence in support of the observation of CDH_2-CD_3 was observed in the C-H stretching mode region in Figure 22, it would not then be expected to see a more intense secondary mode appearing in the C-D stretching mode region. Additionally, if the band observed at 2216 cm^{-1} were to be assigned to motion of CDH_2-CD_3, then a mode at approximately 2185-2190 cm^{-1} would be expected. As no significant absorption is evident in that region, it seems clear that the CDH_2-CD_3 isomer is not significantly present based on all pieces of evidence. By contrast, significant evidence in support of the CD_2H-CD_2H isomer is present in the experimental spectrum.

Finally, it is worth noting that the predicted spectrum of CD_2H-CD_2H should have an infrared absorption shifted approximately -70 cm^{-1} from the most intense C-D stretching feature of C_2D_6. Thus, one would expect to see a feature corresponding to CD_2H-CD_2H near 2160 cm^{-1}. There is one feature in this region

at 2158 cm^{-1} which grows with the same behaviour as the rest of the set B features. However, the calculations also predict that this mode attributed to CD_2H-CD_2H should also be shifted approximately +40 cm^{-1} from the second most intense C-D absorption of C_2D_6 in this region, near 2115 cm^{-1}. At first, this seems not evident by the spectrum of C_2D_6, which shows no significant absorption near 2115 cm^{-1}, in contradiction with the predicted spectrum. However, a set of two absorptions at 2134 cm^{-1} and 2085 cm^{-1} for C_2D_6 are observed, due to Fermi resonance.[15] A further analysis of this missing aspect of Figure 23 is presented in the discussion section. On the basis of the wavenumber shifts relative to C_2D_6, the numbers of absorption bands observed in the C-H and C-D stretching mode regions compared from predicted vibrational spectra, and the associated relative intensities of the products, it seems reasonable to assign the set of features labeled B in this spectrum as originating from vibrations of CD_2H-CD_2H.

5.4 Discussion: gas flow rate and diffusion during matrix deposition

In general, as the flow rate of the gas is increased, the rate of deposition onto the surface of the cold window is accordingly increased. Given that the cooling unit used in our experiments has a fixed rate of removal of heat from the cold tip where a matrix is deposited, the thermal transfer to the apparatus accompanying the higher volume of gas implies that the amount of time necessary for the matrix to completely freeze will be increasing with the increasing flow rate. As a consequence, this suggests that during matrix formation, there is both an enhanced mobility via diffusion of isolated reagents, as well as an enhanced contact time of metal atoms and reagents prior to the complete condensation of the matrix. Correspondingly, one might expect that metal-metal interactions become more and more significant under such conditions.

To investigate the formation of metal-metal aggregates, we have performed experiments of V atoms deposited in pure rare gas matrices in which the flow rate was increased up to 5.00 sccm, using UV-visible spectroscopy as the method of detection. Under the same conditions of metal atom generation as used in our infrared experiments, we have not observed a significant amount of V_2 to be present,[16] and thus it seems reasonable to discount the increased reactivity as metal dimer chemistry, on these grounds. Additional investigation of dimer formation and reactivity was presented in Chapter 4. Since the formation of ethane increases effectively linearly with flow rate for the fixed concentration of ethene, as demonstrated in Figure 20, the enhanced yield must be related to an

increase in the overall reaction time prior to complete matrix condensation. This increase in time would then allow additional reagent molecules to find transient species in the matrix, allowing for an increased number of successful reaction events.

Recently, similar experiments to those presented here have been performed by Cho and Andrews, [3] in which the reactions of V atoms with similar concentrations of ethene in Ar under conditions of matrix isolation have been studied. Interestingly, their spectra show no evidence for the formation of ethane as a major product. Since the sample preparations and reagents are all similar, it seems clear that there can be only reasons of experimental design that are possible for explaining the divergence in the chemistry. There are three primary differences which may account for this difference in observed chemistry. First, the flow rate used in the current work is considerably higher than the flow rate of matrix gas introduced in the work of Cho and Andrews (10 mmol per hour compared with 2-4 mmol per hour). Secondly, the Andrews method uses a laser ablation source for generation of V atoms, while the current work generates V atoms by thermal vaporization. The conditions of thermal metal atom vaporization, by comparison, involve the metal filament behaving as a broadband irradiation source. Thus, there may be considerably more resonance excitation of V atoms, or reaction products having an absorption in the visible, during matrix formation.[4] Finally, the temperature of the cold tip during matrix deposition conditions of Cho and Andrews is considerably colder (8K) than the temperature of the tip used in this work (17 K). Thus, the matrices in this work come to

complete condensation much more slowly than those of Cho and Andrews, allowing for a greater reaction time in our experiments, during matrix condensation. It is likely that a combination of these factors provides the basis for explaining the differences in the chemistry observed in this chapter, and that the current spectra provide evidence for the further reactivity of transient species in the matrix.

5.5 Identification of the CD_2H-CD_2H isomer

It seems clear based on the results section that the series of product features associated with set B in Figure 21 to Figure 23 is due to the CD_2H-CD_2H isotopomer of ethane isolated in Ar. This species represents a key isotopomer for understanding properly mechanistic aspects of catalytic hydrogenation studies involving transition metal hydrides, and thus the proper identification of this species is very important. The presence of the key absorptions associated with set B very close to the gas-phase wavenumber values observed by van Riet[12] for CD_2H-CD_2H supports the identification of this molecule in the matrix. However, the lack of intensity data in van Riet's work, combined with the observation of only a few of the modes of the CD_2H-CD_2H spectrum leaves some doubt. As a result, additional considerations can be made to further clarify this assignment, based on observed patterns in C_2H_6 and C_2D_6 isolated in Ar.

In the spectrum of matrix isolated C_2H_6 in Ar, the most intense absorption corresponding to C-H stretching motion, at 2980 cm^{-1} has a triplet splitting pattern nearly identical to the pattern observed at 2947 cm^{-1} here for CD_2H-CD_2H. The origin of this splitting could well be due to conformational isomerism within the

matrix environment. Given the match of the predicted splitting (13 cm^{-1}) for the *anti* and *gauche* isomers of CD_2H-CD_2H in this region, this may provide one explanation for the splitting pattern.

It is worth noting that the infrared spectrum of C_2D_6 isolated in argon does have a triplet of features similar to those observed near 2230 cm^{-1}, however, the middle feature that appears in Figure 23 (at 2235 cm^{-1}) is significantly intensified in the present work compared from the spectrum of C_2D_6 in Ar. This intensification under the band at 2235 cm^{-1} can only be rationalized as a second product feature growing under the spectrum of C_2D_6, under these conditions. In Figure 23, under the reduced C_2D_4:Ar conditions (1:1000 and 1:500), there is evidence for the set of features labeled B (CD_2H-CD_2H) growing first, before the major onset of growth demonstrated by the features labeled A (C_2D_6). The B set of features do have a mode present at 2235 cm^{-1}. Recalling that the most intense C-H stretching band of this species was split into a triplet, it is not surprising to observe a similar effect for the most intense C-D stretching feature. Additionally, the predicted calculations suggest that the most intense C-D stretching feature in this region for CD_2H-CD_2H should be very nearly overlapped with the most intense C-D stretching absorption due to C_2D_6. Since the set of experimental features corresponding to A and B are overlapping as predicted by the DFT calculations, this seems a further piece of evidence clearly identifying the set of features labeled B as CD_2H-CD_2H.

Finally, the calculated shifts predicted by the DFT calculations suggest that there should be a feature near 2160 cm^{-1} for CD_2H-CD_2H, that is shifted

approximately -70 cm^{-1} from the most intense feature of C_2D_6 (2233 cm^{-1}) in the 2300-2100 cm^{-1} region, and shifted by approximately +40 cm^{-1} from the second most intense feature associated with C_2D_6. Indeed, there is a feature at 2158 cm^{-1} which has the appropriate red-shift (-75 cm^{-1}), however, the blue shift from either of the features associated with C_2D_6 in this region is not in agreement with the same shift predicted by the calculations. The matrix isolated spectrum of C_2D_6 has two absorptions observed at 2134 cm^{-1} and 2085 cm^{-1}. However, the calculated spectrum of C_2D_6 predicts only a single absorption in this region, near 2115 cm^{-1}. As a result, calculated shifts of the feature at 2158 cm^{-1} for CD_2H-CD_2H are either +24 cm^{-1} or + 73 cm^{-1}, respectively. However, the observation of these two absorptions for C_2D_6 is known to be due to Fermi resonance[15] resulting from the coupling of vibrational modes. If the corresponding absorptions were suitably decoupled, then the average position of the absorption bands would serve as a representation of the fundamental position. In this case, the average position would be (2134 cm^{-1} + 2085 cm^{-1}) / 2 = 2115 cm^{-1}. Given that the C_2D_6 calculated spectrum predicts a single absorption near 2115 cm^{-1}, then this decoupled value seems reasonable for comparison of the shift for the 2158 cm^{-1} mode of CD_2H-CD_2H. Under this comparison, the blue shift relative to the absorption of C_2D_6 is +43 cm^{-1}, in much closer agreement with the shift predicted by the calculations. Thus, it seems very clear that CD_2H-CD_2H is the major H containing isomer of ethane present in the spectra.

5.6 Formation of OVH_2 : Reactivity of HO-V-H in the absence of C_2D_4

On co-deposition of V atoms in any matrices containing H_2O, a significant depletion of H_2O is always noted when comparing the spectrum of a metal-containing matrix with that of a matrix in which no metal atoms have been deposited. Additionally, when only H_2O is present in the matrix gas-sample, very weak product features are present in the resultant infrared spectrum of the matrix containing metal atoms that are consistent with the formation of OVH_2.

Annealing of such matrices to 25K results in the increase of features attributed to OVH_2. In contrast to the results of Zhou *et al*.,[9] no evidence for the formation of HO-V-H is observed at 1569 cm^{-1} in our spectra, neither are the features originally assigned at 1583 cm^{-1} to HO-V-H by Kauffman *et al*.[10] Our results confirm that a pathway to OVH_2 formation exists, that does not involve a direct conversion from HO-V-H by a second O-H bond insertion. Instead, we propose that hydrogen elimination from HO-V-H, to form the spin-allowed products OV + H_2, is a major process active in both experimental systems. It is likely that this reaction proceeds spontaneously during condensation, given that the coordination of water and the initial insertion of V into the O-H bond are exothermic by 54.9 kcal mol^{-1}. Since the barrier to elimination of H_2 from HO-V-H is predicted at 35.8 kcal mol^{-1}, this implies that the reaction of V with H_2O to form VO and H_2 is readily accessible, provided that the energy of the initial steps is conserved. Once isolated in the matrix, the insertion of the OV into the H-H bond of H_2 would be a second proposed step, resulting in the observed OVH_2 product.

The calculations performed by Zhou *et al*.[9] do predict that the H_2 addition to OV should be exothermic by approximately 8 kcal mol^{-1}, although a spin crossing is required to convert from the quartet surface of OV to the doublet OVH_2. Given the close relative energies of the reactants and products, it is likely that only a small barrier to the insertion of OV into the H-H bond exists. In high coordination organometallic systems in which adjacent H ligands are present, elimination of H_2 is often facile.[17] For the lower coordination OVH_2, this might suggest that the only barrier to hydrogen elimination is the endothermicity of the elimination reaction, and hence, the reverse insertion reaction should proceed spontaneously. As such, mild annealing of the matrix could provide the necessary energy for the spontaneous formation of OVH_2 when OV and H_2 are present.

In support of this proposal, a further investigation of the spectra published by Zhou *et al*. has been conducted,[9] and it is clear from their spectra that, even once HO-V-H has been depleted (their Figure 1, spectra c – d), further annealing to 30K results in increased formation of OVH_2. This increase in OVH_2 is correlated with the loss of matrix isolated OV. No further evidence for HO-V-H formation is observed in their spectra following the 30K anneal. The observation of free V atom reaction with liberated molecular H_2 following excitation of V atoms with wavelengths > 455 nm suggests that there is significant availability of H_2, resulting from reactivity of V with water. It seems likely that, given the much higher intensity of OV in the spectra of Zhou *et al*, that their matrices contained

similar relative yields of H_2. Thus, the following scheme is proposed to account for the observed products in both experimental systems:

Scheme 1: Reaction of V with H_2O to form transient species of O-H bond insertion by the metal.

Step 1:	$^4V + H_2O \rightarrow {}^4V\cdots OH_2$	Coordination of Water
Step 2:	$^4V\cdots OH_2 \rightarrow {}^4HO\text{-}V\text{-}H$	V insertion into HO-H
Step 3:	$^4HO\text{-}V\text{-}\dot{H} \rightarrow {}^4OV + H_2$	Hydrogen elimination
Step 4:	$^4OV + H_2 \rightarrow {}^2OVH_2$	OV Insertion into H_2

The results are consistent with the steps proposed here, and these steps provide the basis for understanding the formation of ethane isotopomers when ethene is present.

5.7 Formation of $CD_2H\text{-}CD_2H$: Reactivity of HO-V-H in presence of C_2D_4

As the relative amount of C_2D_4 in the matrix gas sample is increased, evidence for metal-water reaction products produced in the later steps of Scheme 1 decreases, rapidly. This suggests that a competitive pathway to the formation of OVH_2 exists, when C_2D_4 is present. Such an observation implies either that a) once formed, the OVH_2 species is consequently reacting with C_2D_4, or b) a precursor to the formation of OVH_2 is reacting with C_2D_4, inhibiting OVH_2 formation. Since the concentration of C_2D_4 is increased in the experiments, the number of collisions of any species isolated in the matrix with C_2D_4 is consequently increasing. Given that evidence for the formation of VH_2 shuts down as C_2D_4 increases, this implies that the rate of H_2 elimination from HO-V-H is being decreased by some competitive step. Correspondingly, when neither the VH_2 or OVH_2 species are observed in the spectra, there is a product with a

new C-H bond formed (CD_2H-CD_2H), and thus it seems evident that the precursor HO-V-H species is being consumed, prior to elimination of H_2. The most likely competitive reaction step would involve a π-coordination of a C_2D_4 molecule into one of the vacant sites of the HO-V-H species. Unlike the repulsive electron configuration of the neutral V atom, the oxidized HO-V-H species should have the capacity to coordinate such a π donating ligand easily, forming an HO-VH(η^2-C_2D_4) isomer.

To generate the final CD_2H-CD_2H product, the formation of the C-H bond must occur. As the HO-VH(η^2-C_2D_4) isomer has the requisite V-H and C_2D_4 unit, an insertion of C_2D_4 into the V-H bond seems likely. This would suggest the formation of an HO-V-CD_2-CD_2H species, under our reaction conditions. This species is analogous to the HO-V-H species, with the V-H bond replaced with a V-CD_2CD_2H group. Elimination of the alkyl group with the H from the HO- moiety would lead to the formation of OV and CD_2H-CD_2H as products. This step is completely analogous to the case of HO-V-H, although one would expect the elimination of an alkane product from HO-V-CD_2CD_2H to be less favourable than the H_2 elimination due to the directionality of the orbital associated with the metal alkyl bond. As such, the barrier to this elimination may be quite large, and this step may require photoexcitation to eliminate the alkane product. Given that the features associated with CD_2H-CD_2H in our experiments behave as one would expect for this proposed chemistry, it is suspected that these steps are involved in the major mechanism governing the formation of CD_2H-CD_2H in these matrix experiments. This chemistry is summarized as Scheme 2, below:

Scheme 2: Proposed reaction steps for the hydrogenation of C_2D_4 following reaction of atomic V with water.

Step1:	$V + H_2O \rightarrow V^{\cdots}OH_2$	H_2O coordination
Step 2:	$V^{\cdots}OH_2 \rightarrow$ HO-V-H	O-H insertion by V
Step 3:	HO-V-H $+ C_2D_4 \rightarrow$ HO-VH(η^2-C_2D_4)	C_2D_4 π-coordination
Step 4:	HO-VH(η^2-C_2D_4) $\rightarrow$ HO-V-CD_2CD_2H	C_2D_4 insertion in V-H
Step 5:	HO-V-$CD_2CD_2H + h\nu \rightarrow$ OV + CD_2H-CD_2H	CD_2H-CD_2H elimination
Net:	$V + H_2O + C_2D_4 + h\nu \rightarrow$ OV + CD_2H-CD_2H	Overall

5.8 Formation of CD_3-CD_3: Reactivity of d_3-vinyl-V-D in presence of C_2D_4

Given that water is significantly desiccated in these experiments, it was first considered that the formation of C_2D_6 could be due to OV chemistry. At lower concentration of C_2D_4 in Ar, irradiation of the formed matrices with light >455 nm caused the increase of features at wavenumber values consistent with the C-H/C-D bond insertion intermediates identified by Cho and Andrews for V atoms reacting with ethene.[3] Similar C-H bond insertion intermediates on which the metal centre bears an O atom would be expected to appear at wavenumber positions significantly blue-shifted from the observed insertion intermediates. This statement is based on the calculated vibrational spectrum of a metal atom C-H bond insertion into ethene, in which the metal atom also bears an O, and supports the claims of Cho and Andrews who suggest that the metal hydride stretching frequency shifts to higher energy as the valency of the V complex increases.[3] Thus, the likelihood of the sacrificial hydrogenation of ethene involving OV is low.

The presence of significant C_2D_6 with the maximum concentration of C_2D_4 at 0.5% in Ar demonstrates that there is significant availability of C_2D_4 molecules to matrix isolated species during deposition. The only possible formation mechanism of C_2D_6 involves the reaction of at least two C_2D_4 molecules. Given that V atoms must also be excited by a photon prior to direct reaction with C_2D_4, plenty of C_2D_4 must be available near a metal atom under high C_2D_4 concentration deposition conditions to compete with resonant emission. This suggest that following absorption of a photon, the reaction of excited V atoms with C_2D_4 is quite rapid, and that the rate of collision with C_2D_4 is much greater than the rate of V atom collision with H_2O. Indeed, the onset of C_2D_6 as the major reaction product at higher concentrations of C_2D_4 suggests that the excitation of V and subsequent reaction steps exclusively with C_2D_4 units must be very rapid in order to compete with CD_2H-CD_2H formation efficiently.

It is anticipated that the C_2D_6 that we observe is generated via the reaction of additional C_2D_4 units with the metal C-D insertion intermediates, as characterized by Cho and Andrews, which can be generated by light from the filament, during deposition. Under low concentration of C_2D_4 in Ar, features very similar to the C-D bond insertion intermediates identified by Cho and Andrews are observed in the infrared spectra, immediately following deposition. Thus it is proposed that, when the concentration of C_2D_4 is raised, these insertion species are rapidly consumed in a fashion analogous to HO-V-H (in Scheme 2). The analogous steps following V atom insertion into the C-D bond of C_2D_4 are summarized as Scheme 3.

Scheme 3: Proposed reaction steps for the sacrificial hydrogenation of C_2D_4 following reaction of photoexcited V with 2 C_2D_4.

Step 1:	$V + h\nu \rightarrow V^*$	photoexcitation of V
Step 2:	$V^* + CD_2{=}CD_2 \rightarrow D_2C{=}DC\text{-}V\text{-}D$	C-D insertion by V
Step 3:	$D_2C{=}DC\text{-}V\text{-}D + C_2D_4 \rightarrow D_2C{=}DC\text{-}VD(\eta^2\text{-}C_2D_4)VD_2$	C_2D_4 π–coordination
Step 4:	$D_2C{=}DC\text{-}VD(\eta^2\text{-}C_2D_4) \rightarrow D_2C{=}DC\text{-}V\text{-}CD_2\text{-}CD_3$	C_2D_4 insertion in V-D
Step 5:	$D_2C{=}DC\text{-}V\text{-}CD_2\text{-}CD_3 + h\nu \rightarrow (\eta^2\text{-}C_2D_2)V + CD_3\text{-}CD_3$	C_2D_6 elimination
Net:	$V + 2\ C_2D_4 + h\nu \rightarrow (\eta^2\text{-}C_2D_2)V + C_2D_6$	Overall

Following this scheme, the associated vinyl group on the initial C-D insertion intermediate is analogous to the hydroxyl group of the HO-V-H species. The absorption of the V-H stretch in the infrared for both the HO-V-H and $H_2C{=}HC\text{-}V\text{-}H$ species is quite similar (1567 cm^{-1} and 1573 cm^{-1}), supporting the similar chemical properties of these two ligands. Additionally, in the structure of the vinyl hydride given by the calculations of Cho and Andrews, the geometry of the vinyl group is such that the requisite hydrogen on the CH_2 end is present in a favourable geometry for elimination, as proposed in Step 5 of Scheme 3.

As additional support of all three schemes, spectroscopic evidence consistent with observations of all of the primary transient species, such as HO-V-H and the $D_2C{=}DC\text{-}V\text{-}D$ has been observed. Additionally, in most cases, no spin conversion is required to form products. In the case of the initial transient species formed in Scheme 3, the requirement of photons > 420 nm to induce the C-D bond insertion is definitely necessary, and certainly the light emit by the filament during metal deposition experiments yields significant intensity in this region. Given that the experiments have demonstrated conclusively that species

in the matrix can then be expected to interact with a further C_2D_4 molecule, all of the steps listed in these schemes seem plausible.

The absence of spectroscopic features corresponding to some of the transient species implicated in these schemes is, at first, somewhat perplexing. Considering first that several of the implicated steps involve the formation of OV as a final product, it is interesting to note that, even under the conditions where the largest yields of ethane isotopomers are generated, no significant absorption at 987 cm^{-1} corresponding to matrix-isolated OV is observed.[9] However, under most conditions, a significant amount of C_2D_6 is observed, which requires that a larger fraction of the V atoms are reacting selectively with C_2D_4, and not with water. As a result, the total number of V atoms reaching the matrix must be distributed between OV and (η^2-C_2D_2)V species (or their further reaction products). Thus, the lack of observation of these key species in the spectra is due to the small concentrations limited by the number of V atoms. As a result, while these species must be formed, their weak absorption spectra inhibit their direct observation.

The absence of newly proposed intermediates such as HO-VH(η^2-C_2D_4), HO-V(-CD_2CD_2H), D_2C=CD-VD(η^2-C_2D_4) or D_2C=CD-V-CD_2-CD_3 can be explained using thermodynamic arguments. Thermochemical calculations involving second-row transition metal atom hydrides reacting with ethene are expected to have only a small barrier to, or even a barrierless, insertion of ethene into the M-H bonds of L_nMH_x species.[18] This argument, or a similar one, for first row transition metal species with increasing numbers of coordinated ligands may

still hold true. If the insertion of C_2D_4 into the V-H bond of HO-V-H(η^2-C_2D_4) were barrierless, HO-V-CD_2-CD_2H would be formed rapidly and thus the precursor would not be observed. Once formed in the matrix, HO-V-CD_2-CD_2H would be subject to prolonged irradiation by the filament, and thus would have a high probability of absorbing a photon to eliminate the CD_2H-CD_2H product.

In each of the schemes presented above, the π-coordination of the ethene molecule which formally ends up as the ethane product occurs at the monohydride intermediate. Given that key species implicated in these schemes are not directly observed, it is not immediately possible to eliminate a mechanism by which the π-coordination occurs following a second insertion of V into additional O-H or C-D bonds of the HO- or D_2C=DC- coordinated ligands. However, given that both of the dihydrido- products require spin conversion, it is very likely that the formation of these species is slow by direct O-H or C-D insertion, due to a kinetic impediment. Thus, it seems more likely to coordinate the alkene to the monohydride intermediates in all cases, for which all of the following steps in the schemes proceed via spin conserved surfaces, rather than invoking steps in which spin interconversion must first occur.

As one final additional mechanistic point, if the proposed alkene insertion were near barrierless, such an alkene insertion might be somewhat reversible, for which the insertion/elimination of C_2D_4 into V-H bonds formed through V atoms reacting with H_2O may be expected to exhibit small amounts of H/D scrambling. The likely reverse mechanism would proceed via $\tilde{\beta}$-hydrogen elimination from the coordinated –CD_2-CD_2H, and due to rotation about the C-C

bond, this should result in β-H or β-D elimination in the mixed isotope experiments. The additional broad, yet weak, C-H stretching features that appear near the expected C-H position of the CD_2H-CD_2H isomer in Figure 22, may be evidence of such H/D scrambling resulting from insertion/β-elimination of ethene. However, when Nb atoms are used, the peaks potentially associated with the CDH_2-CD_3 isomer still appear, but are not intensified in the same way that there is an intensification of the C_2D_6 and CD_2H-CD_2H spectra. Thus, although it is not possible to conclusively rule out the possibility of H/D scrambling, it is not expected to be a major mechanism, overall.

5.9 Absence of V + H_2O + C_2D_4 chemistry in related work

Under conditions where ethane was originally observed, it was noted that there was a significant loss of ethene dimer,[19] and the ethene:water 2:1 hydrogen bonded complex.[20] The former is further explored in detail, in Chapter 6. Similar experiments with C_2D_4 in high concentration showed the formation of C_2D_6 and CD_4 only, while losses of the ethene dimer and ethene:water 2:1 complex were still observed. As a result, it was concluded that ethane formation involving H_2O as the formal source of hydrogen was not directly involved in the overall hydrogenation process.[1] Clearly, the formation of CD_2H-CD_2H under these new reaction conditions implicates parallel reactivity involving H_2O, which ultimately leads to ethane formation. Thus some explanation explaining the lack of H_2O observed reactivity in the other work is required.

The simplest explanation seems to lie in the impact of concentration of ethene, for which the earlier results employed a concentration of ethene that was

approximately 10-20 fold increased, compared from the most concentrated experiments in this work. Noting that a mere 2 fold increase in the concentration of C_2D_4 in this work results in significant increase in the C_2D_6 product, then it is not unreasonable to expect that the same process at 10-20 times the C_2D_4 concentration would ultimately dominate, outcompeting every other mechanism completely. If such a supposition were true, then the formation of reaction products involving V + H_2O chemistry may not be significantly observed, compared from the overwhelming C_2D_4 chemistry. Thus, while the chemistry may have been present, the product yields may simply have been too small to observe, in deference to the formation of C_2D_6.

5.10 Summary and conclusions

Vanadium hydrides formed by the insertion of the metal atom into the O-H bonds of water or the C-D bonds of C_2D_4 are able to further react with additional deuterated ethene molecules to form isotopomers of ethane as major products. Consequently, the major features of the infrared spectrum of CD_2H-CD_2H isolated in an argon matrix have been observed for the first time. A mechanism involving C-H or O-H bond insertion by V atoms, alkene insertion and subsequent elimination of ethane is proposed. These mechanisms are consistent with the infrared data observed in this work.

5.11 References for Chapter 5

[1] Thompson, M.G.K.; Parnis, J.M. *J. Phys. Chem. A.*, **2005**, 109, 9465.

[2] Ritter, D.; Carroll, J. J.; Weisshaar, J.C. *J. Phys. Chem.*, **1992**, 96, 10636.

[3] Cho, H.G.; Andrews, L. *J. Phys. Chem. A*, **2007**, 111, 5201.

[4] Devore, T.C. *J. Chem. Phys.*, 1975, 62, 520

[5] Frisch, M. J.; Trucks, G. W.; Schlegel, H. B.; Scuseria, G. E.; Robb, M. A.; Cheeseman, J. R.; Zakrzewski, V. G.; Montgomery, Jr.; J. A.; Stratmann, R. E.; Burant, J. C.; Dapprich, S.; Millam, J. M.; Daniels, A. D.; Kudin, K. N.; Strain, M. C.; Farkas, O.; Tomasi, J.; Barone, V.; Cossi, M.; Cammi, R.; Mennucci, B.; Pomelli, C.; Adamo, C.; Clifford, S.; Ochterski, J.; Petersson, G. A.; Ayala, P. Y.; Cui, Q.; Morokuma, K.; Rega, N.; Salvador, P.; Dannenberg, J. J.; Malick, D. K.; Rabuck, A. D.; Raghavachari, K.; Foresman, J. B.; Cioslowski, J.; Ortiz, J. V.; Baboul, A. G.; Stefanov, B. B.; Liu, G.; Liashenko, A.; Piskorz, P.; Komaromi, I.; Gomperts, R.; Martin, R. L.; Fox, D. J.; Keith, T.; Al-Laham, M. A.; Peng, C. Y.; Nanayakkara, A.; Challacombe, M.; Gill, P. M. W.; Johnson, B.; Chen, W.; Wong, M. W.; Andres, J. L.; Gonzalez, C.; Head-Gordon, M.; Replogle, E. S.; Pople, J. A.; Gaussian 98, Revision A.11.2, Gaussian, Inc.: Pittsburgh, PA, 2001.

[6] Becke, A. D. *J. Chem. Phys.* **1993**, *98*, 5648.

[7] Lee, C.; Yang, E.; Parr, R. G. *Phys. Rev. B.* **1988**, *37*, 785.

[8] S. I. Gorelsky, SWizard program, http://www.sg-chem.net/

[9] Zhou, M.; Dong, J.; Zhang, L.; Qin, Q. *J. Am. Chem. Soc.*, **2001**, 123, 135.

[10] Kauffman, J.W.; Hauge, R.H.; Margrave, J.L. *J. Phys. Chem.*, **1985**, 89, 3547.

[11] Xiao, Z. L.; Hauge, R. H.; Margrave, J. L. *J. Phys. Chem.*, **1991**, 95, 2696.

[12] Van Riet, R. *Ann. Soc. Scient. Brux.*, **1957**, 71, 102.

[13] Scott, A.P.; Radom, L. *J. Phys. Chem.*, **1996**, 100, 16502.

[14] Merrick, J. P.; Moran, D.; Radom, L.; *J. Phys. Chem. A.*, **2007**, ASAP Alert, doi: 10.1021/jp073974n.

[15] Herzberg, G. *Infrared and Raman Spectra of Polyatomic Molecules*, Van Nostrand Reinhold Company: New York, **1988**, p. 345.

[16] Ford, T.A.; Huber, H.; Klotzbuecher, W.; Kuendig, E.P.; Moskovits, M.; Ozin, G.A.; *J. Chem. Phys.,* **1977,** 66, 524**.**

[17] A) See for example: *The Organometallic Chemistry of the Transition Metals*, 4th Ed, Crabtree, R.; John Wiley & Sons, Inc.: Hoboken, NJ, **2005**. b) Cotton, F.A.; Wilkinson, G.; *Advanced Inorganic Chemistry,* 5th Ed.; Wiley, New York, **1988.** c) *Catalytic Chemistry*, Gates, B.C.; John Wiley & Sons, Inc: Hoboken, NJ, **1992.**

[18] Siegbahn, P. E. M. *J. Am. Chem. Soc.*, **1993**, 115, 5803.

[19] a) Cowieson, D.R.; Barnes, A.J.; Orville-Thomas, W.J. *J. Raman Spec.*, **1981**, 10, 224. b) Rytter, E.; Gruen, D.M. *Spectrochim. Acta,* **1979**, 35A, 199.

[20] Thompson, M.G.K.; Lewars, E.G.; Parnis, J.M. *J. Phys. Chem. A.*, **2005**, 109, 9499.

Chapter 6

Reaction of V with C_2H_4 under high concentration of ethene: Sacrificial hydrogenation of ethene under matrix isolation conditions

6.0 Introduction[h]

In earlier chapters, when V atoms were cocondensed with ethene in Ar matrices, the surprising formation of ethane as a major product in the infrared spectrum was observed. Isotopic experiments, as presented in Chapter 5, suggested two competitive mechanisms leading to ethane formation, involving transient species resulting from either O-H or C-H bond insertion by the metal as the initiating step. The first mechanism proposed steps involving metal atom insertion into the O-H bond of water, and the subsequently formed transient species reacting with an ethene molecule, leading to ethane formation. The second mechanism proposed a metal atom insertion into the C-H bond of ethene, and the transient species reacting with an additional ethene molecule, ultimately leading to ethane formation. This chapter aims at exploring the second reaction channel, involving M + C_2H_4 chemistry as the initiating step, for the overall reaction: M + C_2H_4 + C_2H_4 → C_2H_6 + other products. The similarity of

[h] A similar but modified version of this chapter has appeared as: Thompson, M.G.K.; Parnis, J.M.; *J. Phys. Chem. A.*, **2005**, 109, 9465.

the two proposed reaction mechanisms suggests that reactivity of ethene with M-H bond containing species is a general process which could be explored with other H-containing precursors. In this particular investigation, the focus of this chapter is to explore the reactivity of metal atoms with relatively high concentrations of ethene, in which ethene is both the target, and initiating species in the observed hydrogenation.

6.1 Experimental Details

In these experiments, matrices were deposited for 1.5 hours (unless otherwise noted) with a gas flow rate of 0.5 sccm. Otherwise, the parameters described in Chapter 3 have been employed, with no major deviations. Niobium and titanium metals used in these experiments were of 99.9% purity, from A.D. McKay.

6.2 Reactions of 1:10 C_2H_4:Ar with metal atoms: C_2H_6 formation

Portions of the infrared spectra obtained prior to, and following, the co-condensation of gas-phase Ti, V or Nb atoms with 10% ethene in argon are given in Figure 24. For comparison, the spectrum of 0.1% ethane in argon is also shown, which demonstrates clearly that the major product obtained in the metal-containing matrices is unperturbed matrix-isolated ethane. The major unobscured ethane absorptions obtained by metal atom reactions with ethene are observed at 2944.9, 2919.4, 2885.9, 1465.0, and 1373.1 cm^{-1}, wavenumber positions that are identical to those observed for matrix-isolated ethane deposited using an ethane/argon mixture. Methane is also formed as a product, giving rise to an absorption at 1304 cm^{-1}. Other minor features sometimes appear in the

spectra of the metal-containing matrices associated with CO_2 (2349 cm^{-1}, 667 cm^{-1}) and CO (2137 cm^{-1}).[1] Both species are well-known matrix isolation impurities, in this case generated as byproducts of metal vaporization by desorption from the apparatus walls during sample formation. In accord with this supposition, the intensities of these features varied from experiment to experiment in a manner that did not correlate with production of ethane or methane.

For each metal used, a new absorption was sometimes observed at 1193 (Ti), 1205 (V), or 1263 cm^{-1} (Nb). In each case, the absorption could be photobleached during irradiation of the matrix with visible light. There was no other apparent change in recorded spectra upon elimination of this species. The yield of this species varied significantly between similarly prepared samples, despite the fact that production of ethane was essentially constant. Therefore, this set of absorptions is likely due to the production of a metal-containing species, via a competitive metal atom reaction, which is not investigated in this work due to the irreproducibility of the features.

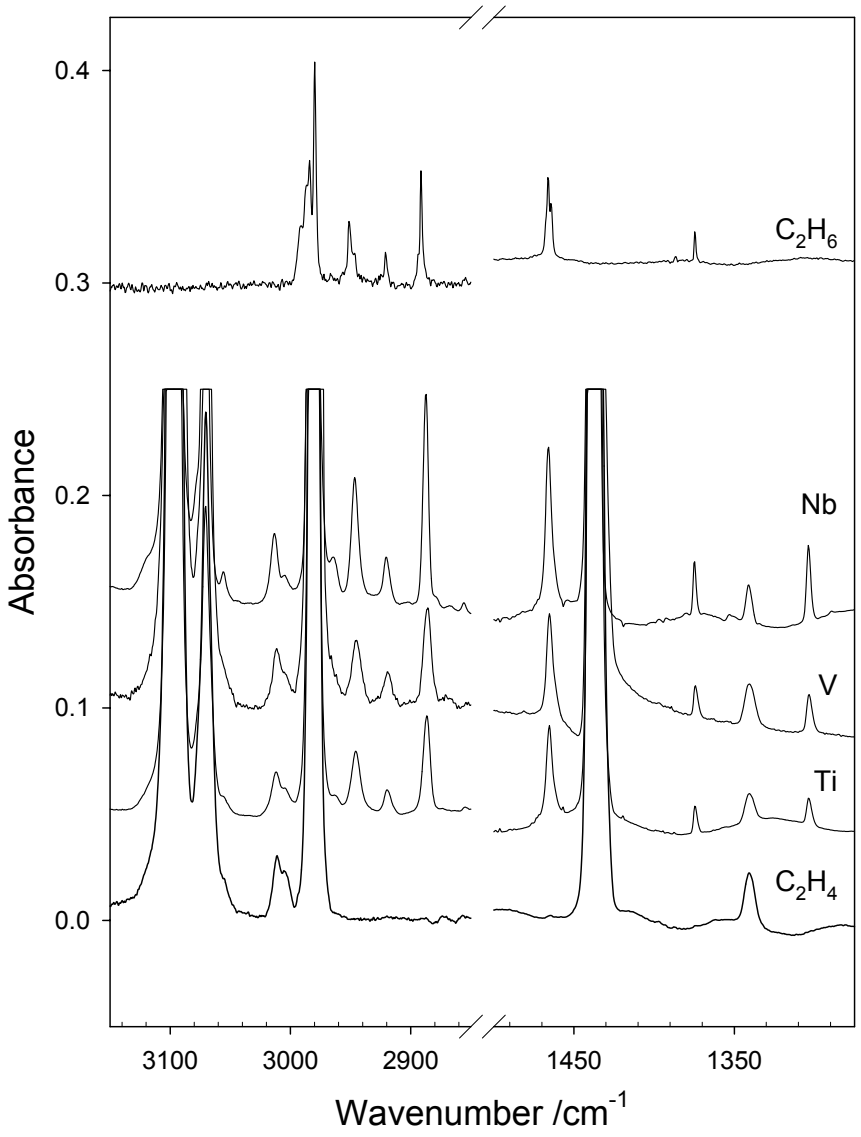

Figure 24: Portions of FTIR absorption spectra of argon matrices containing (from bottom to top) 10% ethene, 10% ethene with Ti atoms, 10% ethene with V atoms, 10% ethene with Nb atoms, and 0.1% ethane.

6.3 Reduced ethene concentration and V/C-H insertion intermediates

Codeposition of Ti or V atoms with lower-concentration mixtures of ethene in Ar (1:70 ethene:Ar) gave rise to diminished yields of ethane, accompanied by new features in the region of 1650-1450 cm^{-1}. In the case of Ti, these absorptions have been previously identified in 1:200 ethene:Ar matrices by Lee *et al.* [2] as being associated with $HTiC_2H_3$ (1500 cm^{-1}) and $H_2TiC_2H_2$ (1585, 1611 cm^{-1}). These features show identical photochemical behavior to that described previously by Lee *et al., e.g.*, irradiation of deposition samples containing both species with 466 nm light gave rise to depletion of $HTiC_2H_3$ and significant growth of $H_2TiC_2H_2$. Prolonged irradiation of such matrices resulted in the complete destruction of both titanium hydride species, in accord with the observations of Lee *et al.* However, in the present work, such prolonged irradiation also resulted in concomitant production of both ethane and methane, an observation not previously reported for Ti.

Features analogous to those of the $H_2TiC_2H_2$ species were seen at 1552 and 1644 cm^{-1} when V atoms were employed with 1:70 ethene:Ar gas mixtures (see Figure 25), after the matrix sample was subjected to a sequence of irradiations similar to those employed by Lee *et al.* in the Ti work noted above. These are the features which were the main result of Chapter 4, and are due to the H-V-C_2H_3, and $H_2V(C_2H_2)$ species. Irradiation with light of wavelength >455 nm for 10 min resulted initially in the growth of features due to these molecules, however, further irradiation at these wavelengths resulted in their modest depletion. Subsequent irradiation with broad-band UV-visible light for 10 minutes

resulted in further depletion of these features, with the complete destruction of these features following prolonged irradiation (~15 hours). Following irradiations of the sample containing V atoms with visible light there is a very small increase in the features associated with ethane. Subsequent broadband UV-visible irradiation of the sample gave a more pronounced growth of the ethane features, particularly following prolonged irradiation (see Figure 25, top spectrum).

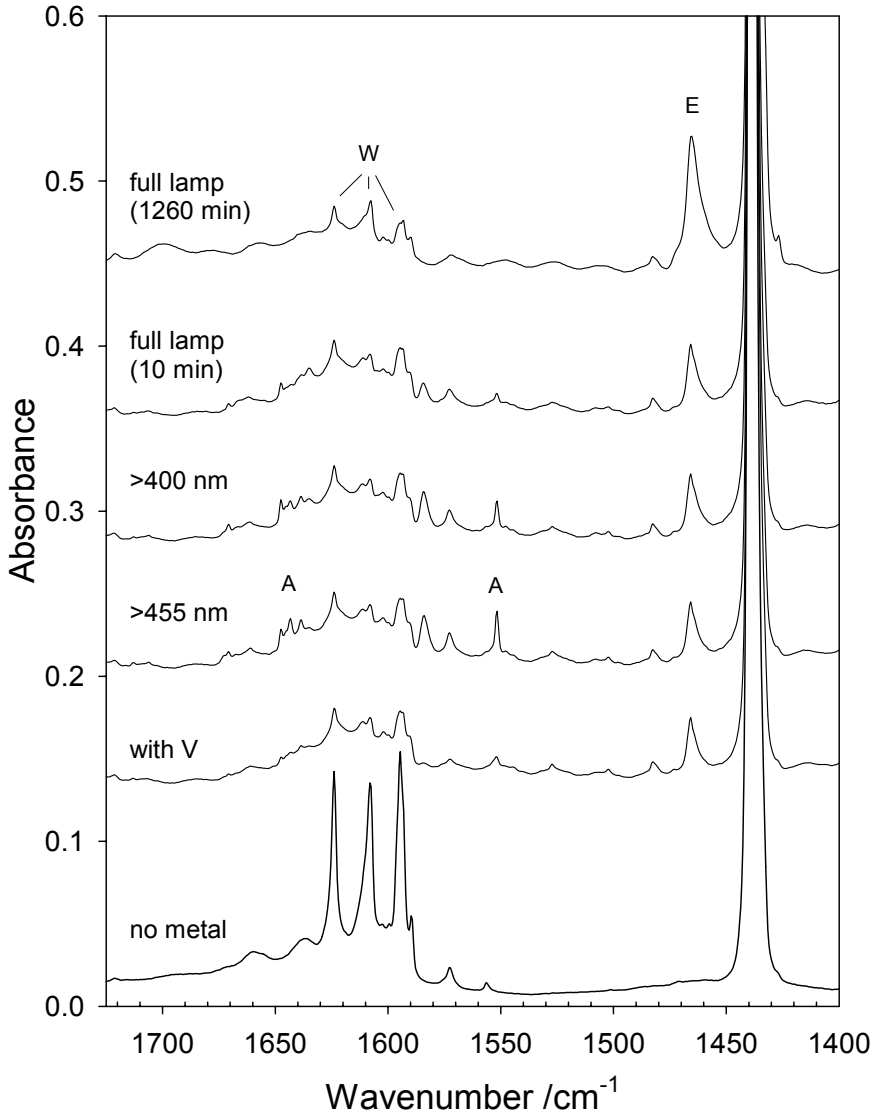

Figure 25: Portions of the infrared spectra of argon matrices containing ethene (1:70 ethene:Ar) with (bottom to top): 5 hour deposition with no metal, 4.5 hour deposition with V atoms, following 10 minute irradiation >455 nm, following additional 10 minute irradiation >400 nm, following additional 10 minute irradiation with full UV-visible output of lamp, and following additional 1260 minute irradiation with full UV-visible output of lamp. Features associated with matrix-isolated ethane, water and those assigned in the text to $H_2VC_2H_2$ are denoted E, W and A respectively.

6.4 Metal atoms in pure C_2H_4 matrices

Similar experiments were done with Ti, V or Nb atoms in pure ethene matrices. In these cases, the yield of ethane was substantially greater than in 1:10 ethene:Ar matrices, but otherwise no other significant changes were noted beyond some changes in peak shape. Methane was also produced in amounts that appear to be correlated with the increase in ethane production.

6.5 Ethane formation and the ethene dimer

Production of ethane was in all cases accompanied by measurable depletion of absorptions due to matrix-isolated ethene dimers,[3] which give rise to absorptions at 3096 and 2980 cm^{-1} in the C-H stretching mode region. This depletion is specific, and can be seen in samples where the dimer coexists with the monomer, in that only the dimer features diminish when metal atoms are present with respect to reference spectra. Figure 26 shows the spectra in the C-H stretching region of matrices generated with a 1:70 ethene:argon mixture, with and without the inclusion of V metal atoms. The presence of metal atoms results in both the production of ethane and the depletion of ethene dimer, as can be clearly seen in the figure.

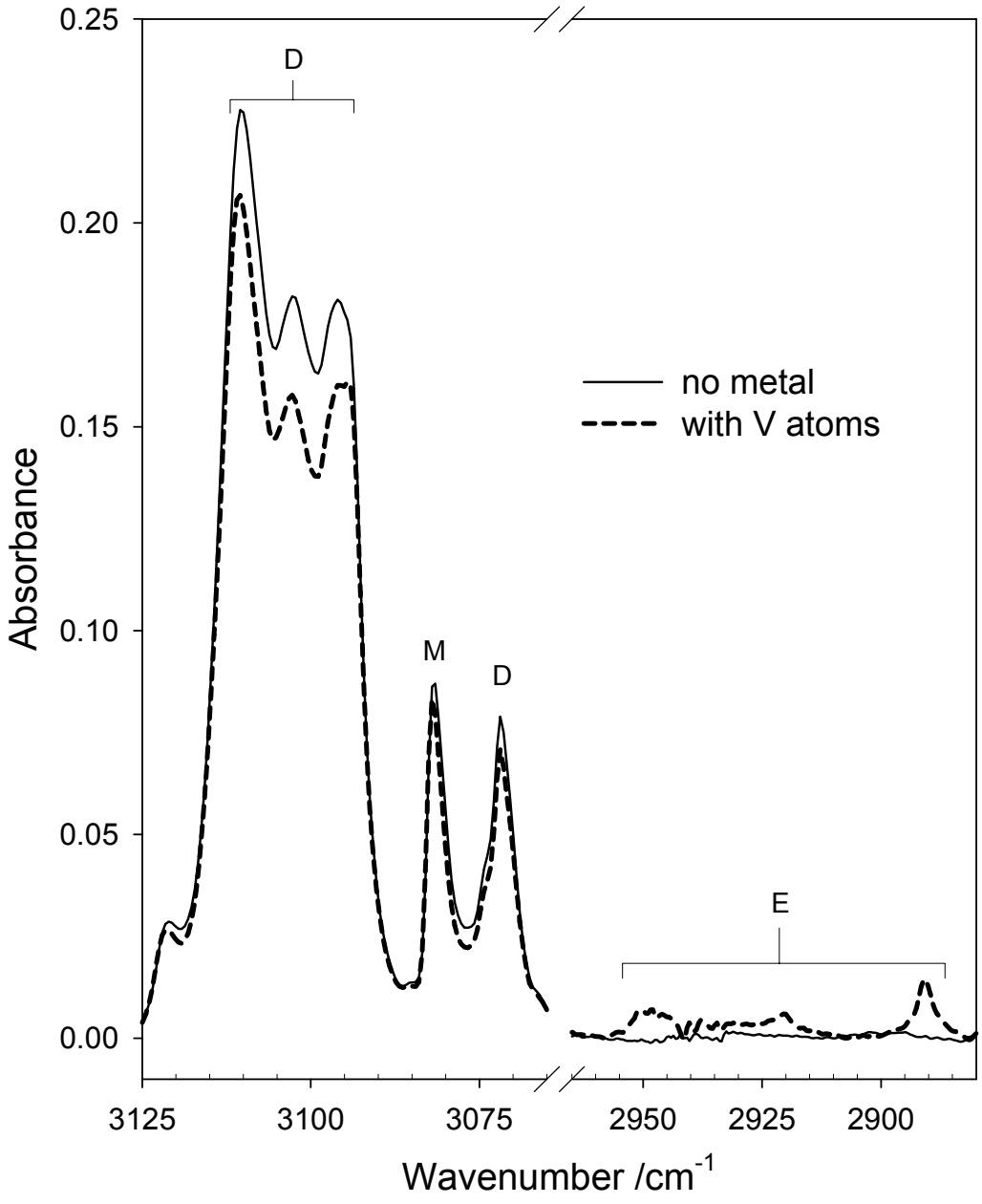

Figure 26: Portions of the infrared spectra of argon matrices containing ethene (1:70 ethene:Ar), with (dotted line) and without (solid line) V atoms. Features associated with ethane, the ethene monomer and ethene dimer are labeled E, M and D respectively.

6.6 Reactions of V with ethene isotopomers

For vanadium atoms, the analogous reactions were carried out with argon containing 10% perdeuteroethene (C_2D_4). Portions of the resultant spectra are given in Figure 27, along with the corresponding spectrum for 0.1% perdeuteroethane (C_2D_6). The results of these experiments confirm that perdeuteroethane is the only major hydrocarbon product in these reactions. Absorptions due to CO_2, CO, and traces of CH_4 associated with the metal vaporization approach were also observed, as noted above for the C_2H_4 reactions. A feature at 993 cm^{-1} is also observed which is assigned to CD_4[4] by comparison with spectra of CD_4 in an Ar matrix.

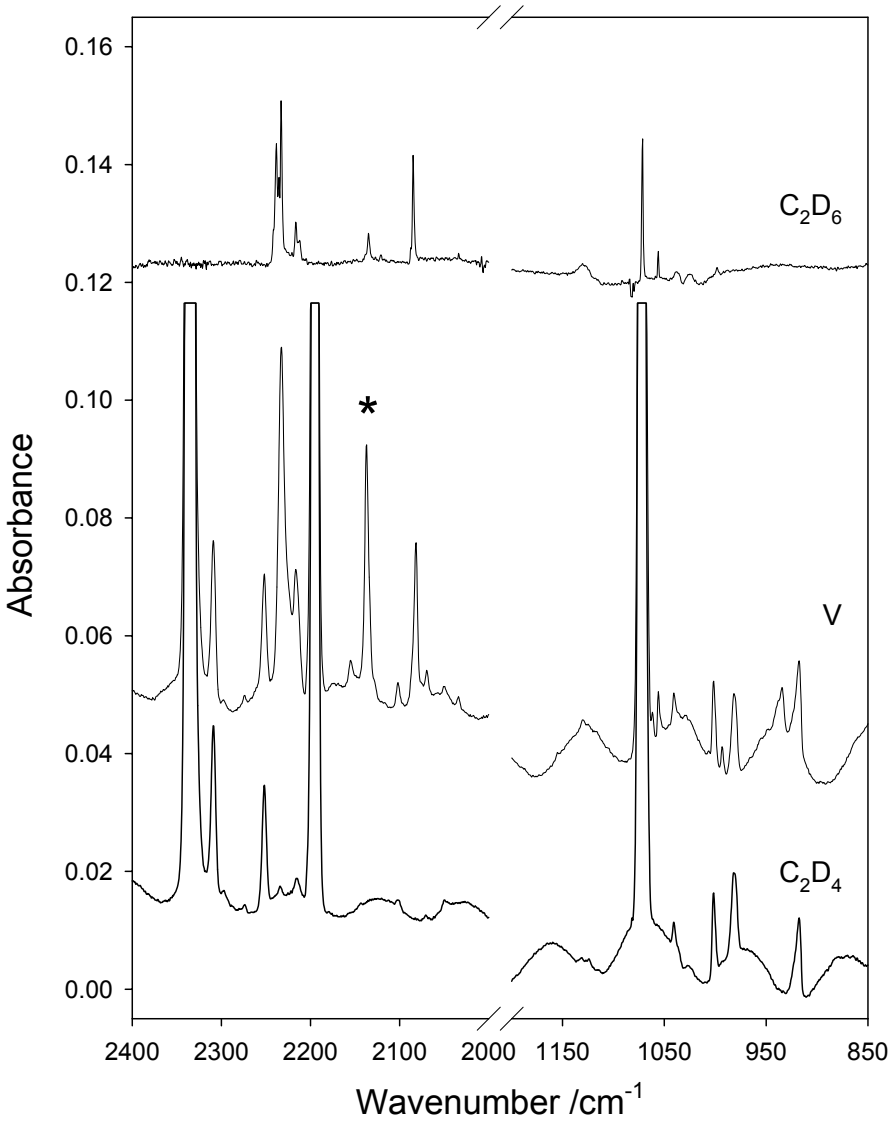

Figure 27: Portions of FTIR absorption spectra of argon matrices containing (from bottom to top) 10% perdeuteroethene, 10% perdeuteroethene with V atoms, and 0.1% perdeuteroethane. Asterisk (*) denotes a feature due to matrix-isolated CO, generated by thermal desorption of CO in the apparatus during sample preparation.

The reaction of an equimolar mixture of 5% each of C_2H_4 and C_2D_4 with vanadium atoms was also studied. Infrared spectra obtained for this reaction show numerous weak and broad features in the C-H and C-D stretching regions. Many of these absorptions correspond to features associated with ethane (C_2H_6) and perdeuteroethane (C_2D_6). The additional observed absorptions are likely associated with one or more isotopomers of ethane, due to the close proximity of these absorptions to the known modes of the isotopically-pure ethanes. Spectral congestion did not allow for the identification of mixed isotope product(s).

6.7 Discussion: Factors promoting ethane formation in matrices

The results presented above demonstrate that ethane is the major infrared-observable, matrix-isolated, product for the reactions of Ti, V, or Nb atoms with ethene in matrices where the ethene dimer is prone to form during matrix condensation. Specifically, evidence is given that metal atoms react with at least two ethene molecules to form ethane, in regions where the ethene dimer would otherwise be formed on deposition in the absence of metal. Organometallic species that are believed to be precursors to dehydrogenation products are observed in our work when relatively low concentrations of ethene are employed. In the case of Ti, these species have been identified previously as titanocyclopropene dihydride and vinyl titanium hydride[2], and similar results have been observed with vanadium. At intermediate concentrations, where a relatively low abundance of the ethene dimer coexists with the matrix-isolated ethene monomer, production of ethane and metal hydride species can be observed simultaneously.

At higher ethene concentrations (1:10 ethene:Ar and higher), metal hydride species are not observed, which suggests that if they are formed they exist only as transient species under these conditions due to their rapid consumption in the formation of ethane. This is supported by the results presented in Chapter 5, and in the theory work of Siegbahn which suggests that second-row transition metal hydride species can incorporate an ethene molecule[5] by a barrierless process involving direct insertion of the ethene molecule into the M-H bond. For Ti and V, this argument may involve photoexcitation of the metal hydride species, since photoinduced reactivity can also be observed in the matrix. Such a process would result in formation of $HM(C_2H_2)C_2H_5$ or $H_2C{=}HC\text{-}M\text{-}C_2H_5$, which would be expected to be possible precursors to ethane in our experiments. Ethane formation could occur from the former by reductive elimination of the hydride and alkyl fragments, or from the latter by a 1,3-elimination of C_2H_6 to yield $M(C_2H_2)$. Note that, since insertion of bare transition metal atoms into C-H bonds is generally exothermic, such a reductive elimination process should be expected to exhibit a significant potential energy barrier. In order to overcome such a barrier, the process would need to be photon-assisted or exhibit significantly different thermodynamics than that of the bare metal atom. The latter possibly could result from the presence of one or more additional ligands on the metal atom.

The production of ethane in the matrix isolation environment following the reaction of iron atoms with ethene has been previously reported by Kafafi *et al.* at 13.5-15 K.[6] Cardenas and Shevlin also observed production of ethane following

warm-up of matrices containing iron atoms in ethene deposited at 77K.[7] In the work of Kafafi *et al.*, absorptions assigned to ethane (C_2H_6) at 1465.9 and 1374.5 cm^{-1} and methane (CH_4) at 1305.1 cm^{-1} were observed on co-condensation of iron atoms with high concentrations of ethene in argon ($Fe:C_2H_4:Ar$ = 0.6:12.4:100) .[6] Prolonged UV irradiation of such matrices resulted in an increase in ethane and methane absorptions, with concomitant decrease in the diethene-iron complex ($Fe(C_2H_4)_2$). They propose that methane and ethane are produced following the disproportionation of the diethene-iron π-complex, in which production of an unobserved iron carbide species is speculated. Note that an increase in the amount of ethane upon prolonged irradiation of the matrices in this work is also observed. Gentle annealing of the matrix is always a feature of prolonged irradiations with broad band light, and it is expected that such annealing results in additional metal atom reactions occurring with matrix isolated ethene dimer.

Vibrational modes of ethane are also evident in earlier published matrix-isolation work on the reaction of transition metal atoms with ethene in argon. Huber *et al.* have studied the reaction of nickel atoms with ethene under relatively concentrated conditions of ethene in argon, and in pure ethene.[8-12] They have assigned several observed vibrational modes to $Ni(C_2H_4)_2$, which appear at exactly the same positions of major ethane modes (2945, 2886, 1465 cm^{-1}, for 1:10 C_2H_4:Ar) observed here in argon. The published spectra also show absorptions at 2918 and ~1375 cm^{-1}. The first of these modes has been assigned to ν(C-H) of $Ni(C_2H_4)_3$,[8] but given both the close wavenumber matching

and observation of the other three fundamental modes of ethane, it is highly likely that these absorptions are also due to ethane. A similar group of bands (2943, 2888, 1463 cm^{-1})[i] assigned by Huber *et al.* to $Pd(C_2H_4)_2$[13] are almost certainly due to ethane features as well. The remaining modes of the group of bands assigned by Huber *et al*., to $Ni(C_2H_4)_2$ have been reassigned to $Ni(C_2H_4)$ by Merle-Mejean *et al.*[14], and confirmed in the work of Lee *et al.* [15] Interestingly, Merle-Mejean *et al.* did not observe the feature at 1465 cm^{-1} under their experimental conditions, though they do predict a vibrational mode of $Ni(C_2H_4)$ to occur at about 1460 cm^{-1}, resulting from the coupling of C=C stretching and CH_2 deformation motions. This mode has subsequently been reported by Lee *et al.*[15] at 1468 cm^{-1}, following co-condensation of Ni vapour with ethene in argon matrices. As the spectra of Lee *et al.* show no evidence for any of the other modes of ethane, and the experiments were carried out at relatively low ethene concentrations where ethene dimers are not formed in the matrix substantially, it is likely that the mode observed by Huber *et al.* [8] at 1465 cm^{-1} is due to matrix-isolated ethane, but the mode reported at 1468 cm^{-1} by Lee *et al.* is due to NiC_2H_4. The latter assignment is confirmed by the observation of a ^{13}C shift in the 1468 cm^{-1} mode of -15.5 cm^{-1}, as anticipated for a metal-ethene π-complex,[14,15] and far greater than the shift of -4 cm^{-1} observed in this work for ethane, when $^{13}C_2H_4$ is used. The observation of features attributable to ethane in the work of Huber *et al.* are most likely due to metal atom reactions with ethene that would otherwise form dimers during deposition, in their matrices,

[i] average values quoted from various ethene, Ar or Xe matrix experiments.

given the high ethene concentrations employed. Additionally, their results may be due to photoexcitation from the metal source used in their experiments. In cases where there is doubt about the origin of the 1465 cm^{-1} mode, ^{13}C-isotopic substitution could be used profitably to distinguish between formation of ethane, and the formation of a metal-ethene π-complex.

6.8 Mechanistic considerations of ethane formation

It is obvious by stoichiometric considerations alone that the production of ethane from ethene must involve the reaction of at least two ethene molecules, provided there is no other source of hydrogen available. However, the ubiquitous presence of water in all matrix samples raises the concern that water may be the source of hydrogen incorporated into ethane, as was observed in Chapter 5. When metal atoms are co-deposited with samples containing ethene and argon there is a significant loss of features associated with water. To investigate water as a hydrogen donor in our work, experiments which incorporated D_2O in the sample gas were performed in order to determine if any D atoms would be included in the observed ethane. No evidence for inclusion of deuterium was observed when the concentration of ethene was 10%, thereby eliminating water as the formal source of hydrogen in the major results of these experiments. Clearly, these results are in direct contrast with the results observed in Chapter 5. However, the dramatic increase in concentration of ethene in this investigation likely causes a $V + C_2H_4 + C_2H_4$ mechanism to dominate the previously observed $V + H_2O + C_2H_4$ chemistry. Since the depletion of water is evident in all metal containing experiments, it is clear that some reaction of metal atoms with water is

occurring on deposition. Indeed, a feature near 1584 cm^{-1} which may be attributed to a metal hydride stretch associated with a metal-water reaction product (see Figure 25) is observed. Note that such a feature near this position has been attributed to HVOH by Kauffman *et al.*[16], and to a vanadium cluster/water reaction product by Zhou *et al.*[17] Additionally, the results of Chapter 4 suggest this could simply be an isomer of H-V-C_2H_3, as well. However, it would appear that these results do give evidence for vanadium water chemistry occurring, and that such chemistry is unrelated to the major mechanism leading to formation of ethane in this work.

The hydrogenation of ethene involving a second ethene molecule requires one of the ethene molecules to act as a sacrificial hydrogen atom donor, while the other ethene molecule acts as a hydrogen atom acceptor. Mechanistic steps required for such a process are supported by: a) the calculations of Porembski and Weisshaar for early transition metals,[18,19] b) experimental and theoretical investigations by Carroll *et al.*,[20] and c) the theoretical work on metal hydrides and ethene by Siegbahn.[21] In the first of these cases, early second row transition metal atoms are predicted to coordinate ethene through the π–bond to form a metallocyclopropane species. Zr atom reactions with C_2D_4[22] show no kinetic isotope effect in the rate of atom removal, thus supporting the supposition that π-complexation of ethene is the initial reaction step. For Ti and V, π–complexation must involve photoexcitation of the metal atom, since experimental gas-phase measurements of the rate of depletion of both of these metals by ethene show that the ground states of both elements are not

reactive.[23] Further, the first allowed excited states of Ti and V are accessible with visible light corresponding to wavelengths (629, 611 nm)[24] present in emission from the heated Ti or V filaments in the current experiments. In both cases, such excitation would lead to an electronic configuration similar to that of ground state niobium atoms (having partial occupancy of the valence s-orbital), and therefore it is reasonable to suggest that this excitation will result in similar chemistry between the three metallic elements, as is reflected in the results.

The initial coordination step is believed to be followed by insertion of the coordinated metal into a C-H bond to form hydrido-, and subsequently dihydrido-, organometallic intermediates. The barrier for the first of these insertions for early transition metals has been calculated to be fewer than 2 kcal/mol for Y and Zr,[18,19,20] and nonexistent for Nb.[20] In the work of Siegbahn,[21] metal hydrides are predicted to be able to insert ethene directly into a M-H bond without prior formation of a π-bonded ethene complex. Such a direct insertion is predicted to be barrierless[21] for early second-row transition metals up to Nb, for each of the mono-, di-, or trihydrides, and increasingly thermodynamically favored for the di- and trihydride compared with the monohydride.

These studies together provide the basis for development of a formal scheme for alkene hydrogenation through sacrificial hydrogen donation by a second alkene. The observation of perdeuteroeth*ane* (C_2D_6) in this work for the analogous reaction of V atoms with perdeuteroeth*ene* (C_2D_4) conclusively demonstrates that the formal hydrogen atom source must be ethene. The observation of depletion of the ethene dimer following complete matrix

condensation, correlated strongly with the production of ethane, suggests that matrix environments favouring the ethene dimer are the *actual* source of hydrogen in our work. Thus, it is believed that the production of ethane by disproportionation of ethene at transition metal atom centers is a general reaction in environments where the ethene dimer is formed near a metal atom, as can be prepared under high ethene concentration conditions in low-temperature matrices. The generality of this process is demonstrated by the production of ethane both in this work with early transition metal atoms, and in the work of others using late transition metals. The general observation of ethane production under conditions of higher ethene concentration demonstrates that there exists a richer chemistry for metal atom reactions with ethene than has been previously recognized, specifically under conditions where a second ethene molecule is available to react immediately with primary products.

The following reaction scheme (Scheme 4) is proposed as a framework for understanding the present work:

Scheme 4: Reaction mechanism for production of ethane from ethene disproportionation with transition metal atoms.

$$M + C_2H_4 \xrightarrow{h\nu} H_2C{=}HC\text{-}M\text{-}H^*$$

$$H_2C{=}HC\text{-}M\text{-}H^* + C_2H_4 \longrightarrow H_2C{=}HC\text{-}M\text{-}C_2H_5$$

$$H_2C{=}HC\text{-}M\text{-}C_2H_5 \xrightarrow{h\nu} (C_2H_2)M + C_2H_6 \quad \textbf{or}$$

$$H_2C{=}HC\text{-}M\text{-}C_2H_5 \xrightarrow{h\nu} (C_2H_2)M(H)(\text{-}C_2H_5)$$

$$(C_2H_2)M(H)(\text{-}C_2H_5) \xrightarrow{h\nu} MC_2H_2 + C_2H_6$$

$$(C_2H_2)M \longrightarrow \longrightarrow MC_2 + H_2$$

All steps in this scheme must be fast following irradiation from the filament, since no other intermediates are observed on deposition that show concentration relationships that link them to ethane production. The alternative mechanism listed in the later steps is also a viable mechanism, and may well be active in these experiments. In total, this mechanism is completely analogous to that described in the Schemes of Chapter 5. No experiment can be performed under the conditions used in this study to differentiate clearly between the two possible mechanisms presented in the scheme above.

One can understand why the yield of ethane increases non-linearly with ethene concentration, since the formation of ethene dimer in the matrix is lower in 1:70 ethene:Ar samples, but essentially the only form ethene takes in 1:10 ethene:Ar matrices. As well, the production of additional ethane following prolonged irradiation in 1:70 samples is in accord with the idea that photoannealing of the matrix over very long periods of time will cause an increase in the number of metal atoms in close proximity to matrix-isolated ethene dimer, yielding additional production of ethane. Subsequent destruction of the MC_2H_2 species is implicit in the lack of observation of any other products save methane, which it cannot generate directly.

The overall reaction process would be $M^* + 2\ C_2H_4 \rightarrow MC_2 + C_2H_6 + H_2$ which would give rise to no new major spectroscopically observable hydrocarbon products, other than ethane. While there is no evidence for a metal carbide product, it must be present for the validity of these reactions, and simply the

infrared spectrum is not sufficiently intense to be observed under our conditions. Note that Kafafi *et al.* proposed the formation of a similar metal carbide species involving iron atoms following prolonged irradiation of their matrix samples, which was also not observed in their work.[6] The fundamental of NbC has been experimentally determined to occur at 993 cm^{-1} (ω_e).[25] TiC and VC are predicted to have ω_e in the range 869-1006 cm^{-1}. The MCC dicarbides of Ti, V and Nb are known to have a M-C fundamental mode in the range of 500-600 cm^{-1}.[26-28] As ethene in argon matrices (1:10; ethane:Ar) has strong IR absorption in the range 920-985 cm^{-1}, it is possible that spectral features due to metal monocarbides are obscured by the strong ethene absorptions in this spectral range. However, given the low concentration of metal in this work, it is more likely that features due to metal carbide species are simply too weak to observe.

The reaction of niobium atoms with ethene has been studied in the gas phase, both by Weisshaar[20] and ourselves,[29] using fast-flow metal atom reactors. In both cases, Nb atoms are removed by ethene at rates very close to the gas-kinetic collision frequency, supporting a barrierless association reaction to form a π-complex as a first, rate-limiting step. In other flow reactor work, product mass data indicates that production of NbC_2H_2 is the major active process in the gas phase. As well, the kinetic behavior of the reaction of this product with a second ethene molecule exhibits sequential addition behavior. The observation of NbC_2H_2 as the major product in the gas phase contrasts the current matrix-isolation work, in which no product except ethane is observed. This difference is undoubtedly due to the fact that the gas-phase processes involve only the ethene

monomer, whereas the current matrix work involves both the ethene monomer and dimer. Intermediates such as those identified by Lee *et al.*[2] are likely the precursors to the gas phase reactivity, leading to partial or full dehydrogenation of ethene. Ethane production would likely be observed in the gas phase, if the gas-phase reaction process were to be carried out at high enough partial pressures of ethene for reaction of two ethene molecules at the metal center before any metal-alkene bond cleavage were to occur.

In both this work, and the work of Kafafi *et al.*, the observation of absorptions attributed to CH_4 are observed,[6] the latter involving photoexcitation of a metal atom - ethene complex. In the analogous reactions with C_2D_4, the formation of CD_4 (993 cm^{-1}) demonstrates that the presence of methane in the resultant spectra must be due to a competitive metal atom-ethene reaction. In the absence of any further spectroscopic information related to methane production, we can only speculate on the mechanism for methane formation by early transition metal atoms. It is clear that the mechanism must involve a C-C bond cleavage as a critical step. Such a process likely involves further reaction of hydridic metal complexes from reactions of metal atoms with ethene, likely involving the intermediates such as HMC_2H_3 and $H_2MC_2H_2$ identified by Lee *et al.* for Ti and proposed for V in this work. That water is depleted in many experiments, may also implicate M + H_2O, or even MO chemistry, but no evidence in support of these two claims is available from the current data.

6.9 Summary and conclusions

In summary, the production of ethane is a general process in the chemistry of matrix-isolated ethene with metal atoms, when the concentration of ethene is sufficiently high for the ethene dimer to be present. A proposed general mechanistic scheme for ethene disproportionation to form ethane, molecular hydrogen and metal carbides at the expense of matrix-isolated ethene dimer is also presented. This mechanism is supported not only in the current work, but in observations obtained in previous work with ethene and metal atom reactions. It has been shown that gas-phase and matrix-isolation reaction chemistries are distinct, and that differences in observed chemistry are likely due to the photochemical activation of the metal, and the availability of a second ethene molecule to react promptly with primary organometallic products.

6.10 References for Chapter 6

[1] Nakamoto, K. *Infrared and Raman Spectra of Inorganic and Coordination Compounds,* 4th ed.; Wiley; New York, **1978**.

[2] Lee, Y.K.; Manceron, L.; Papai, I. *J. Phys. Chem. A* **1997**, *101*, 9650.

[3] Rytter, E.; Gruen, D.M.; *Spectrochim. Acta A.*, **1979**, *35A*, 199.

[4] Nielsen, A.H.; Nielsen, H.H. *Phys. Rev.* **1938**, *54*, 118.

[5] Siegbahn, P.E.M.; Blomberg, M.R.A.; Svensson, M. *J. Am. Chem. Soc.* **1993**, *115*, 1952.

[6] Kafafi, Z.H.; Hauge, R.H.; Margrave, J.L. *J. Am. Chem. Soc.* **1985**, *107*, 7550.

[7] Cardenas, G.; Shevlin, P.B. *J. Org. Chem.* **1984**, *49*, 4726.

[8] Huber, H.; Ozin, G.A.; Power, W.J. *J. Am. Chem.Soc.* **1976**, *98*, 6508.

[9] McIntosh, D.; Ozin, G.A. *J. Organomet. Chem.* **1976**, *121*, 127.

[10] Ozin, G.A.; Power, W.J.; *Inorg. Chem.* **1977**, *16*, 212.

[11] Ozin, G.A.; Power, W.J.; Upton, T.H.; Goddard III, W.A.; *J. Am. Chem. Soc.* **1978**, *100*, 4750.

[12] Parker, S.F.; Peden, C.H.F.; Barrett, P.H.; Pearson, R.G. *Inorg. Chem.* **1983**, *22*, 2813.

[13] Huber, H.; Ozin, G.A.; Power, W.J.; *Inorg. Chem.* **1977**, *16*, 979.

[14] Merle-Mejean, T.; Cosse-Mertens, C.; Bouchareb, S.; Galan, F.; Mascetti, J.; Tranquille, M. *J. Phys. Chem.* **1992**, *96*, 9148.

[15] Lee, Y.K.; Hannachi, Y.; Xu, C.; Andrews, L.; Manceron, L. *J. Phys. Chem.* **1996**, *100*, 11228.

[16] Kauffman, J.W.; Hauge, R.H.; Margrave, J.L. *J. Phys. Chem.*, **1985**, *89*, 3547.

[17] Zhou, M.; Dong, J.; Zhang, L.; Qin, Q.; *J. Am. Chem. Soc.*, **2001**, *123*, 135.

[18] Porembski, M.; Weisshaar, J.C. *J. Phys. Chem. A* **2001**, *105*, 4851.

[19] Porembski, M.; Weisshaar, J.C. *J. Phys. Chem. A* **2001**, *105*, 6655.

[20] Carroll, J.J.; Haug, K.L.; Weisshaar, J.C.; Blomberg, M.R.A.; Siegbahn, P.E.M.; Svensson, M. *J. Phys. Chem.* **1995,** *99*, 13955.

[21] Siegbahn, P.E.M. *J. Am. Chem. Soc* **1993**, *115*, 5803.

[22] Porembski, M.; Weisshaar, J.C. *J. Phys. Chem. A*, **2000,** *104,* 1524.

[23] Ritter, D.; Carroll, J.J.; Weisshaar, J.C.; *J. Phys. Chem.*, **1992**, *96*, 10636.

[24] Moore, C.E.; Circ. U.S. Natl. Bur. Stand., **467**, 1, 1947.

[25] Simard, B.; Presunka, P.I.; Loock, H.-P.; Bérces, A.; Launila, O. *J. Chem. Phys.* **1997,** *107,* 307.

[26] Wang, X.; Ding, C.; Wang, L.S. *J. Phys. Chem.* **1997**, *101*, 7699.

[27] Li, X.; Wang, L.-S. *J. Chem. Phys.* **1999**, *111*, 8389.

[28] Zhai, H.-J.; Liu, S.-R.; Li, X.; Wang, L.-S. *J. Chem. Phys.* **2001**, *115*, 5170.

[29] Parnis, J.M.; Escobar-Cabrera, E.;, Thompson, M.G.K.; Jacula, J.P; Lafleur, R.D.; Guevara-Garcia, A.; Martinez, A.; Rayner, D.M.; *J. Phys. Chem.,* **2005**, 109, 7046.

Chapter 7

Summary and Future Direction

7.0 Conclusions and Future Outlook

Thermally generated vanadium atoms have been shown to insert into the O-H bonds of water, or the C-H bonds of ethene, forming transient species that are implicated in the hydrogenation of ethene. The final product is ethane in these cases, which is believed to result from elimination of an alkyl fragment coordinated to the metal, with a second hydrogen atom on the initiating species (H_2O or C_2H_4).

The mechanism for hydrogenation is proposed to involve the alkene insertion into an M-H bond, with a subsequent elimination of the alkyl group, following a second metal atom O-H/C-H insertion, or by a 1,3-elimination alkane elimination route. That there is such similarity in the mechanistic steps describing the overall hydrogenation following the reaction of the metal atom with either H_2O or C_2H_4 as the initiating species suggests that this hydrogenation mechanism may become active with a wider variety of other H-containing sources, as well. Alcohols, aldehydes, or other main-group hydrides such as

H_2S, may well represent additional areas worth exploring, to determine the limitations, if any, of hydrogenation where M-H bond formation is an initial step.

In these results, ethene has been the focus of the observed hydrogenation in all cases. Additional investigations exploring the insertion of other alkenes into M-H bond containing species would represent another aspect worth exploring. Furthermore, other π-bond containing molecules, such as C_2H_2, CO, or even N_2 may react by analogous mechanisms, leading to a wider array of products.

Finally, the observed sacrificial hydrogenation for various metals (Ti, V, Nb, Ni, Pd, Fe) suggests that this hydrogenation is a general reaction among the transition elements, and factors exploring the reactivity of each metal with respect to the proposed mechanisms may give rise to additional insight as well. All of these aspects represent excellent starting points for further characterizing the limitations of the work which has been presented in the previous chapters.

Appendix

Table 5: Comparison of infrared spectra features for new molecules isolated in argon matrices for the reaction of V atoms with isotopomers of ethene.

Molecule A: C_2H_4 results		Molecule A: C_2D_4 results				Molecule A: C_2D_4 results			
Wavenumber	**product identity**	**Wavenumber**	**product identity**	**shift**	**ratio**	**Wavenumber**	**product identity**	**shift**	**ratio**
1557.6	^{4}H-V-C_2H_3 conformation								
1552	^{4}H-V-C_2H_3 conformation	1119.8	^{4}D-V-C_2D_3 conformation	-432.2	1.39	1551.6	^{4}H-V-C_2H_3 conformation	**-0.4**	1.00
1547.4	^{4}H-V-C_2H_3 conformation								
1069	^{4}H-V-C_2H_3 conformation					1040.9	^{4}H-V-$^{13}C_2H_3$ conformation	**-28.1**	1.03
Molecule B2: C_2H_4 results		**Molecule B2: C_2H_4 results**				**Molecule B2: C_2H_4 results**			
Wavenumber	**product identity**	**Wavenumber**	**product identity**	**shift**	**ratio**	**Wavenumber**	**product identity**	**shift**	**ratio**
1667.8	$^2H_2V(C_2H_2)$ conformation	1205.1	$^2H_2V(C_2H_2)$ conformation	-462.7	1.38	1672.6	$^2H_2V(^{13}C_2H_2)$ conformation	4.8	1.00
1645.8	$^2H_2V(C_2H_2)$ conformation					1647.6	$^2H_2V(^{13}C_2H_2)$ conformation	1.8	1.00
Molecule C2: C_2H_4 results		**Molecule C2: C_2H_4 results**				**Molecule C2: C_2H_4 results**			
Wavenumber	**product identity**	**Wavenumber**	**product identity**	**shift**	**ratio**	**Wavenumber**	**product identity**	**shift**	**ratio**
1584.5	^{4}H-V-C_2H_3 conformation	1142.6	^{4}D-V-C_2D_3 conformation	-441.9	1.39	1589.7	^{4}H-V-C_2H_3 conformation		
						1582.2	^{4}H-V-C_2H_3 conformation		
1561.5	^{4}H-V-C_2H_3 conformation								
						1345.8	^{4}H-V-C_2H_3 conformation		
		681.7	^{4}D-V-C_2D_3 conformation						
						854.8	^{4}H-V-C_2H_3 conformation		
						847.6	^{4}H-V-C_2H_3 conformation		
						844.2	^{4}H-V-C_2H_3 conformation		
591.9	^{4}H-V-C_2H_3 conformation					569.9	^{4}H-V-C_2H_3 conformation	-22	1.04
575.7	^{4}H-V-C_2H_3 conformation					566.5	^{4}H-V-C_2H_3 conformation		
						563.8	^{4}H-V-C_2H_3 conformation		

Note: Wavenumber values are in cm^{-1} units. Shift values are relative to the corresponding modes of the C_2H_4 species. Additionally, ratios are calculated as the values for the C_2H_4 divided by the value for the corresponding isotopomer. Modes which have no corresponding entry in the row of the table have no corresponding observations.

Appendix

Throughout this thesis, a number of physical constants are used. The following is a listing of the major physical constants that appear in this work, along with their associated units. Additional constants, when necessary in other applications, can typically be found in the front of standard physical chemistry textbooks.

Symbol	**description**	**value**	**units**
c:	speed of light	2.9979248×10^{8}	m/s
π:	pi	3.14159265	none
k:	Boltzmann's constant	1.38066×10^{-23}	$J.K^{-1}$
h:	Planck's constant	6.626×10^{-34}	J.s
N_a:	Avogadro's number	6.022×10^{23}	$mole^{-1}$
R:	ideal gas constant	8.31451	$J.K^{-1}.mole^{-1}$